

TNASA-CR-65023

# FINAL REPORT RADIANT HEATING SIMULATION

By

T. K. Pugmire and R. W. Liebermann

prepared for

NATIONAL AERONAUTICS AND SPACE ADMINISTRATION  
MANNED SPACECRAFT CENTER  
HOUSTON, TEXAS

3 May 1965

Technical Report  
RAD-TR-65-6  
Contract NAS 9-3507

N65-24996

FACILITY FORM 602

(ACCESSION NUMBER)	(THRU)
<u>136</u>	<u>1</u>
(PAGES)	(CODE)
<u>CR 65023</u>	<u>33</u>
(NASA CR OR TMX OR AD NUMBER)	(CATEGORY)

GPO PRICE	\$	<u>          </u>
OTS PRICE(S)	\$	<u>          </u>
Hard copy (HC)		<u>4.00</u>
Microfiche (MF)		<u>1.00</u>

RESEARCH AND ADVANCED DEVELOPMENT DIVISION  
AVCO CORPORATION  
Wilmington, Massachusetts

RQT-29925

# FINAL REPORT RADIANT HEATING SIMULATION

By

T. K. Pugmire and R. W. Liebermann

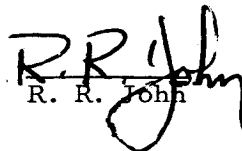
prepared for

NATIONAL AERONAUTICS AND SPACE ADMINISTRATION  
MANNED SPACECRAFT CENTER  
HOUSTON, TEXAS

3 May 1965

Technical Report  
RAD-TR-65-6  
Contract NAS 9-3507

APPROVED

  
R. R. John

RESEARCH AND ADVANCED DEVELOPMENT DIVISION  
AVCO CORPORATION  
Wilmington, Massachusetts

SYMBOLS (Cont'd)

<u>Symbol</u>	<u>Description</u>
P	Pressure
$P_1$	Initial pressure driven tube
Q	Heat flux
$\dot{q}$	Heat transfer rate
$\dot{q}_{st}$	Stagnation point heat transfer rate
$\dot{q}_r$	Radiative heat transfer rate
$R_n$	Nose radius of hemispherical body
T	Absolute temperature, transmissivity
$V_s$	Traveling normal shock velocity
$V_\infty$	Flight velocity
$V_e$	Flight velocity
W	Vehicle weight
$\dot{a}_\lambda$	Apparent absorption coefficient
$a_\lambda$	True absorption coefficient
$\delta$	Shock detachment distance
$\epsilon$	Emissivity
$\delta$	Shock detachment distance
$\mu$	Micron ( $10^{-4}$ cm)
$\lambda$	Wavelength
$\rho_o$	Reference density at STP (air)

SYMBOLS (Concl'd)

<u>Symbol</u>	<u>Description</u>
$\rho$	Density (used as representing stagnation density)
$\Omega$	Solid angle
$\sigma$	Conductivity
<u>Subscripts</u>	
$g$	Gage property
$\infty$	Flight, free stream condition
$s$	Stagnation point gas property



TABLES

Table	I	Operating and Performance Data for Carbon Arc Double Elliptical Mirror Image Furnaces .....	24
	IIA	Main Data of High Wattage Xenon, Mercury, and Mercury-Xenon Compact Arc Lamps .....	35
	IIB	Main Data of High Wattage Xenon, Mercury, and Mercury-Xenon Compact Arc Lamps .....	36
	III	Source Evaluation Summary.....	69
	B1	Continuum Radiation Data of Air .....	87
	D1	Total Normal Emissivity of Copper .....	114

## SYMBOLS

<u>Symbol</u>	<u>Description</u>
a	Entry Angle
°	
Å	Angstrom units ( $10^{-8}$ cm)
A	Area, altitude
$C_D$	Drag coefficient
c	Velocity of light
$C_{L_{max}}$	Lift coefficient
D	Aerodynamic drag
$E_t$	Total equilibrium radiation per unit gas volume
$E_c$	Continuum radiation per unit gas volume
$f(V_\infty)$	Function of flight velocity
$F_1$	Shock layer shape correction factor
$F_2$	Thin film gage geometric view factor
h	Plank's constant
$h_s$	Stagnation point enthalpy
$h_\infty$	Ambient enthalpy
I	Intensity
$J_\lambda$	Radiant flux per unit wavelength
k	Boltzman's constant
L	Aerodynamic lift
n	Number density, exponent
$n_e$	Electron number density

ILLUSTRATIONS (Cont'd)

Figure	38	Spectral Radiance Measurements for Argon .....	61
	39	Spectral Radiance Measurements for a Carbon Arc .....	62
	40	Spectral Radiance Measurements of Various Gases .....	64
	41	Spectral Radiance of Argon at 14,000° K for Pressures from 1 to 6 Atmospheres .....	65
	42	Spectral Radiance of Argon with a Trace of Cesium..	66
	A-1	Normalized Equilibrium Radiation Data of Air versus Flight Velocity .....	76
	A-2	Normalized Equilibrium Radiation Data of Air versus Flight Velocity .....	77
	A-3	Normalized Equilibrium Radiation Data of Air versus Flight Velocity .....	78
	A-4	Normalized Equilibrium Radiation Data of Air versus Flight Velocity .....	79
	A-5	Composite of Normalized Equilibrium Radiation Data of Air versus Flight Velocity .....	80
	A-6	Shock-Tube Data Reported by Flagg .....	82
	A-7	Shock-Tube Data Reported by Hoshizaki .....	84
	B-1	Continuum Radiation of Air versus Temperature at Constant Pressures .....	89
	B-2	Continuum Radiation of Air versus Density at Constant Pressures and Temperatures .....	90
	B-3	Continuum Radiation of Air versus Flight Velocity at Constant Pressures and Temperatures .....	91
	B-4	Density of Air versus Flight Velocity at Constant Pressures and Temperatures .....	92

ILLUSTRATIONS (Concl'd)

Figure	B-5	Continuum Radiation of Air versus Temperature at Constant Density .....	93
	B-6	Total Equilibrium Air Radiation versus Temperature at Constant Density Ratios (theory versus extended data) .....	94
	B-7	Comparison of Nitrogen UV (0-0.11 $\mu$ ) Estimated Continuum Radiation with Experimental Data Covering the 0.25-2.5 $\mu$ ) Spectral Range .....	96
	B-8	Sketch of Constricted Arc .....	98
	C-1	Radiant Heating Source .....	102
	C-2	$l^2 - l_0^2$ versus $\dot{q}_r (l_0)t$ .....	104
	D-1	Reflectivity of Silver After Damage by Particle Impact .....	112
	D-2	Talysurf Profile of Alumina Surface .....	113
	D-3	Four 125-Microinch RMS Finishes .....	116
	D-4	Illustration of Deficiencies of RMS Method in Defining Surface Roughness .....	117
	D-5	Comparison of the Effective Emissivity of the Cylinder with that of the New Shape Black Body .....	118

## ILLUSTRATIONS

Figure	1	Velocity Altitude Profile .....	5
	2	Velocity-Time Entry Histories .....	6
	3	Stagnation Point Heat Transfer Time History, Reentry $V_e = 26,000$ ft/sec, $L/D = 1.2$ .....	7
	4	Stagnation Point Heat Transfer Entry Histories, $V_e = 36,500$ ft/sec, $L/D = 1.2$ .....	8
	5	Stagnation Point Heat Transfer Entry Histories, $V_e = 36,500$ ft/sec, $L/D = 0.6$ .....	9
	6	Stagnation Point Heat Transfer Time Histories, Reentry $V_e = 36,500$ ft/sec, $L/D = 1.2$ .....	10
	7	Equilibrium Radiation Data and Uncertainty Band...	12
	8	Typical Stagnation Point Radiation Heating .....	13
	9	Normalized Equilibrium Radiation Data of Air versus Temperature (Arc-Column Data Estimates versus Shock-Tube Data) .....	14
	10	Summary of Radiance Measurements for all Carbon Dioxide-Nitrogen Mixtures .....	15
	11	Comparison of Predictions: Radiance of Equilibrium Air $T = 8000^\circ\text{K}$ , $\rho/\rho_0 = 1$ .....	16
	12	Spectral Radiance of Equilibrium Air (1000-100,000Å and $L = 1$ cm) .....	17
	13	Normal Shock Integrated Nonequilibrium Radiation for 9 percent $\text{CO}_2$ - 90 percent $\text{N}_2$ - 1 percent A ...	18
	14	Solar Furnace Flux Stability Test .....	22
	15	Arc-Image Furnace Flux Stability Test .....	25
	16	Arc-Image Furnace Flux Variation .....	26
	17	Reinforcing Mirror Around Anode .....	28

ILLUSTRATIONS (Cont'd)

Figure	18	Carbon Vapor Lamp .....	29
	19	Conical Carbon Resistor .....	31
	20	Carbon Radiation Source Element .....	32
	21	High Pressure Compact Arcs .....	34
	22	Cross Section of Constricted Arc .....	38
	23	Plasma Generator Radiation Source .....	39
	24	Vortex Stabilized Radiation Source .....	40
	25	Vitro Arc Sketch .....	42
	26	Schematic of Modified Tandem Gerdien Combined Radiative and Convective Heating Arc Source.....	43
	27	ROVERS Facility .....	44
	28	Carbon Arc Furnaces - Reflector Systems .....	48
	29	Use of Secondary Reflectors to Fold Back Rays ....	50
	30	Paraboloid - Spherical Reflector .....	51
	31	Flux Enhancement for Optically Thin Sources .....	53
	32	Percentage Reflectence of an Aluminum Mirror ....	55
	33	Transmission Characteristics of Quartz, Various Glasses, and Water .....	56
	34	Spectral Radiance Measurements for Nitrogen - One Atmosphere .....	57
	35	Spectral Radiance Measurements for Oxygen - One Atmosphere .....	58
	36	Spectral Radiance Measurements for Nitrogen - 7.7 Atmospheres .....	59
	37	Spectral Radiance Measurements for Xenon .....	60

## CONTENTS

I.	Summary .....	1
II.	Introduction .....	2
	A. Program Objectives.....	2
	B. Program Organization.....	2
III.	Definition of Radiant Heat Inputs For Manned Missions.....	4
	A. Estimates of Radiation Heat Fluxes .....	4
	B. Spectral Distribution (Air) .....	11
IV.	Relationships of Flight Parameters to Simulation Requirements..	19
V.	Source Evaluation .....	21
	A. Radiation Sources .....	21
	1. Solar-Radiation .....	21
	2. The Carbon Arc.....	23
	3. Electrical Resistors .....	27
	4. High Pressure Compact Arcs .....	33
	5. Plasma Generator .....	37
	6. Electron-Beam Radiation Sources.....	45
	7. Lasers as Radiation Sources .....	46
	B. Radiation Source Optics .....	47
	1. Arc Imaging.....	47
	2. Types of Optical Systems .....	47
	3. Imaging System Performance Limitations .....	49
	C. Spectral Radiance of Sources.....	54
	D. Source Selection .....	63
	1. Carbon Arc Lamps.....	63
	2. Plasma Arc Lamps .....	67
VI.	Recommendations For Future Research .....	70

CONTENTS (Concl'd)

Appendixes

A.	Experimental Radiation From Shock-Heated Facilities .....	75
1.	Reduction of Shock-Tube Data .....	75
2.	Reduction of Flagg's Data .....	81
3.	Reduction of Nerem's Data .....	83
4.	Reduction of Hoshizaki's Data .....	83
5.	Reduction of Page's Data .....	85
6.	Conclusions and General Remarks .....	85
B.	Estimates of Continuum Radiation Based on Experimental Results From an Arc-Heated Plasma .....	86
1.	Estimates of the Continuous Spectrum .....	86
2.	Comparison with Theory .....	88
3.	Comparison with Shock-Tube Data .....	88
4.	UV Radiation .....	95
5.	Plasma Diagnostic Techniques and Experimental Apparatus - A Standard Arc Source .....	97
C.	Evaluation of Experimental Results of a Material Subject to Radiative Heating .....	101
D.	The Effect of Electromagnetic Radiation on Solids .....	105
1.	Theory of the Thermal Radiation Parameters .....	105
2.	Characterization of Surfaces .....	111
E.	References .....	119



## I. SUMMARY

The overall objective of this study program was to define the requirements for Simulation of the radiant heating attendant to atmospheric entry by manned spacecraft and assessment of techniques for achieving this simulation. Phase I of the study defined the radiant heating inputs for manned missions. For this Phase the objectives were met, insofar as possible, with existing data.

While attempting to establish the environment definition, it was observed that the data reduction procedures for shock-tube radiation data could be improved on. This was done, and the results are presented in this report. It was also observed that the recently developed technique of arc-column diagnostics provided applicable data for estimating radiative fluxes. This data was utilized to produce engineering-type curves for flux estimates. An attempt was also made to relate the environment parameters to the simulation requirements. This was the area in which the greatest difficulty was encountered, due to the significant void of information or data. In several areas, particular information voids are discussed and illustrated. Possible action to improve this condition has been recommended.

During Phase II of the program, an extensive investigation was made of potential radiation sources. This data has been presented. For the third and last Phase, an evaluation was made of the sources on the basis of the simulation requirement definition. Additional studies have been recommended here, particularly in the area of the spectral distribution match requirement.

To meet the present NASA-MSD requirement for radiation simulation testing of heat-shield materials, the procurement of two types of sources is recommended. First, a plasma arc generator in which the model may be brought into close proximity to the arc column for small-scale material screening and phenomenon investigation. Second, a plasma generator with the required associated optics suitable for imaging the radiative flux on larger models in conjunction with or without a convective heating source.

## II. INTRODUCTION

This is the Final Report submitted under contract NAS 9-3507 and covers the period of 23 September 1964 through 26 February 1965.

### A. PROGRAM OBJECTIVES

#### 1. Phase I - Definition of Radiant Heat Inputs for Manned Missions

a. This phase of the program included definition and characterization of the radiant heating environments. Consideration was given to reentry velocities from those characteristic of Apollo (35,000 to 45,000 ft/sec) to those characteristic of manned planned planetary missions (50,000 to 70,000 ft/sec and greater).

b. An investigation was made of the available scaling and other simulation criteria necessary for predicting material behavior under entry-radiant heating conditions. Particular emphasis was placed on investigating the necessary sample model size, test time, the required spectral distribution of the energy from the radiant source, and the necessity for programing the radiant heat input.

#### 2. Phase II - Evaluation of Existing Radiant Heater Technology

a. A study was carried out on those radiant sources which might be utilized in entry simulation facilities. The following radiation sources were evaluated: 1) Solid and gas discharge lamps; 2) Electron beam heaters; 3) Resistance or induction heaters; 4) Solar furnace and 5) Direct arc column heating.

b. The evaluation of the performance characteristics of the sources included: 1) Maximum radiant flux attainable; 2) Spatial and temporal uniformity of flux at test section; 3) Spectral distribution of the radiant flux; 4) Compatibility with convective heating sources; 5) Operational characteristics; and 6) Economics.

#### 3. Phase III - Definition of Future Research and Development Requirements

a. On the basis of existing technology of radiative and combined convective-radiative simulators the state-of-the-art was defined.

b. Comparison was made between the state-of-the-art of radiant heater technology and the future reentry environment requirements. On the basis of this comparison, specific recommendations for future development efforts have been made in those areas where the existing technology is not adequate.

## B. PROGRAM ORGANIZATION

This program originated from the Structures and Mechanics Division of the NASA Manned Spacecraft Center. Mr. D. H. Greenshields, Thermo-Structures Branch, is the Technical Representative for NASA-MSC. The Project Director at Avco RAD is Dr. R. R. John. Mr. T. K. Pugmire is the Project Engineer. Other participants in this study are Drs. S. Bennett, T. Laszlo, R. Schlier, and R. Timmins; and Messrs. P. Andrews, Mr. Hermann, R. Liebermann, J. Morris and F. Viles. P. Andrews, M. Hermann and J. Morris contributed in the area of environment definition. S. Bennett, M. Hermann, T. Laszlo, and R. Timmins provided analyses pertinent to the evaluation of the simulation requirement. T. Laszlo provided data on a variety of radiation sources. R. Schlier and F. Viles contributed information on several particular sources. S. Bennett contributed the discussion on source optics.

### III. DEFINITION OF RADIANT HEAT INPUTS FOR MANNED MISSIONS

#### A. ESTIMATES OF RADIATION HEAT FLUXES

A literature search to establish the limits of possible radiant heating for the manned entry corridor (limits established by  $C_{Lmax}$ , 12g undershoot,  $C_{Lmax}$ , overshoot;  $L/D_{max}$ , 12g undershoot; and  $L/D_{max}$  overshoot) provided somewhat disappointing results. In general, predictions at the higher velocities of 40,000 ft/sec differ by factors of more than 2.<sup>1-8</sup>

For flight velocities less than 40,000 ft/sec, the agreement among investigators is relatively good. Comparison studies were made of the available radiation data obtained in shock-heated facilities. The data studied is shown in appendix A together with a discussion of reduction and application of this data.

Radiant heating fluxes pertinent to the manned entry corridor are demonstrated by the trajectories shown in figure 1. Figure 2 provides a velocity versus time plot of these flight profiles. For the reentry trajectories shown, the following other conditions apply:

$C_{Lmax}$ :	$W/C_D A$	=	42 psf
	a	=	60 degrees
	L/D	=	0.6
$L/D_{max}$	$W/C_D A$	=	147 psf
	a	=	30 degrees
	L/D	=	1.2

The specific equilibrium radiation data used to predict the radiation heat transfer for these conditions was that of Allen and Textoris<sup>4</sup> and where considered applicable and valid, the results of Kivel and Bailey<sup>3</sup>. (The earlier resumes of Kivel and Bailey considerably overestimate the radiative intensity at temperatures above 9000°K.) For these calculations, stagnation-point shock-detachment distances were estimated assuming a two-dimensional flow. Heating distributions were made for the windward side assuming a plane, optically thin slab model with linear temperature and density gradients normal to the surface. The shock geometry was derived from NASA-Langley Schlieren photographs. Non-equilibrium radiation calculations were based entirely on the experimental data of Allen et al.<sup>7</sup> No density dependence was considered and an arbitrary altitude cutoff of 280,000 feet was assumed. The heating rates for these conditions are shown in figures 3-6. Some of the results are contained in reference 9.

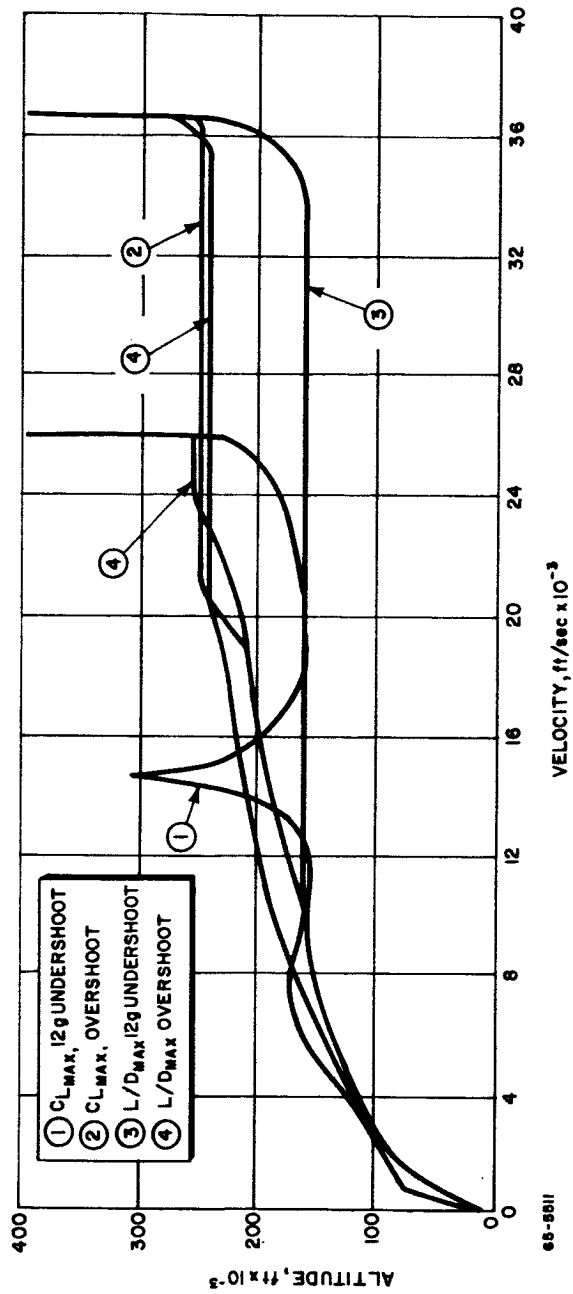


Figure 1 VELOCITY ALTITUDE PROFILE

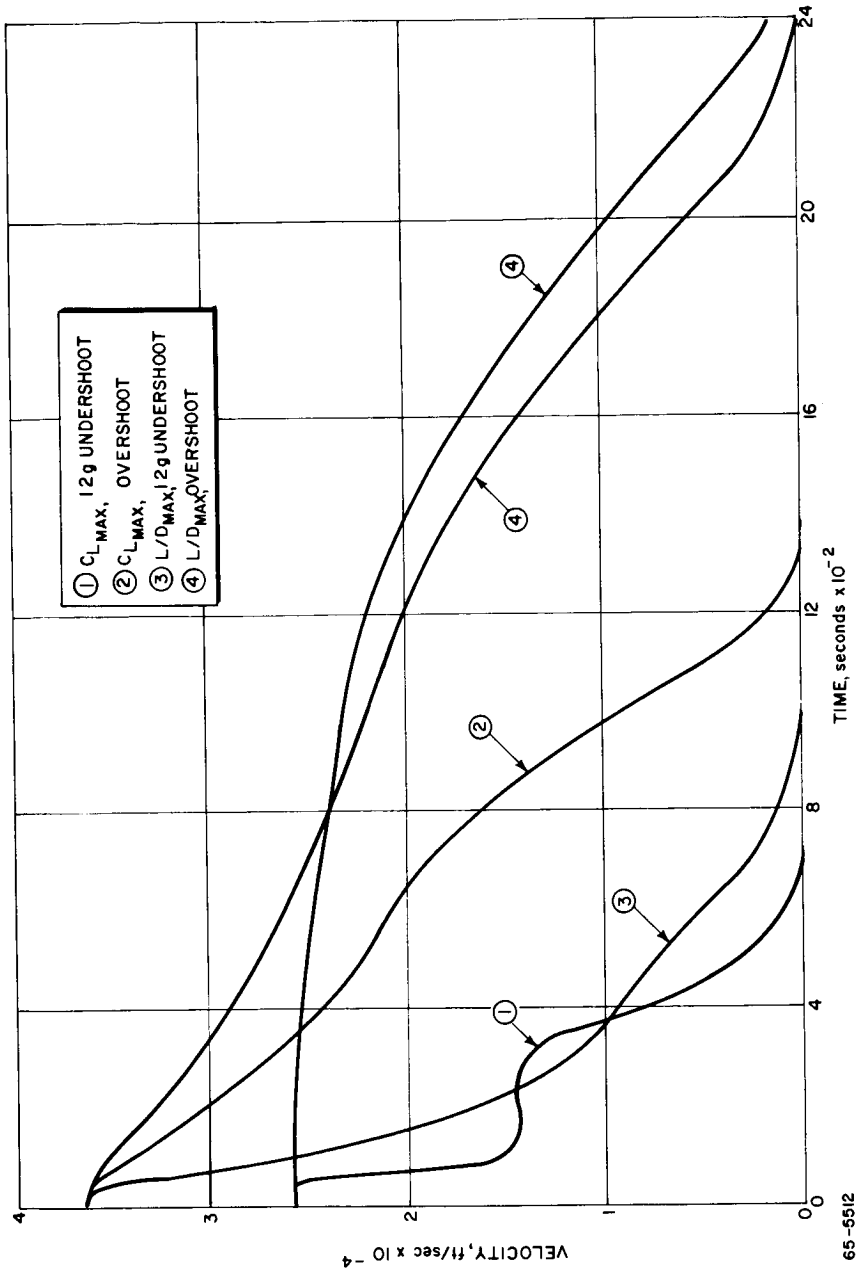


Figure 2 VELOCITY-TIME ENTRY HISTORIES

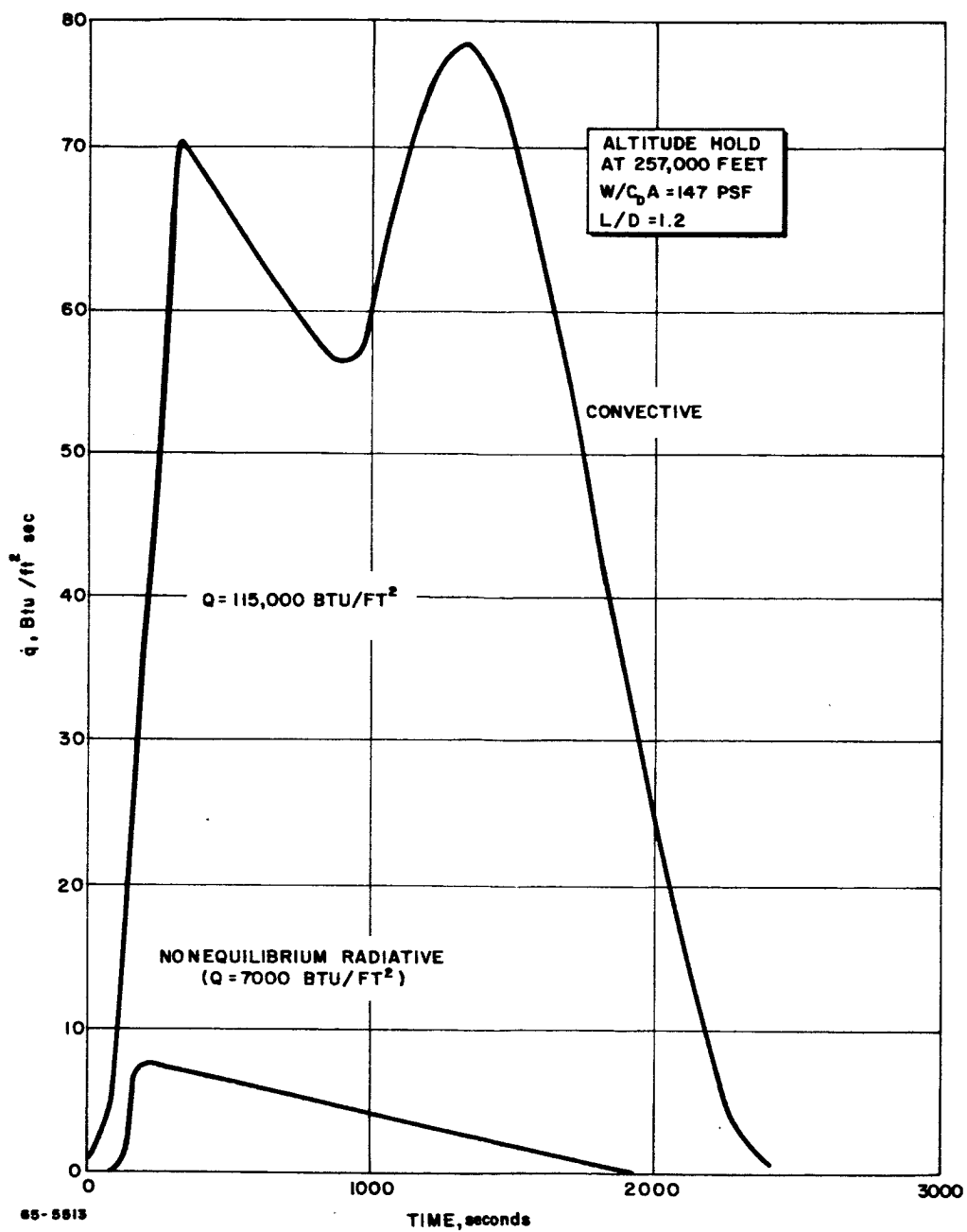


Figure 3 STAGNATION POINT HEAT TRANSFER TIME HISTORY, REENTRY  
 $V_e = 26,000$  FT/SEC,  $L/D = 1.2$

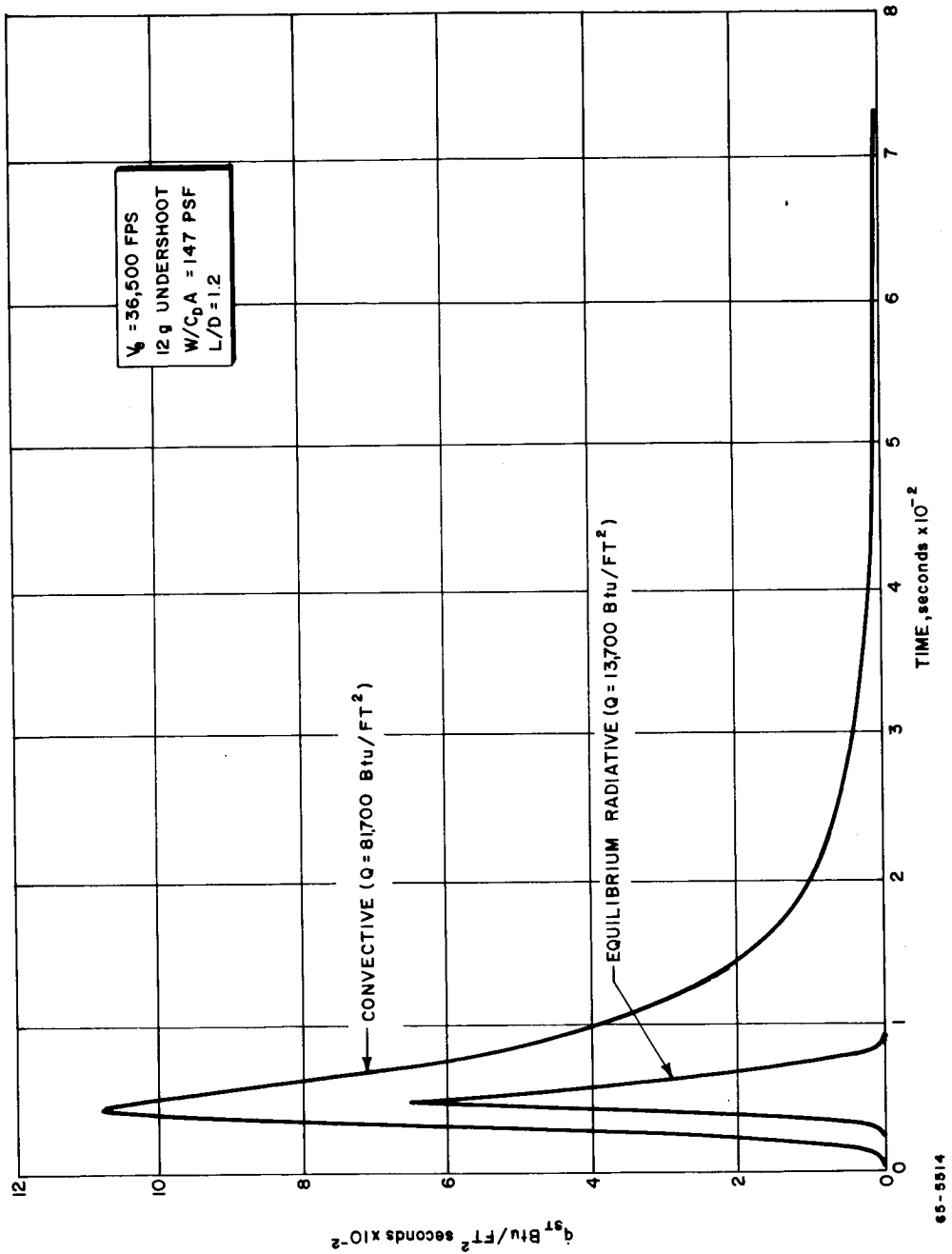


Figure 4 STAGNATION POINT HEAT TRANSFER ENTRY HISTORIES,  
 $V_e = 36,500 \text{ FT/SEC}$ ,  $L/D = 1.2$



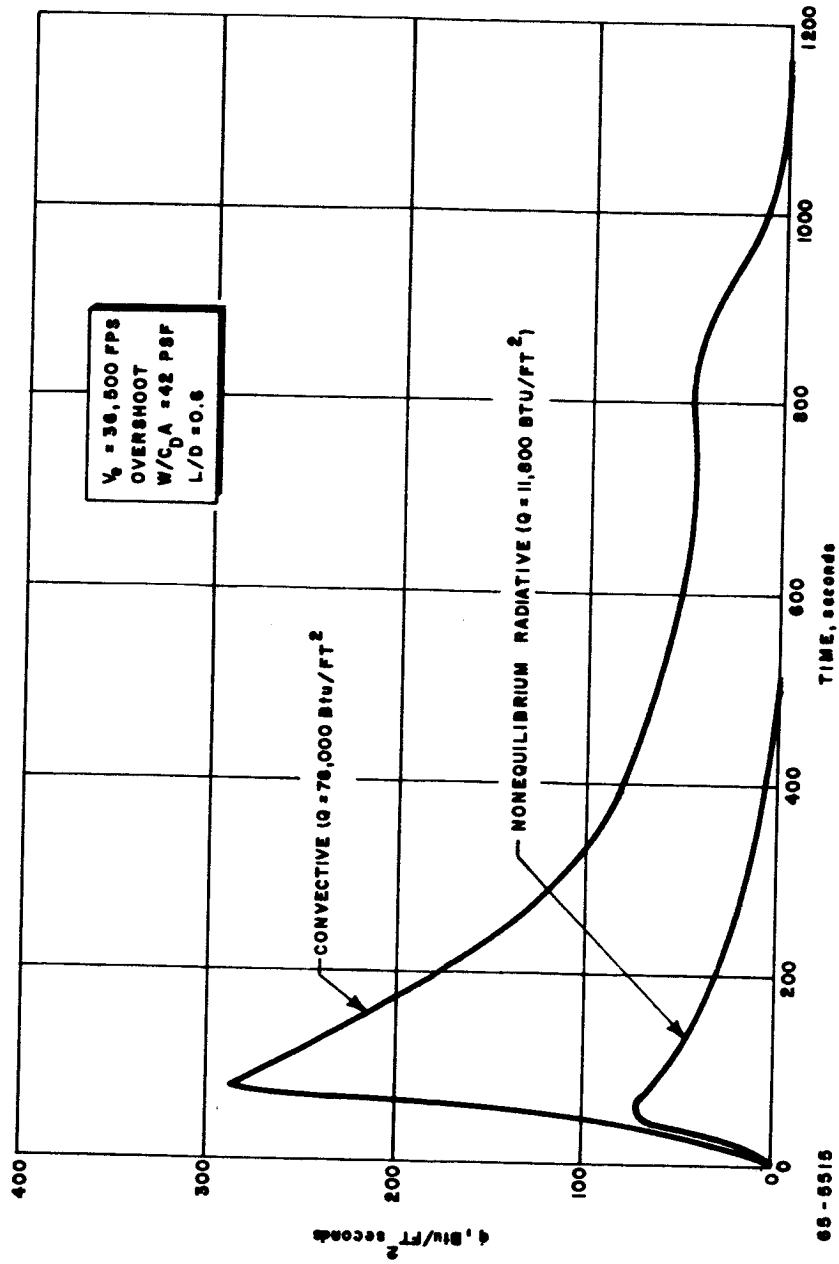
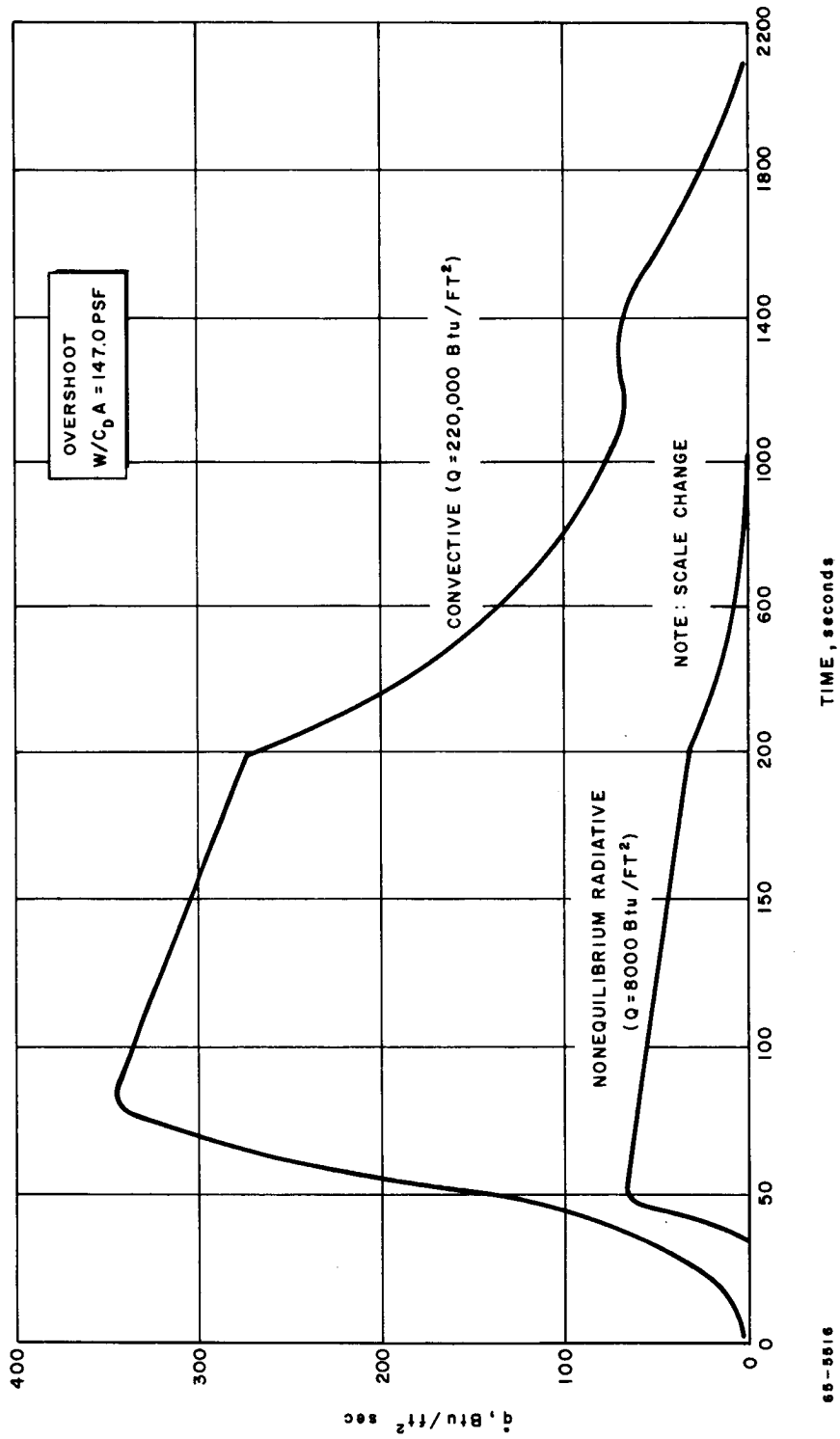


Figure 5 STAGNATION POINT HEAT TRANSFER ENTRY HISTORIES,  $V_e = 36,500 \text{ FT/SEC}$ ,  $L/D = 0.6$



65-5516

Figure 6 STAGNATION POINT HEAT TRANSFER TIME HISTORIES, REENTRY  
 $V_e = 36,500$  FT/SEC,  $L/D = 1.2$

As indicated previously and in appendix A, there exists an uncertainty as to the radiant heating expected for flight velocities over 40,000 ft/sec. Figure 7 indicates a generalization of this uncertainty for velocities up to 65,000 ft/sec. (Data used for this generalization are from references 1-8.) With only order-of-magnitude results being required for the purpose of outlining general radiation heating simulation requirements, the stagnation point heating history curve of figure 8 is felt to be an adequate guide. This curve is representative of the heating that can be expected to be associated with the earth reentry following a planetary or space probe type mission.

Recently a technique has been developed to provide estimates of continuum radiation from high temperature gases. This technique is based on spectroscopic analysis of arc-heated plasmas. The technique is described in detail in appendix B of this report, however, a comparison of estimates obtained from the experimental measurements of arc-heated gas is shown in figure 9. Utilizing data obtained by this technique, engineering estimates of radiant flux versus a spectrum of flight conditions are given in appendix B.

A generalized band, including the results of various investigators<sup>10-14</sup> of radiant heating for entry into planetary atmospheres of any combination mixture of carbon dioxide and nitrogen, is shown in figure 10. By selection of the appropriate flight conditions, this band will provide adequate order of magnitude results for entry into the atmospheres of Mars and Venus.

#### B. SPECTRAL DISTRIBUTION (AIR)

A literature search for the spectral radiance distribution for high-temperature air provided difficulties similar to those encountered when attempting to establish the magnitude of radiation-heating rates. The relatively current (in open literature) variation of spectral radiance of equilibrium air at 8,000°K for  $\lambda = 0.1 - 1.3$  microns is shown in figure 11. A generalization of the distribution for several temperatures for 1000-100,000 Å is shown in figure 12. For comparison purposes, a plot of normal shock nonequilibrium radiation for 9 percent CO<sub>2</sub>, 90 percent N<sub>2</sub>, and 1 percent A from reference 12 is shown in figure 13. Additional spectral radiance data for several gases are shown in the section on Spectral Radiance of Sources. Current theories<sup>15, 2</sup> have suggested that the integrated continuum spectrum of the vacuum UV-region is comparable in magnitude to those previously estimated for the near UV, visible and near IR-regions of the spectrum<sup>16, 17</sup>. A comparison of data obtained in the constricted arc for nitrogen with recent theories is shown in appendix B.

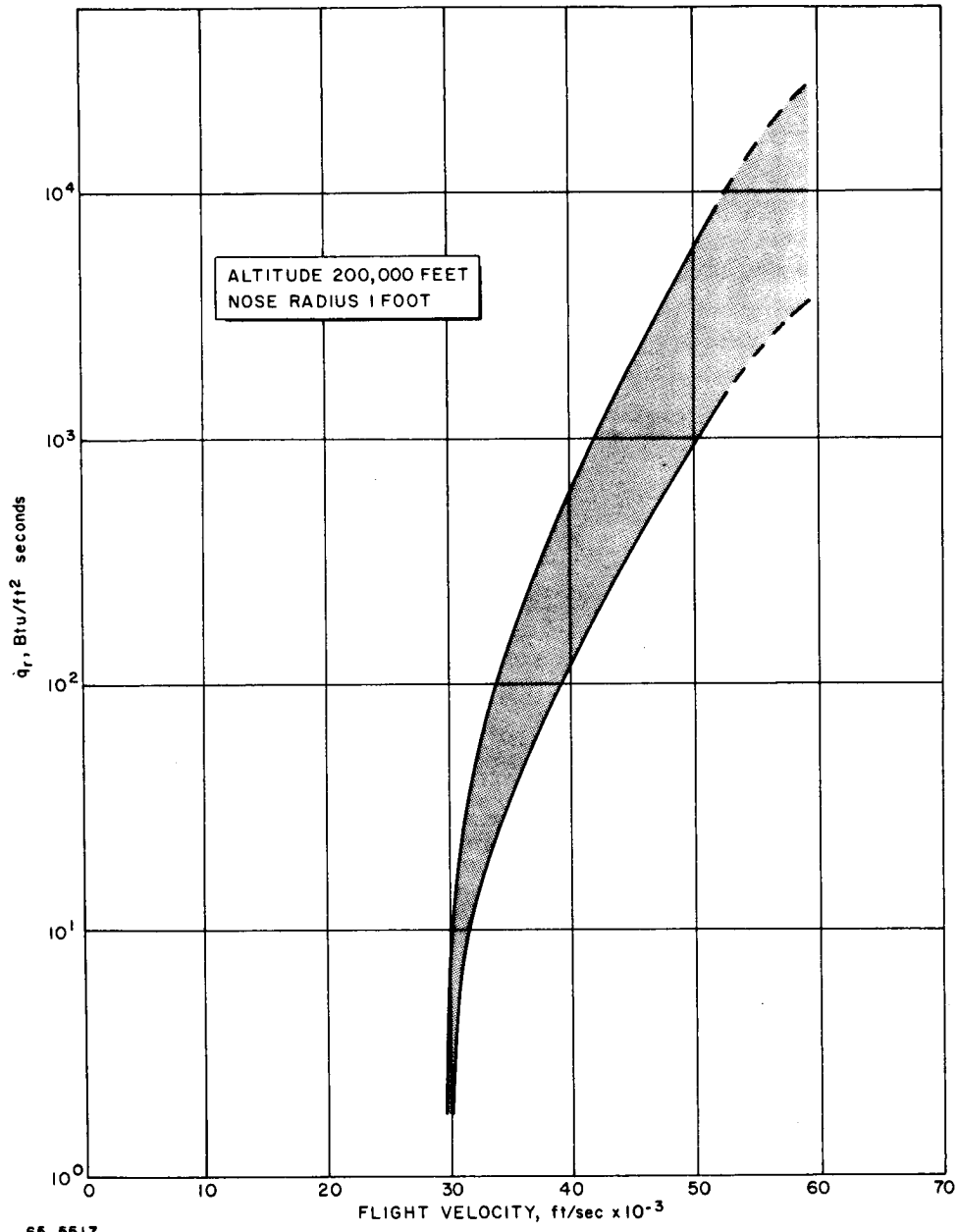
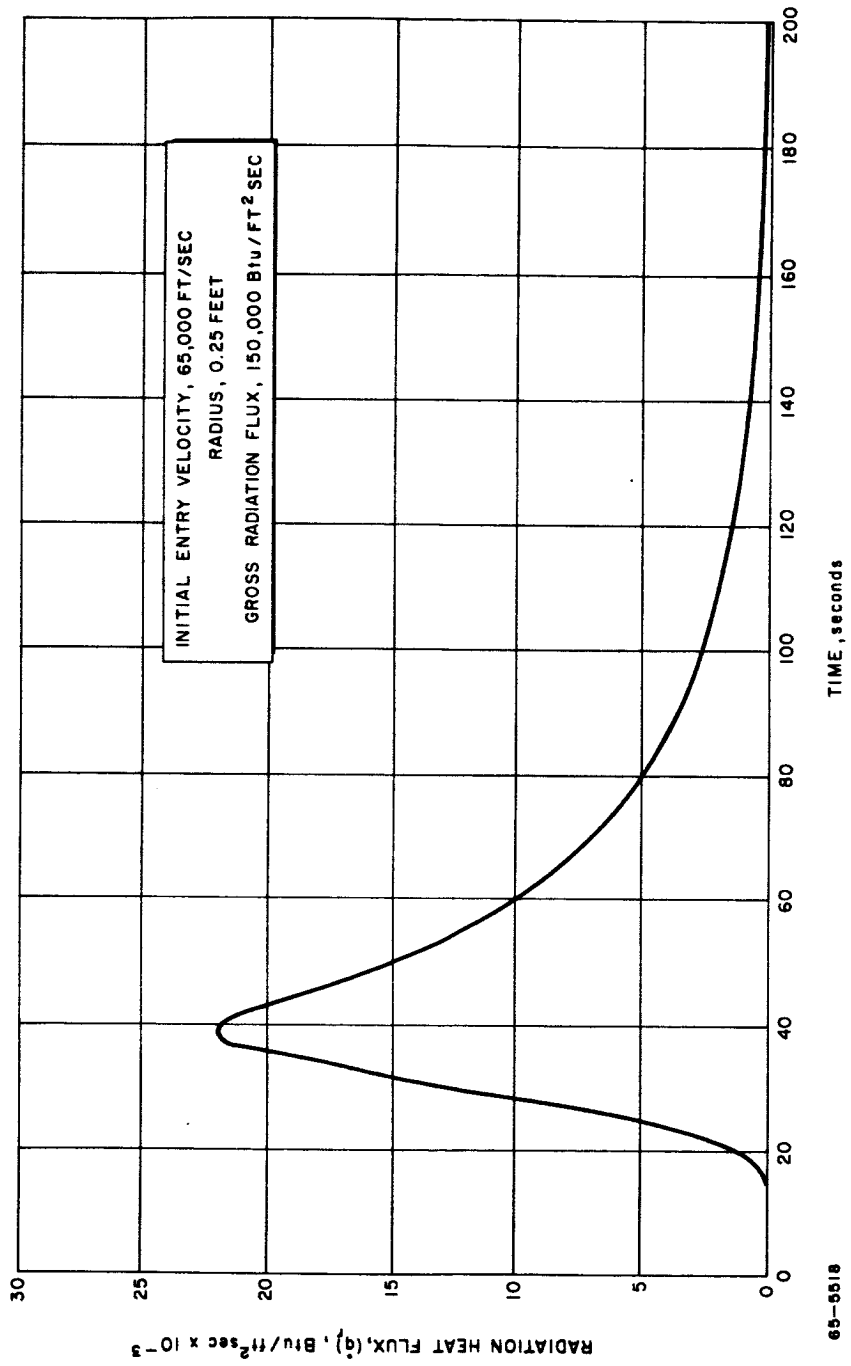


Figure 7 EQUILIBRIUM RADIATION DATA AND UNCERTAINTY BAND



65-5518

Figure 8 TYPICAL STAGNATION POINT RADIATION HEATING

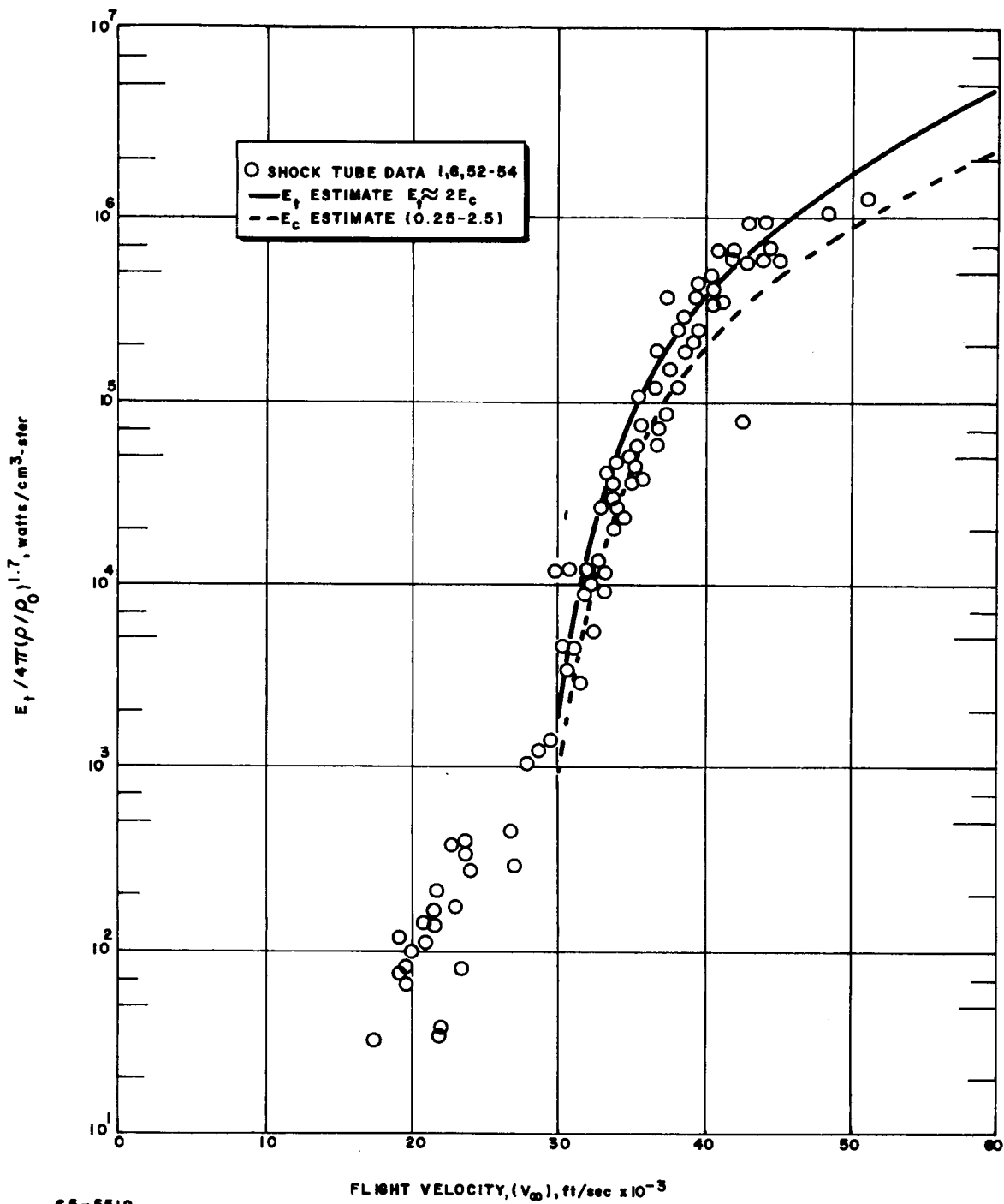
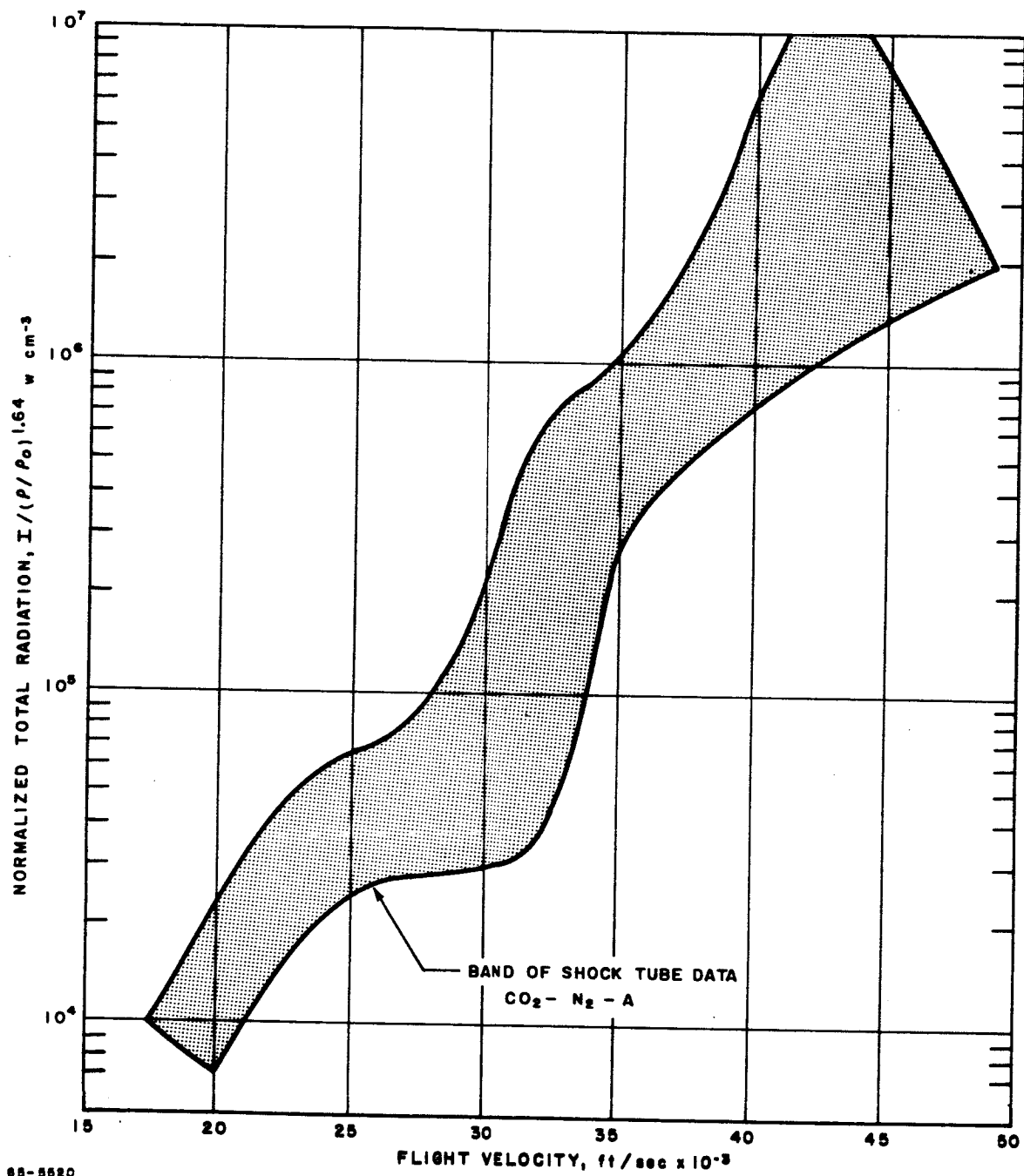
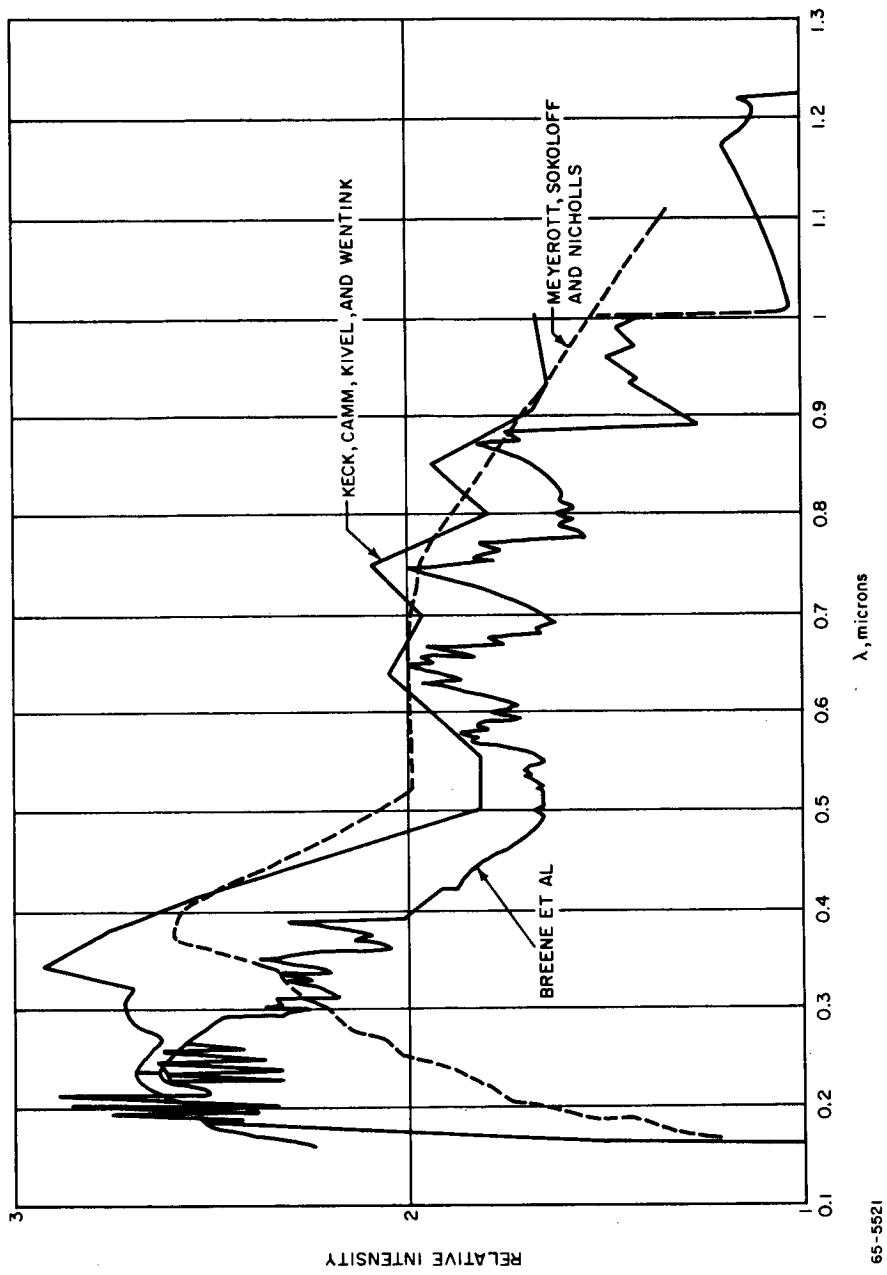


Figure 9 NORMALIZED EQUILIBRIUM RADIATION DATA OF AIR VERSUS TEMPERATURE (ARC-COLUMN DATA ESTIMATES VERSUS SHOCK-TUBE DATA)



68-5520

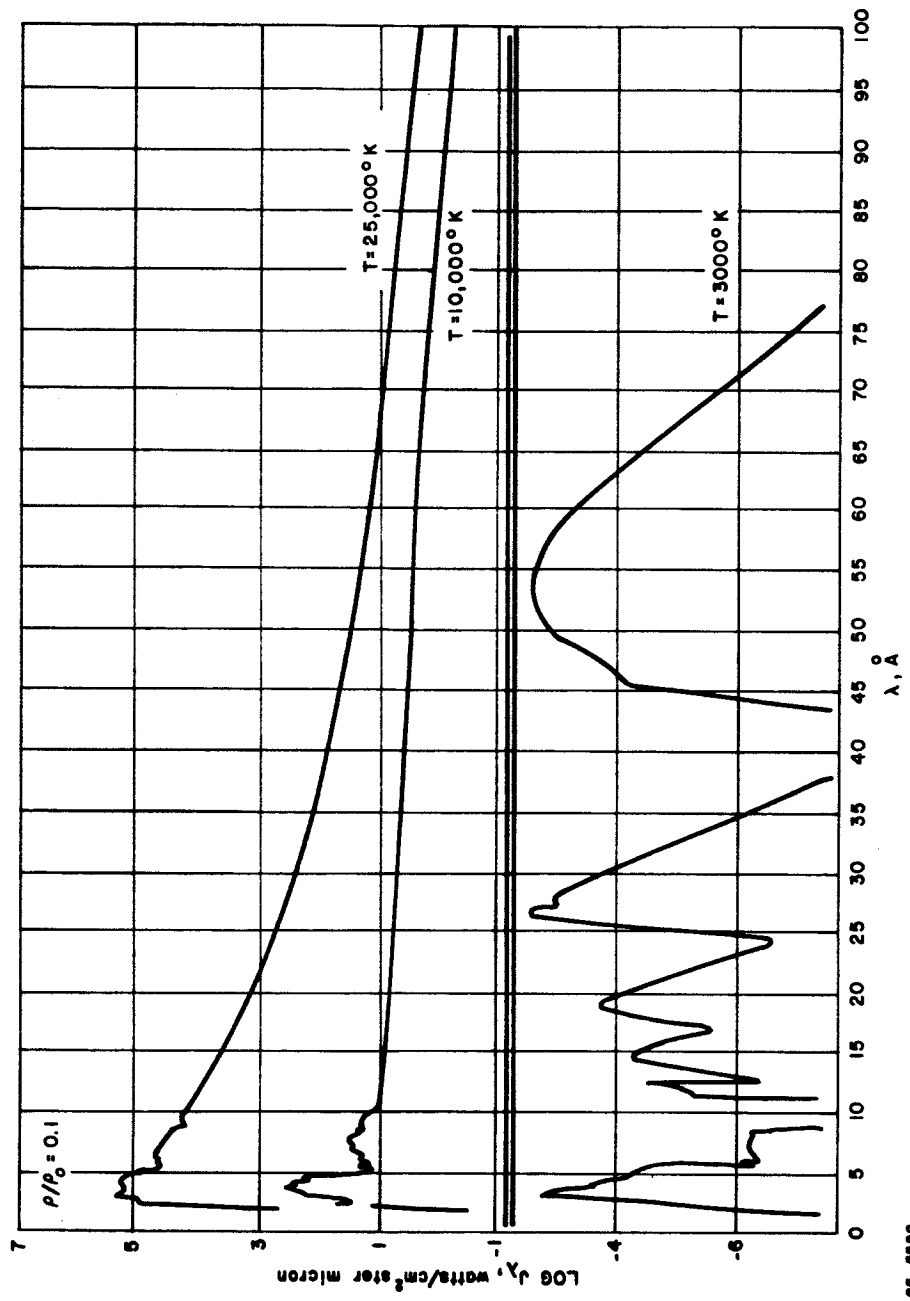
Figure 10 SUMMARY OF RADIANCE MEASUREMENTS FOR ALL CARBON DIOXIDE - NITROGEN MIXTURES



65-5521

Figure 11 COMPARISON OF PREDICTIONS: RADIANCE OF EQUILIBRIUM AIR  
 $T = 8000^{\circ}\text{K}$ ,  $p/p_0 = 1$





66-5822

Figure 12 SPECTRAL RADIANCE OF EQUILIBRIUM AIR (1000-100,000 $\text{\AA}$  AND  $L = 1 \text{ CM}$ )

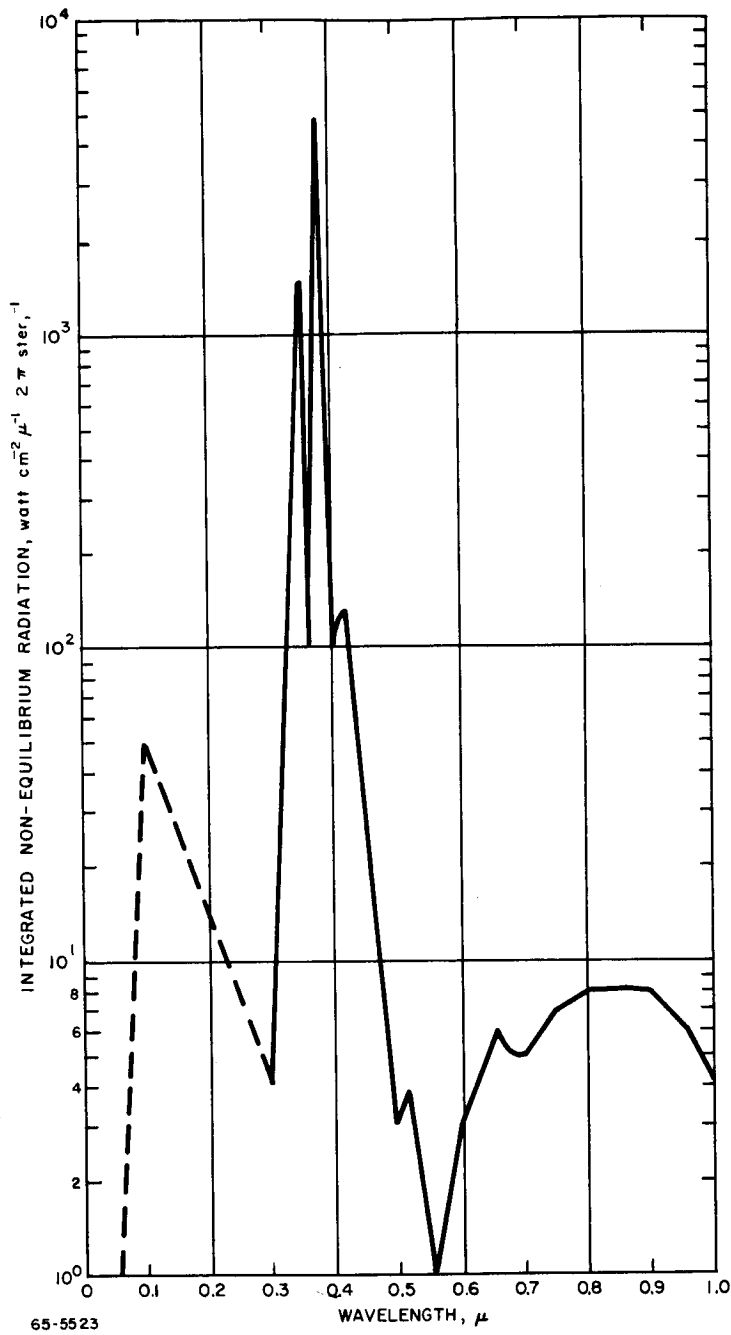


Figure 13 NORMAL SHOCK INTEGRATED NONEQUILIBRIUM RADIATION FOR  
9 PERCENT CO<sub>2</sub> - 90 PERCENT N<sub>2</sub> - 1 PERCENT A

#### IV. RELATIONSHIP OF FLIGHT PARAMETERS TO SIMULATION REQUIREMENTS

The spectral radiance of a gas significantly varies with composition, pressure, and temperature. Therefore, the spectral distribution of radiant energy from the gas cap as seen by the heat-shield material represents a rather complicated phenomenon. There are not only pressure, temperature, species, and composition variations and gradients, but also gas-phase and surface combustion, radiation absorption, blocking and reradiation<sup>8</sup>. Production of all of these parameters can only be accomplished in a flight test. However, experience has shown in other aspects of laboratory simulation that meaningful evaluations and engineering design data can be obtained from less than exact duplication of flight conditions. What now remains is the establishment of relative importance of the several factors mentioned, necessary model sizes, combined radiative and convective heating, and the effects on all of the factors resulting from parameter changes associated with the entry trajectory. As there are only several facilities capable of obtaining useful data in this field, there is very little actual data on which to base decisions. The more significant reports are those of Howe and Viegas<sup>8</sup>, Diaconis et al<sup>18</sup>, Lundell et al<sup>19</sup>, Howe<sup>20</sup>, Lundell et al<sup>21</sup>, Louis et al<sup>22</sup>, and various internal reports. While reports of the nature of the latter classification are not generally available, they can provide additional useful data. In this regard, references 23-25 have applicable data.

In spite of the availability of references, data in this field are sparse and inconclusive. One is not able at this time to specify which parameters in radiant heating simulation of entry conditions must be duplicated.

From data on the more simple heat-protection materials such as teflon, graphite, and phenolic nylon, it would appear that if the total net heat to the material surface occurs with a constant surface temperature, then the material performance is nearly constant regardless of the ratio of convective to radiative heating. This is confirmed in the data of Lundell et al<sup>21</sup>. It should be noted that considerable significance can be attached to duplication of the total net heating input and the maintenance of a surface temperature equivalent to that which would be associated with flight conditions. Constant gross heating with variations of the ratio of convective and radiative heating seem to produce significant changes in total net heating.

Source uniformity is another interesting parameter that appears to be greatly influenced by the material to be tested. Several investigators have noted that a source that is quite nonuniform, exhibiting a particular high brightness in the center, can be used to test materials that are char-forming without causing any apparent nonuniform heating. However, it has also been noted that such a source will directly reflect the source nonuniformities on materials such as teflon. Therefore, source uniformity must also be assessed according to the types of materials to be evaluated.

The importance of the length of a test has been a difficult parameter to assess even for straight convective heating. In convective heating this parameter is strongly dependent on the type of material being tested and the particular application of interest. After conferring with test engineers in several material test laboratories, a consensus was obtained that, in general, if a material was being subjected to convective heating fluxes of less than 100 BTU/ft<sup>2</sup> sec, it would require 10 minutes of test time for the material to arrive at a steady state. For fluxes of about 200 BTU/ft<sup>2</sup> sec, it would take on the order of 2 minutes. For fluxes greater than 500 BTU/ft<sup>2</sup> sec, it would take 30 seconds or less. All of the test engineers questioned, however, cautioned that these estimates may be only applied in general, and that they might not apply at all to a given particular type of material. For pure radiative or for a combined radiative and convective heating test, the general test time applicable for convective heating might have to be doubled or even quadrupled, due to the factors of surface reflectance or boundary layer blocking. It should be noted that in many ballistic vehicle applications, the heat-shield material does not reach a steady-state condition during the reentry. Under conditions such as this, one may not need to test until a steady-state condition is achieved. It therefore appears necessary that both the application and the particular material must be examined, and perhaps, some preliminary material tests will be required to establish this parameter.

Importance of a matched spectral distribution in a radiation simulator cannot be determined at the present time. Data in this area are extremely sketchy, and in one instance even contradictory. At low net flux levels, less than a few watts/cm<sup>2</sup>, it has been observed that certain organic materials may react differently chemically. A good example of this is the film coatings which produce different colors dependent on the spectral distribution of the incident radiation. It is also a well established fact that a material's emissivity is wavelength dependent. Though slight, this has some effect on reradiation and hence the net heat flux. In several cases similar heat-shield type materials have evidenced similar performance when tested with either a pure radiative heating flux, an argon arc lamp or a pure convective heating flux, from a typical arc plasma heater. Some data and analysis are cited in Appendix C to demonstrate this point.

Due to the paucity of specific materials test data in this particular field, appendix D has been prepared as a general discussion of governing parameters and effects of electromagnetic radiation on solids.

## V. SOURCE EVALUATION

### A. RADIATION SOURCES

The radiation heating source consists primarily of the radiant energy source and, in some instances, an optical system for the concentration, focussing, and modulation of the radiant energy.

#### 1. Solar Radiation

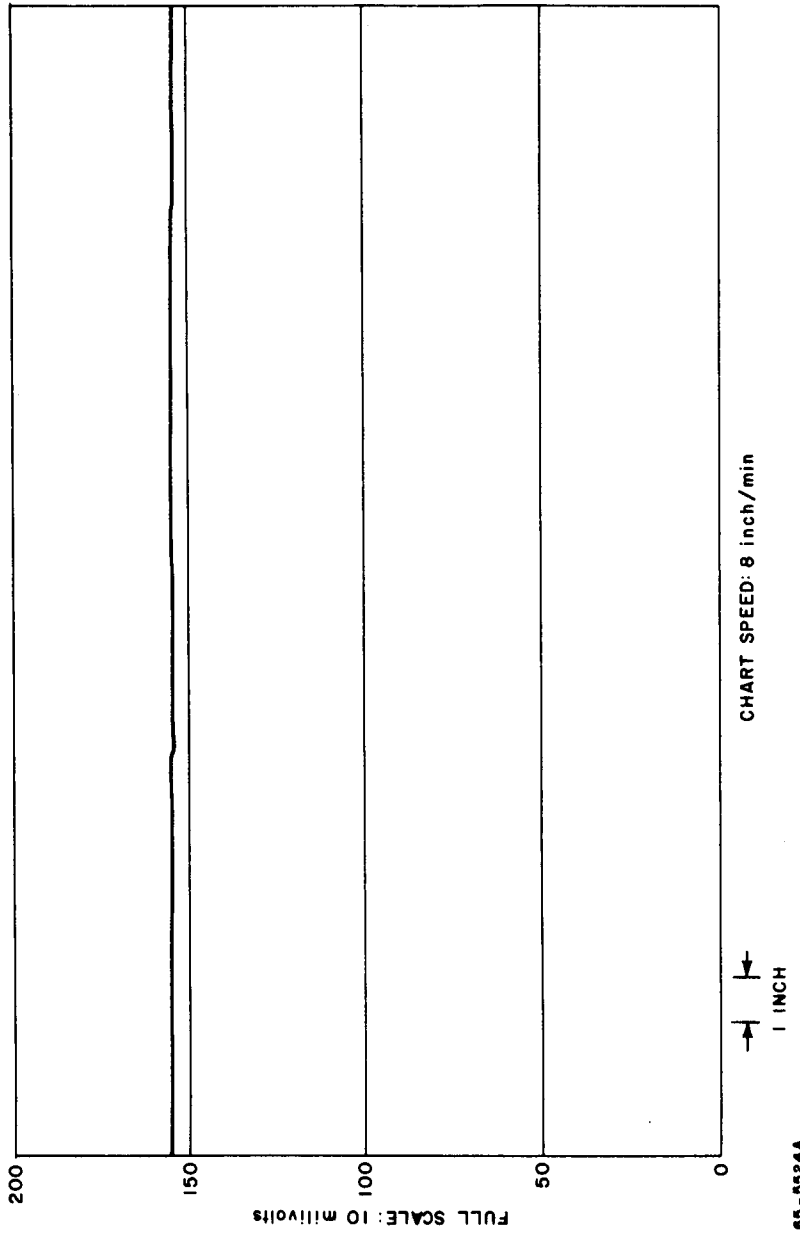
The oldest, and very likely the most spectacular, source for radiant energy is the sun.

Solar radiation is attractive because the source is freely available and the radiation arrives at the surface of the Earth with a sufficiently high intensity and in nearly parallel beams. The intensity of normal incidence solar radiation may be as high as  $1.5 \text{ cal/cm}^2\text{-min}$  at certain suitable sites. It is imperative to consider the normal incidence and not the total solar radiation, since only the well-collimated fraction of the solar radiation can be concentrated in solar furnaces. This is the reason why dry, desert areas with high yearly solar-irradiation values are not necessarily suitable sites for solar furnaces. The fine dust particles, which stay in the atmosphere above deserts for weeks after sand storms, disperse the solar radiation, causing a drop in the normal incidence value. In regions where good ground cover exists, (vegetation during summer, snow during winter) atmospheric dispersion is small.

The apparent surface temperature of the sun (approximately  $6000 \text{ }^\circ\text{K}$ ) is very difficult to equal with any other radiation source, as is the approximately blackbody distribution of solar radiation. A very important feature of solar radiation is its stability when the sky is clear. It has been reported<sup>26</sup>, that on a clear day the intensity of solar radiation was stable within 5 percent for six hours. Figure 14 is an actual recording illustrating the constancy of the concentrated flux.<sup>27</sup>

The size of the image can be increased, without decrease of the maximum flux, by increasing the aperture of the concentrator. This is an expensive method, but image diameters as large as 5 inches are available in some large solar furnaces. With other sources the image cannot be increased beyond the size of the source without a decrease in flux.

The prime disadvantage of solar radiation, other than the limitation of the maximum flux attainable, is that it is not always available when needed. (This source was used by several laboratories during the mid 1950's as a basic reentry heating simulator).



65-8524A

Figure 14 SOLAR FURNACE FLUX STABILITY TEST

## 2. The Carbon Arc

Perhaps the most widely used radiation source is the carbon arc. Its popularity is attributable to: a) The carbon arc is a familiar convenient laboratory source, ready for use whenever it is needed; b) carbon arc sources are cheaply available from surplus searchlights and cinema projectors. In some cases these arcs are used without modifications; in others, changes in the mechanism are made to better suit the requirements. Typical carbon arc is operated at a current of 150 amperes using a 16-mm anode. With special arrangements the current can be much higher, 300 amperes in the blown arc,<sup>28</sup> and 3000 amperes when the entire mechanism is kept at 10 atmospheres pressure,<sup>29</sup> In one controlled atmosphere carbon arc image furnace, both the source and concentrator mirrors were enclosed in a nine-foot diameter sphere.<sup>30</sup> The sphere could be evacuated or pressurized up to 60 psi. The carbon arc was enclosed in a container which could be pressurized up to 210 psi. It was expected that with such a "concentrated" arc source, such high flux could be radiated that would produce temperatures of 6000° to 10,000°K at the receiver mirror focus. No information on achieving this goal is available. Some systems operate at 2100 amperes without pressure.<sup>31</sup> A correlation between the arc current and flux at the focal area is given<sup>32</sup> for various electrodes in table 1.

A high-pressure arc has been operated with tungsten electrodes in a closed argon atmosphere system.<sup>33</sup> The chamber gas is provided from a liquid argon supply. The arc has been operated up to a pressure of three atmospheres absolute, but could go higher. The maximum current for prolonged lengths of time (several minutes) was over 3000 amperes with 60 volts across the arc. The numerical value of the flux density at the second focus is not available.

The convenience of the carbon arc has to be balanced against its two disadvantages. First, the flux stability is rather poor. The flux at the focal area of a commercial carbon arc image furnace was measured using a Gardon type radiometer, and the result of this measurement is presented in figure 15, (1). Similar measurements were performed on an improved<sup>34</sup> version of this furnace, and the results are presented in figure 16. These results show that there are two major flux instabilities in carbon arc image furnaces. The high-frequency variations are caused by variations in electrode resistance, changes in electrode type configuration, and variations in the solid particle content of the arc gap. The low-frequency variations are caused mainly by changes in the electrode gap, unavoidable even with automatic feed mechanisms. The time/flux variations may be tolerated in certain experiments, when only the average flux is significant. In other cases, these variations may introduce very significant errors.

TABLE I

OPERATING AND PERFORMANCE DATA FOR CARBON ARC DOUBLE ELLIPTICAL MIRROR IMAGE FURNACES

Lamp	Rotating Carbon Reflector Lamp	Gretener Super Venlarc Lamp
Mirror Diameter - inches	18	24
Mirror to crater distance - inches	6.5	7.5
Mirror to mirror distance - inches	70 3/16	96
Nominal magnification at intermediate focus	5.6X	6.5X
POSITIVE CARBON		
Type	High intensity	Modified "Ultrex"
Diameter - mm	11	11
NEGATIVE CARBON		
Type	Rod	Disk
Diameter - mm	8	270
Arc current - amperes	125	140
Arc voltage - dc volts	72-77	70
Arc power - kw	9.3	9.8
Positive consumption-inches/hour	25	50
Positive crater diameter - mm	10.6	9.3
Positive crater depth - mm	8.4	6.1
Center of crater brightness <sup>b</sup>	980	1050
Center of disk <sup>k</sup> brightness <sup>b</sup>	406	465
Brightness ratio-disk to crater	0.42	0.44
Diam. on image for 1/2 peak brightness - mm	8.0	9.0
Max irradiance on image - watts/mm <sup>2</sup>	8.4	11.4
Diam. on image for 1/2-peak irradiance - mm	9.0	10.2
Blackbody temperature equivalent to maximum irradiance - OK	3510	3770
		4000
		4050

a Brightness of a water-cooled surface of MgO at the image position-candles per mm<sup>2</sup>.

b Brightness measured in direction axial to the source.



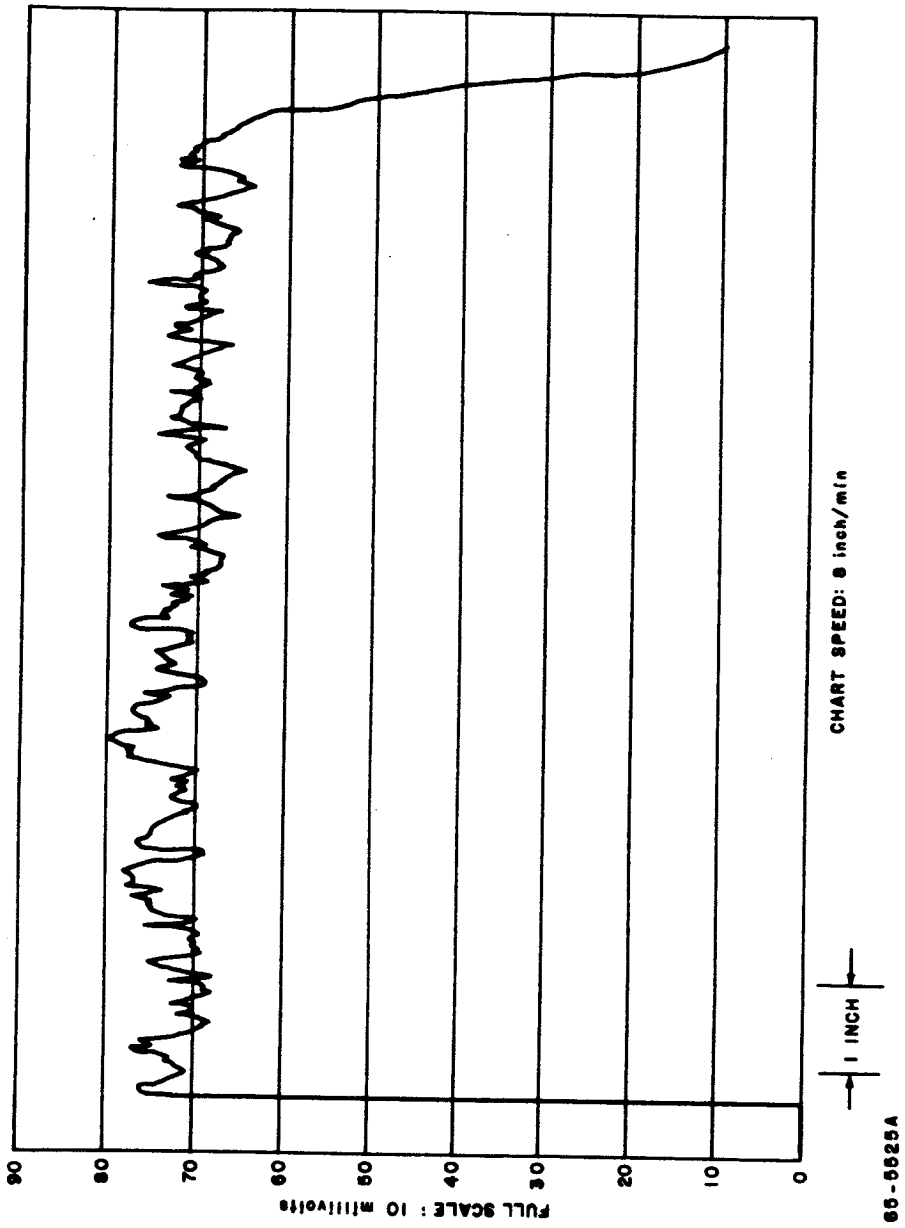
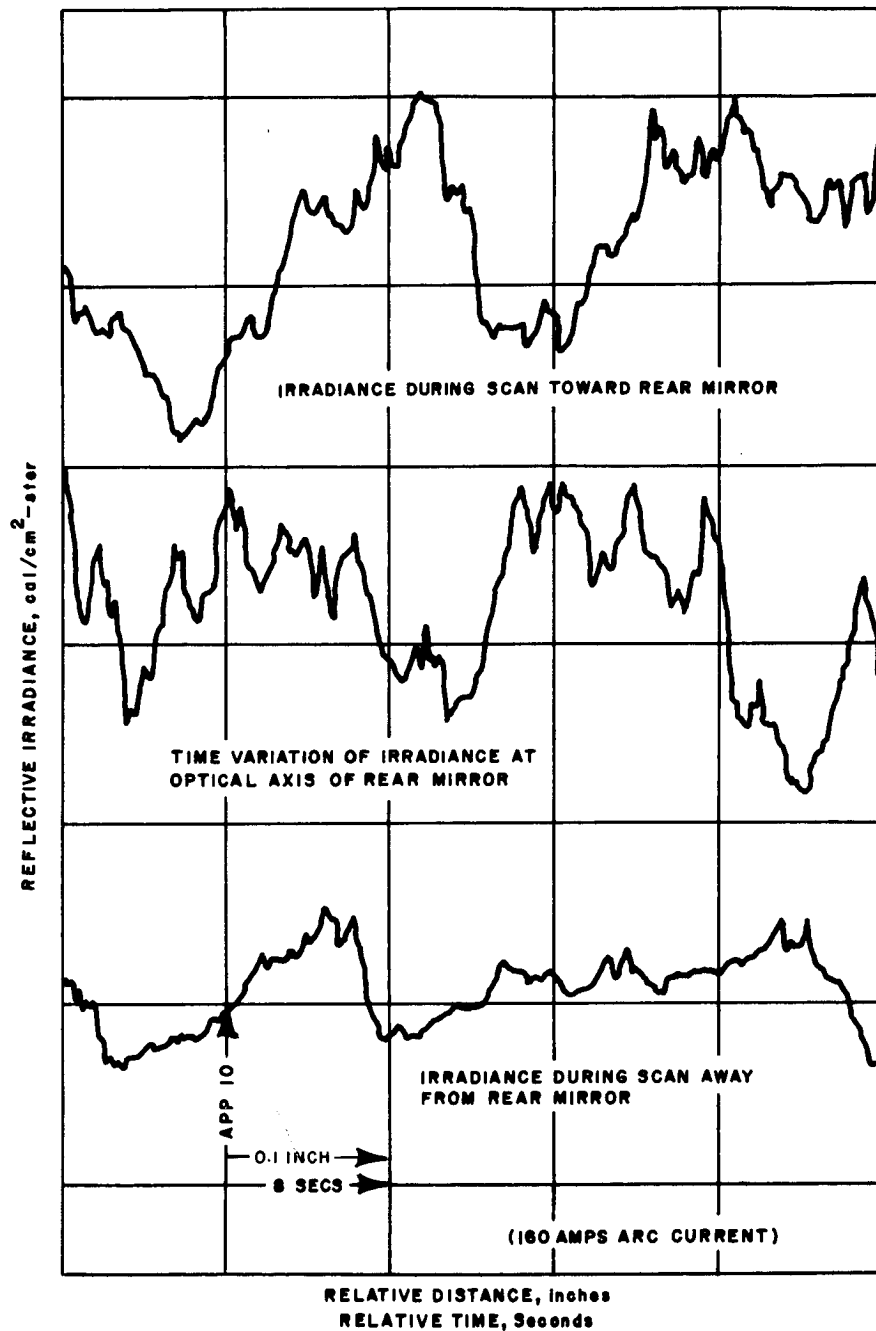


Figure 15 ARC-IMAGE FURNACE FLUX STABILITY TEST



65-5526

Figure 16 ARC-IMAGE FURNACE FLUX VARIATION

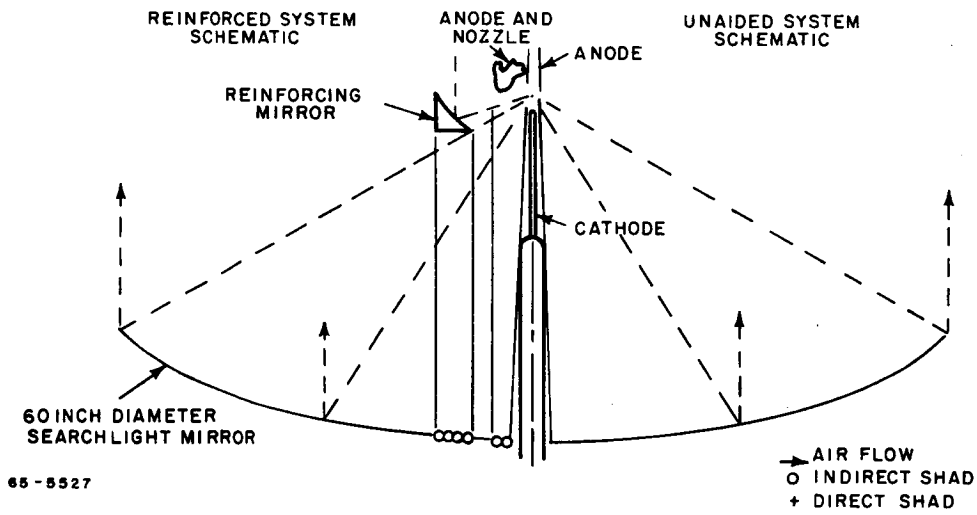
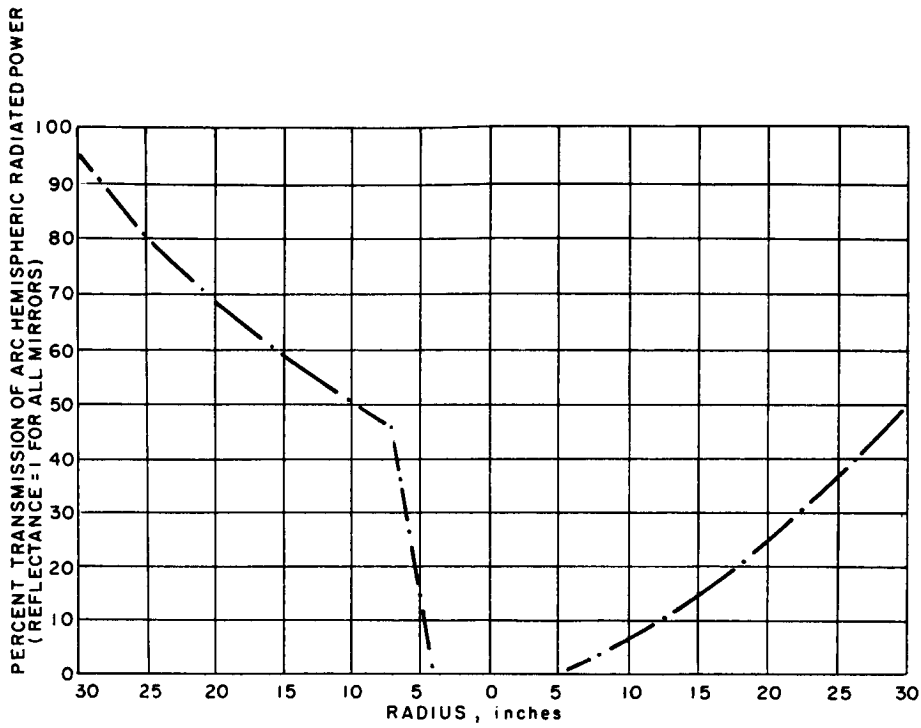
Secondly, the continuous operating time of the carbon arc is limited by the length of the electrodes. At low-current values one electrode lasts approximately 20 minutes, but at higher values only 5 minutes. Recently a new carbon arc has become available which can operate 24 hours without interruption.<sup>35</sup> The carbons, stored in metal cases, are machined at both ends to male-female tapers respectively. The female tapered end of the new carbon is driven by a spring-laden piston toward the male tapered end of the burning carbon. The passage of the joint into the arc is claimed to hardly affect the flux continuity. A second method to overcome this time restriction is the alternate use of two carbon arcs in order to make extended runs possible. The mechanism for switching from one source to the other has to operate very rapidly in order to avoid a harmful temperature drop of the heated specimen. A third disadvantage is that the carbon arc has to be placed at the first focus of the image. Consequently the two electrodes and the related equipment intercept a significant portion of the radiation emitted by the anode. In order to reduce this loss, the use of an auxiliary mirror has been proposed.<sup>31</sup> As illustrated in figure 17, this reinforcing mirror replaces that portion of the image furnace paraboloid which is shaded by the cathode. Although the reinforcing mirror increases the shadow area, the increase in radiation intensity level is claimed to more than offset the increase in shading loss.

A different type of carbon arc, called "carbon vapor lamp" completely eliminates the shadow loss.<sup>36</sup> This source uses three electrodes arranged radially and is supplied with three-phase ac current (figure 18). The arc operates in vacuum, thus reducing electrode consumption caused by oxidation. It is estimated that 8-inch long electrodes would last 8 hours, a significant value for continuous operation.

### 3. Electrical Resistors

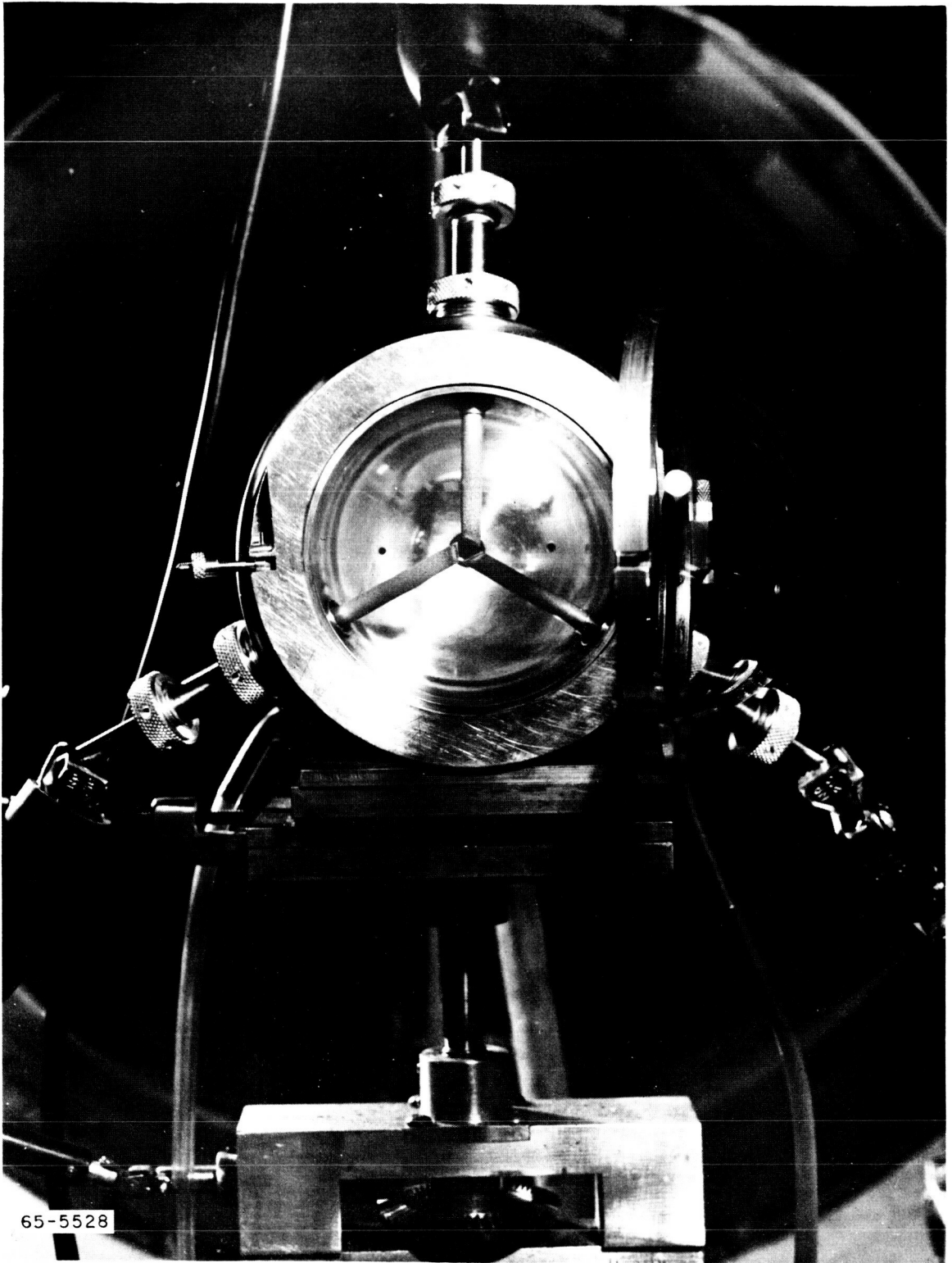
A high-refractory electrical resistor of suitable shape and dimensions can serve as a simple, convenient source. Flux stability is usually excellent, continuous operation for long periods is possible, and flux control is easily achieved at the source.

For low intensity, a resistance-heated tungsten filament projection lamp, G. E. type 2100 T24/8, can be used as a source of radiation. It is rated at 2100 watts when operated at 60 volts; under these conditions the life is 50 hours. As the operating voltage is raised, the expected life of the filament decreases, reaching 10 hours at about 68 volts. The filament consists of 8 parallel coils arranged in two planes. The filament coil assembly is nearly square (~1.2 cm on a side). As a result of use, a dark deposit develops on the inner surface of the glass envelope due to evaporation of tungsten from the filament. This deposit may be removed when necessary by agitating a small quantity of abrasive powder sealed within the bulb.



65-5527

Figure 17 REINFORCING MIRROR AROUND ANODE



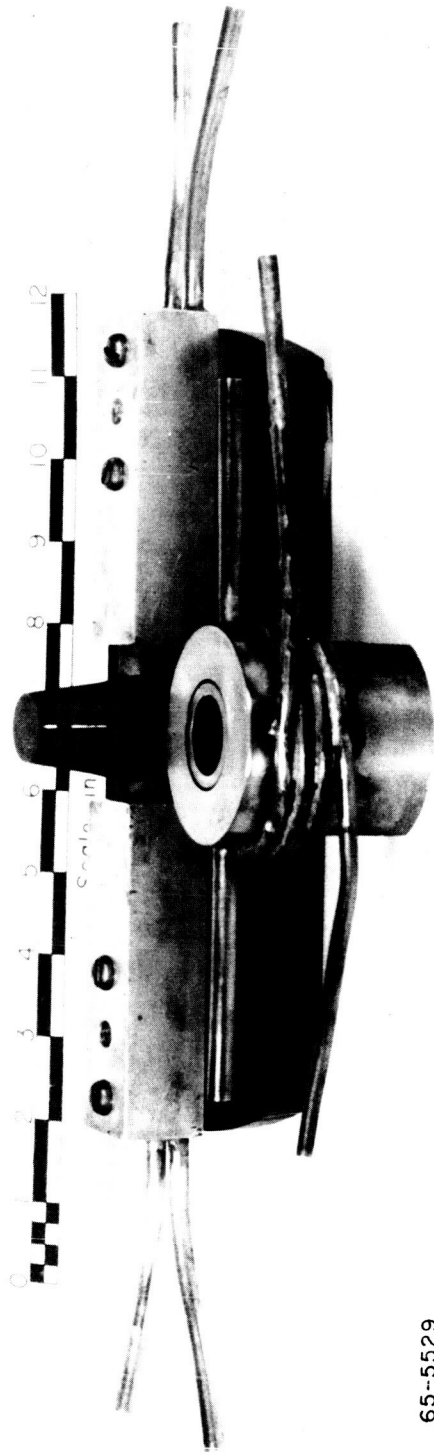
65-5528

Figure 18 CARBON VAPOR LAMP

A 5-kw projection lamp, when placed at the near focus of a 24-inch ellipsoidal mirror, delivered at the far focus approximately  $2 \text{ cal/cm}^2\text{sec}$ .<sup>37</sup> Because of the large size of the filament array, the image is quite diffuse and nonsymmetrical.

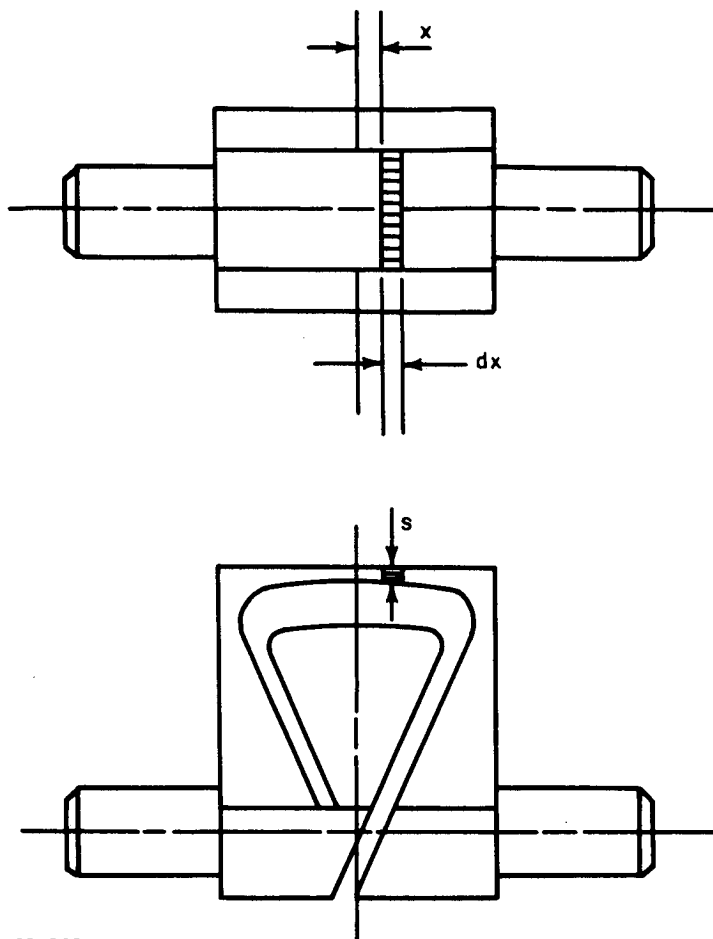
Graphite resistors can be used for obtaining somewhat higher heat fluxes. These radiators are usually designed and fabricated by the experimenter to suit special requirements. When operated under inert gas protection they last long and deliver a very stable flux. A carbon resistor has been designed in such fashion that by using an inert gas it does not require a window.<sup>38</sup> Thus, no solid material of any kind is interposed between the source and the optics that may be required. The resistor mounting is designed so that the face of the resistor disk is the only hot part of the source that can radiate to the optics; the remainder of the resistor is totally enclosed by a water-cooled copper jacket. In addition to confining the effective source to a disk, this jacket makes possible the maintenance of an inert-gas atmosphere around all the hot parts of the resistor by means of a flow of gas through the jacket. The arrangement is such that the gas enters through an opening in the mounting board behind the resistor and exits through a very narrow annular space between the disk and the jacket. The exit gas flow is at high velocity and is directed in such a manner that it converges to a point about 1 inch in front of the disk, thereby forming a protective cone of inert gas. A second gas channel is built into the jacket and is so designed that another slightly larger cone of gas is formed surrounding the first. The two directed gas flows result in a complete gas envelope around the face of the resistor without any physical confinement of the gas and hence without any significant absorption losses. At first, helium was used for both the inner and outer cones, but convection currents led to incomplete cone formation. Since then, argon has been used for the outer cone and helium for the inner cone with entirely satisfactory results. Apparently the heavier argon tends to contain the helium, and convective disruption of the gas flow is prevented. A photograph of the resistor source with the jacket removed is presented in figure 19. (The final vertical cut, which divides the base of the graphite into two sections, has not been made. Due to the fragility introduced by this cut, it normally is not made until the source is to be put into operation.) The success of this design may be judged from the fact that the resistor has been operated continuously for periods exceeding 4 hours at temperatures above  $2,000^\circ\text{C}$  with no visible signs of oxidation. This resistor can be used to sample temperatures up to  $2,200^\circ\text{C}$ .

Another carbon resistor operates in a dry argon atmosphere at 20 psig.<sup>39</sup> The pressure is maintained by the use of a Pyrex hemisphere, and the power leads are water-cooled (figure 20). The resistor is operated at a maximum temperature of  $2840^\circ\text{K}$ , resulting in a flux of  $15 \text{ cal/cm}^2\text{sec}$  at the image. No provision is made for the removal of carbon vapor deposit which might be deposited on the inside wall of the hemisphere.



65-5529

Figure 19 CONICAL CARBON RESISTOR



65-5530

Figure 20 CARBON RADIATION SOURCE ELEMENT

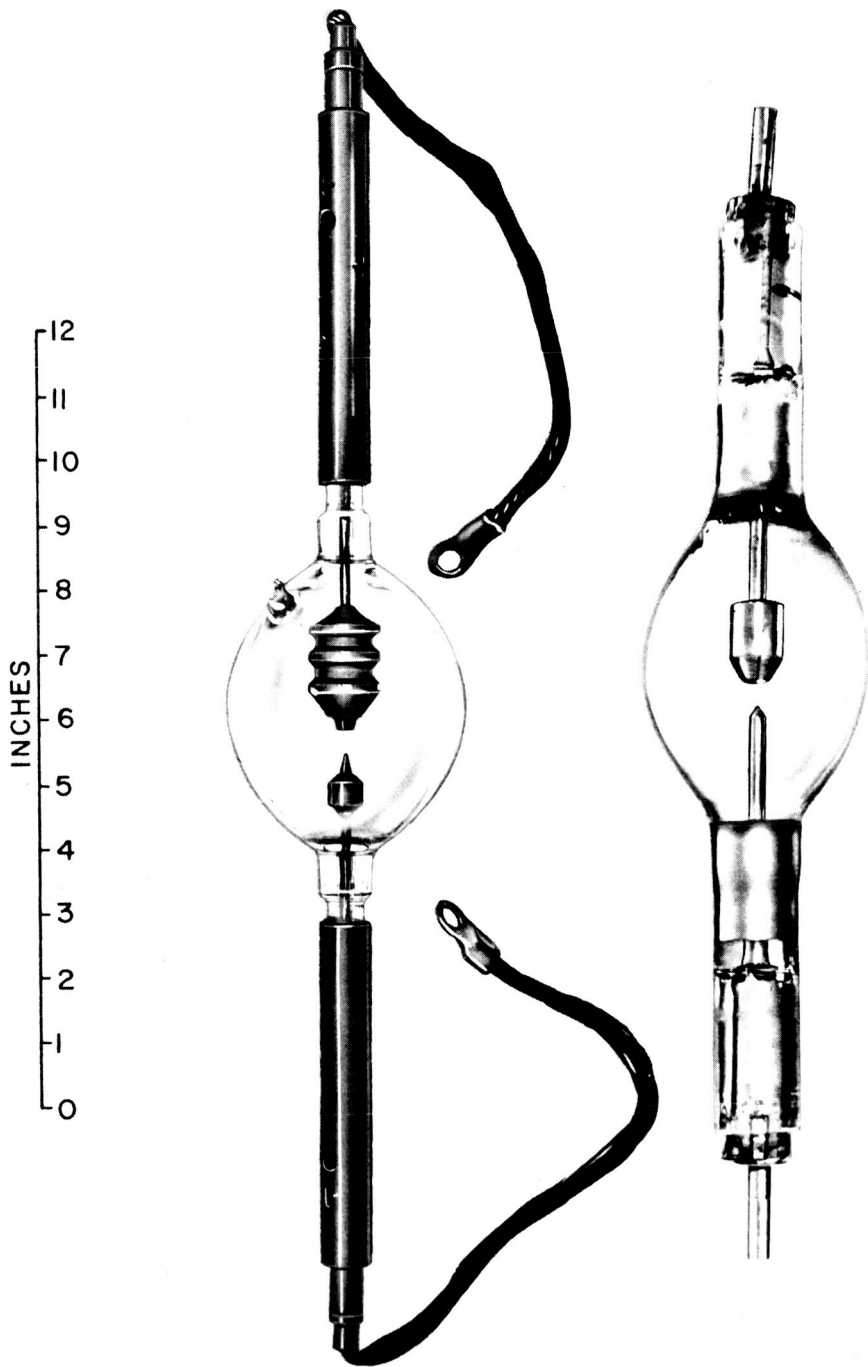


#### 4. High Pressure Compact Arcs

These sources combine the brightness of carbon arcs with the maintenance-free and clean operation of incandescent lamps.<sup>40</sup> They consist of a spherical- or ellipsoid-shape envelope, usually made of clear fused silica. Two diametrically opposed cylindrical extensions contain the hermetic seals, the metallic support, and connecting rods for the two electrodes, and carry the outer electrical contacts. The electrodes are made of solid tungsten and the bulbs are usually filled with xenon (figure 21). In operation, the pressure within the lamp is between 6-30 atmospheres. Due to the high pressure, the arc discharge fills only a small volume directly between the tips of the electrodes and thus forms a highly concentrated source. Operation and the performance data of various lamps are summarized in tables II. A and II. B.<sup>40</sup> Lamps operated with ac give a more uniform brightness distribution than dc lamps. The stability of operation may be affected by the position of the lamp. Xenon dc-arcs burn stably only when the cathode is at the bottom and the anode at the top. An image furnace using a 10-kw xenon arc as a source has been completed recently.<sup>41</sup> It is expected that the lamp will radiate approximately 5.5 kw.

While long, continuous operation is a great advantage of high pressure compact arcs, there are also serious disadvantages. The flux distribution is far from uniform. For example, a 5-kw xenon bulb with a 7-mm electrode gap has a relative brightness which decreases from a maximum of 5000 units at the cathode, to 3000 one millimeter away, to 1500 at two millimeters, and to 300 at the anode. The second disadvantage is that the radiation is emitted on the entire circumference of the envelope, while usually only a narrow beam is utilized. If a reflector is used at the back of the lamp, the reflected radiation passes twice through the fused silica envelope; the absorption losses are increased, the lamp heats up more, and its life decreases.

A design to overcome these disadvantages has been developed recently.<sup>42</sup> The fused silica envelope is replaced by a solid metal block with a cavity of suitable dimensions and highly polished walls. The two electrodes are mounted into the metal block, one directly, the other through an insulator. Thus the arc is formed in the cavity. The radiation undergoes multiple reflections at the wall and, as a consequence, is fairly uniform. This uniform, diffuse radiation, together with the direct radiation from the electrodes, leaves the cavity through a fused silica window. The window can be of any optical shape, thus making it possible to obtain a collimated, convergent or divergent beam. The metal block can be artificially cooled, thus cooling the electrodes as well. This should result in longer electrode life and a more constant flux. The silica window is mounted with gaskets, eliminating the need for a metal-fused silica seal. When the window darkens due to tungsten deposit, it can be easily removed, cleaned, or replaced.



65-5824

Figure 21 HIGH PRESSURE COMPACT ARCS

TABLE II-A

MAIN DATA OF HIGH WATTAGE XENON, MERCURY, AND MERCURY-XENON COMPACT ARC LAMPS\*

No.	Lamp Wattage watts	Type Designation	Gas/Vapor Filling	Max. Bulb Outer Diameter mm	Max. Over-all Length ins.	Arc Length in Operation mm	Internal Operating Pressure atm.	Lamp Operating Voltage volts	Lamp Operating Current
1.	800 AC	SAH800C <sup>a</sup>	Hg	42	9 1/2	8.5	10	70	12
2.	900 DC	XB0900W <sup>b</sup>	Xenon	40	12 13/16	3.4		22	42
3.	1,000 DC	528BC	Hg-Xenon	45	7	6.5		65	16
4.	1,000 AC	SAH1,000A <sup>a</sup>	Hg	51	9 1/2	6.5	25	65	18
5.	1,000 AC	SAHX1,000A <sup>a</sup>	Hg-Xenon	51	9 1/2	6.5	30	65	18
6.	1,600 DC	XB01,600W <sup>b</sup>	Xenon	52	14 9/16	4.2		26	63
7.	2,000 DC	UXL2,000DK <sup>d</sup>	Xenon	53	14 3/16	6		28	70
8.	2,000 DC	XE2,000E	Xenon	54	14 13/16	3.5		22.3	90
9.	2,200 DC	491CC	Xenon	57	12 1/2	4	16	20-23	100
10.	2,500 DC	929BC	Hg-Xenon	64	12 1/2	4	18	45-55	50
11.	2,500 AC	SAH2,500A <sup>a</sup>	Hg	70	13	10	15	65	45
12.	2,500 AC	SAHX2,500A <sup>a</sup>	Hg-Xenon	70	13	10	20	65	45
13.	2,500 DC	SAHX2,500B <sup>a</sup>	Hg-Xenon	70	13	4.5	30	50	50
14.	2,500 DC	XB02,500W <sup>b</sup>	Xenon	57	16 7/8	6.2		30.1	83
15.	4,000 DC	UXL4,000DK <sup>d</sup>	Xenon	86	15 3/4	7		33	120
16.	5,000 DC <sup>4</sup>	932BC	Hg-Xenon	86	13 1/2	5	15	30-60	100
17.	5,000 DC	X35,000E	Xenon	89	19 1/2	7		34.5	145
18.	10,000 DC	XE10,000F	Xenon	92	27 1/2	8	10	40	250
19.	20,000 DC <sup>4</sup>	XE20,000F	Xenon	120	33 1/2	13.5	6	50	400

- a. Westinghouse, USA  
 b. Oeram, West Germany  
 c. Hasovia, USA  
 d. Ushie Kegyo Katsha, Japan  
 e. General Electric, USA  
 f. Daro-Tem, USA
1. In vertical position 8 hours per start  
 2. 12 hours per start  
 3. Preliminary data  
 4. Experimental lamp

TABLE II-B

MAIN DATA OF HIGH WATTAGE XENON, MERCURY, AND MERCURY-XENON COMPACT ARC LAMPS\*

No.	Lamp Wattage watts	Type Designation	Gas/Vapor Filling	Brightness Data - cd/mm <sup>2</sup>		Initial Lumens	Initial Efficiency Lumens/Watt	Rated Life Hours
				Peak	Average for Arc Area of Width & Length mm			
1.	800 AC	SAH800C <sup>a</sup>	Hg	180	380	40,000	50	600
2.	900 DC	XB0900Wb	Xenon			30,500	34	2,000
3.	1,000 DC	528Bc	Hg-Xenon	970	230	52,000	52	1,000 <sup>2</sup>
4.	1,000 AC	SAH1,000Aa	Hg	475		50,000	50	300 <sup>1</sup>
5.	1,000 AC	SAHX1,000Aa	Hg-Xenon	475		50,000	50	400 <sup>1</sup>
6.	1,500 DC	XB01,600Wb	Xenon		430	56,000	35	2,000
7.	2,000 DC	UXL2,000DKd	Xenon		550	70,000	35	
8.	2,000 DC	XE2,000e	Xenon	4,100	820	85,000	42.5	500 <sup>3</sup>
9.	2,200 DC	491CC	Xenon	3,300	440	75,000	34	1,000 <sup>2</sup>
10.	2,500 DC	929Bc	Hg-Xenon	2,050	540	120,000	48	1,000 <sup>2</sup>
11.	2,500 AC	SAH2,500Aa	Hg	325		125,000	50	400 <sup>1</sup>
12.	2,500 AC	SAHX2,500Aa	Hg-Xenon	325		125,000	50	200 <sup>1</sup>
13.	2,500 DC	SAHX2,500Ba	Hg-Xenon	2,050		120,000	48	400 <sup>1</sup>
14.	2,500 DC	XB02,500Wb	Xenon		450	100,000	40	1,500
15.	4,000 DC	UXL4,000DKd	Xenon		600	120,000	30	
16.	5,000 DC <sup>4</sup>	932Bc	Hg-Xenon	2,250	780	230,000	46	
17.	5,000 DC	X35,000e	Xenon	5,900	870	275,000	55	500 <sup>3</sup>
18.	10,000DC	XE10,000f	Xenon	9,500	1,250	480,000	48	500 <sup>3</sup>
19.	20,000 DC <sup>4</sup>	XE20,000f	Xenon	7,500	1,700	1,000,000	50	

a. Westinghouse, USA

b. Oeram, West Germany

c. Hasovia, USA

d. Ushie Kegyo Katsha, Japan

e. General Electric, USA

f. Daro-Tem, USA

1. In vertical position 8 hours per start

2. 12 hours per start

3. Preliminary data

4. Experimental lamp

A 500-watt model of this lamp has been operated successfully, thus proving the feasibility of the design.

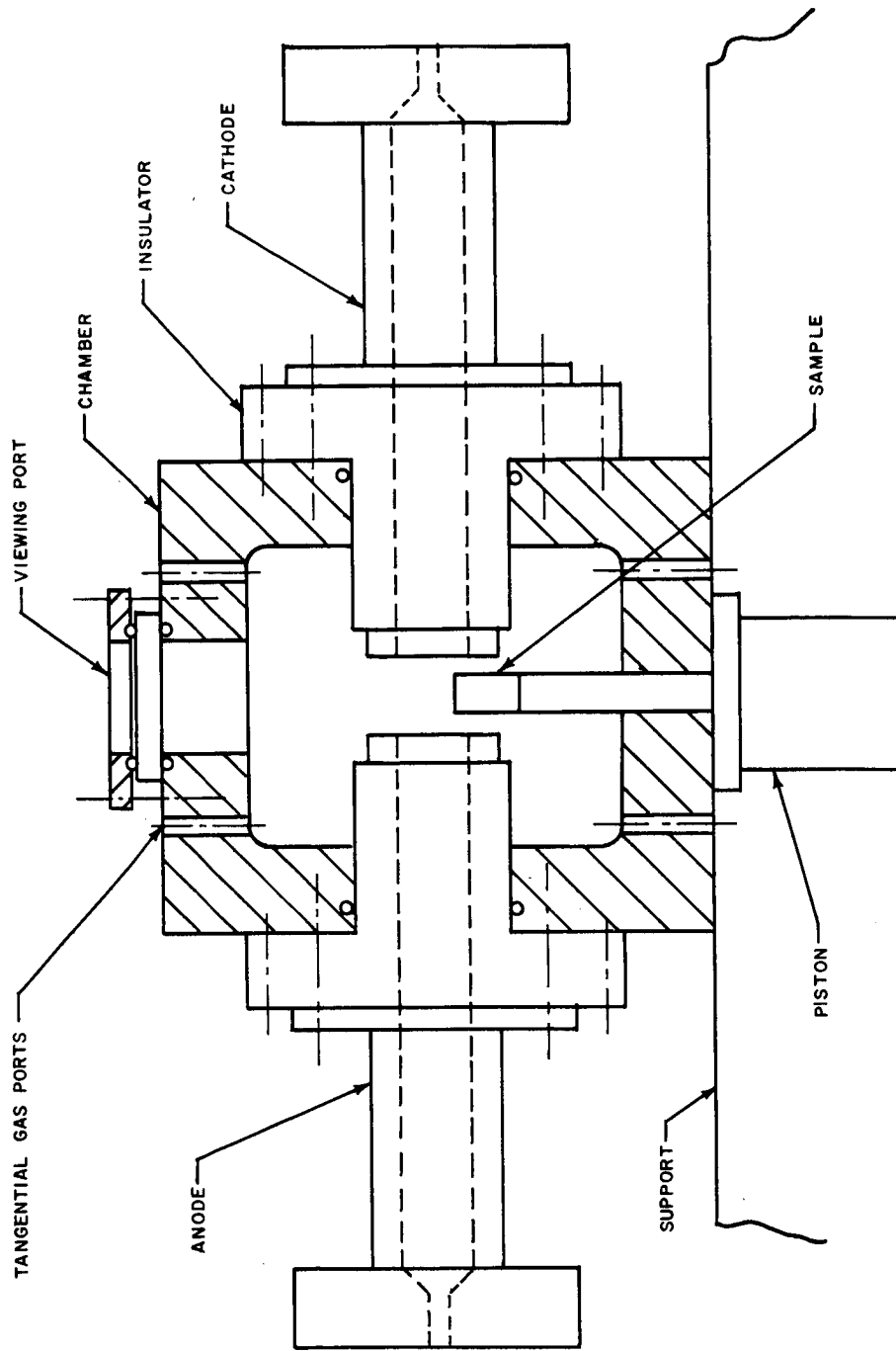
## 5. Plasma Generator

Recently, a concentrated effort has been applied to the study of the plasma arc heater as a possible radiant energy source.<sup>43-46</sup> The plasma arc heater is able to maintain an arc discharge with maximum temperature in excess of 20,000 °K on a continuous time basis. The continuum radiation from such an arc column may be a few watts/cm to several tens of kilowatts/cm depending on the arc current, voltage gradient, pressure level, and type of working fluid. This device has been utilized to provide a radiant and convective heating source for material specimens placed in the area vicinity of the arc column.<sup>44</sup> This type of source is also being developed for the single application of a radiating source.<sup>43, 45, 46</sup> In the latter case, models are placed in the proximity of the column to be irradiated directly (figure 22). Others are being developed with radiation-collecting optics to increase the flux level at the target or model and to permit greater flexibility of model size, shape and placement. Such a device is shown in figure 23.

Based on some experimental results with a plasma generator,<sup>43</sup> it was found that the radiation emitted by the arc column increased with increase in arc current (resulting in higher column temperatures if other factors are kept constant) and pressure level, but decreased with increase in mass flux rates, mean voltage gradient, and external magnetic field. These tests were made utilizing an argon arc column of 100-2000 amperes and pressure levels of 1-10 atmospheres. (Note: Some preliminary results indicate that in spite of the increase in radiation observed with higher pressure, optimum operation may occur at pressure levels between 20 and 50 atmospheres). Spectral distribution of several plasma generators operating with different working fluids was presented in the Phase I report.

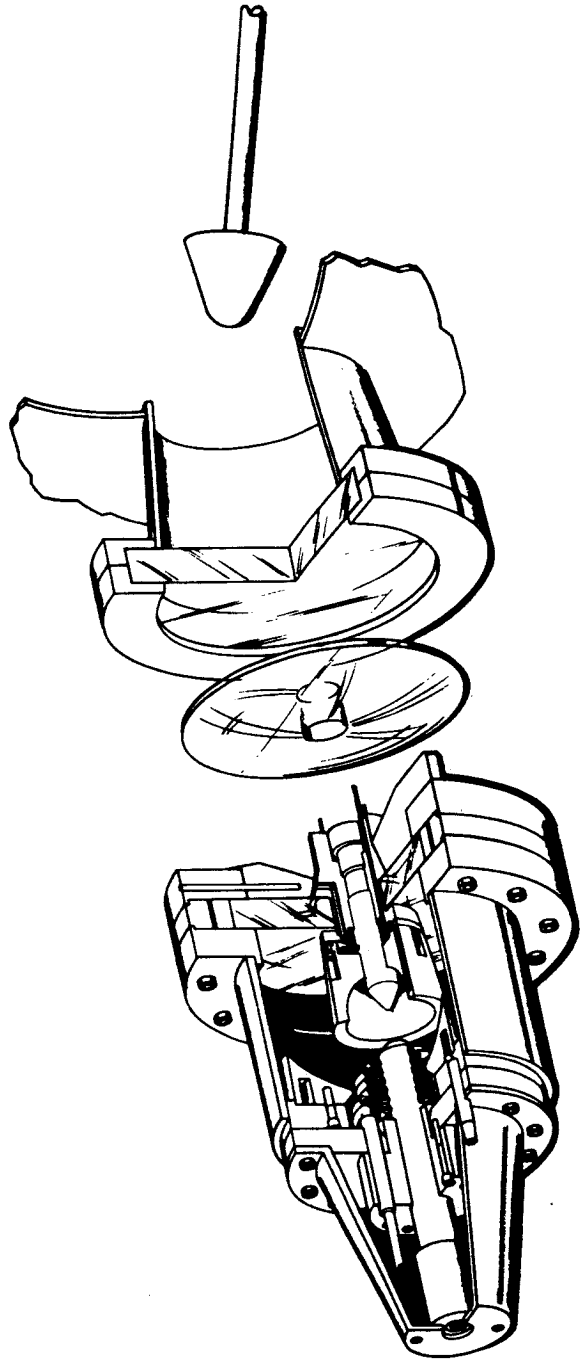
Of the current plasma generators under development or currently being utilized as radiant sources, the following four sources are somewhat representative:

- a. A radiation source under development combines the effects of the vortex-stabilized arc jet and the high-pressure short arc.<sup>46</sup> A prototype of such a source is illustrated in figure 24. The arc chamber pressure is 17 atmospheres and the plasma temperature is approximately 7000 °K. When this source is operated under properly regulated power and gas flow, it produces a cylindrical arc plasma with a diameter approximately equal to that of the anode exhaust aperture. The cool vortex flow continually replaces the gas surrounding the arc, thus greatly reducing the red and infrared radiation as compared to other enclosed arcs. Also the vortex fixes the arc plasma diameter and



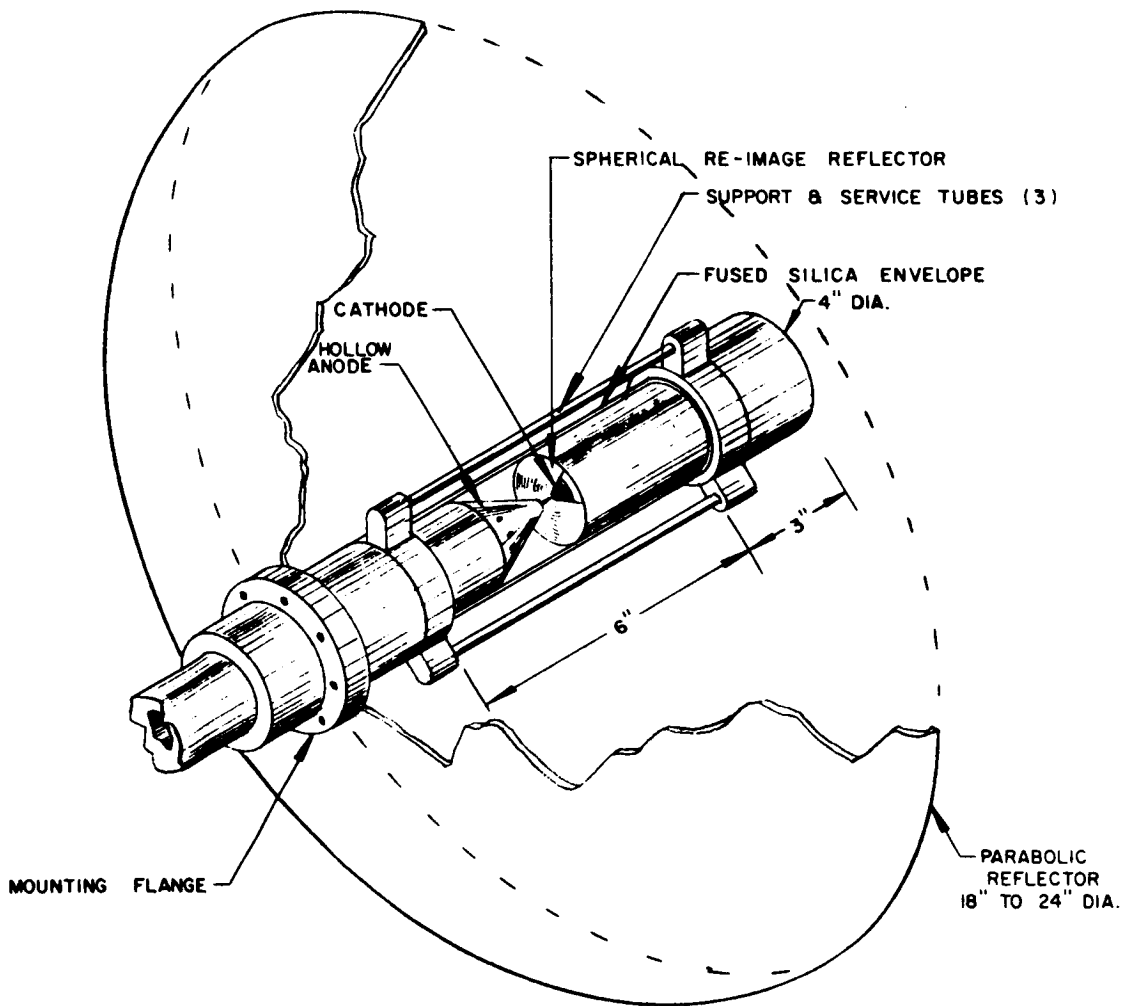
65-5552

Figure 22 CROSS SECTION OF CONSTRICTED ARC



68-5533

Figure 23 PLASMA GENERATOR RADIATION SOURCE



65-5534

Figure 24 VORTEX STABILIZED RADIATION SOURCE



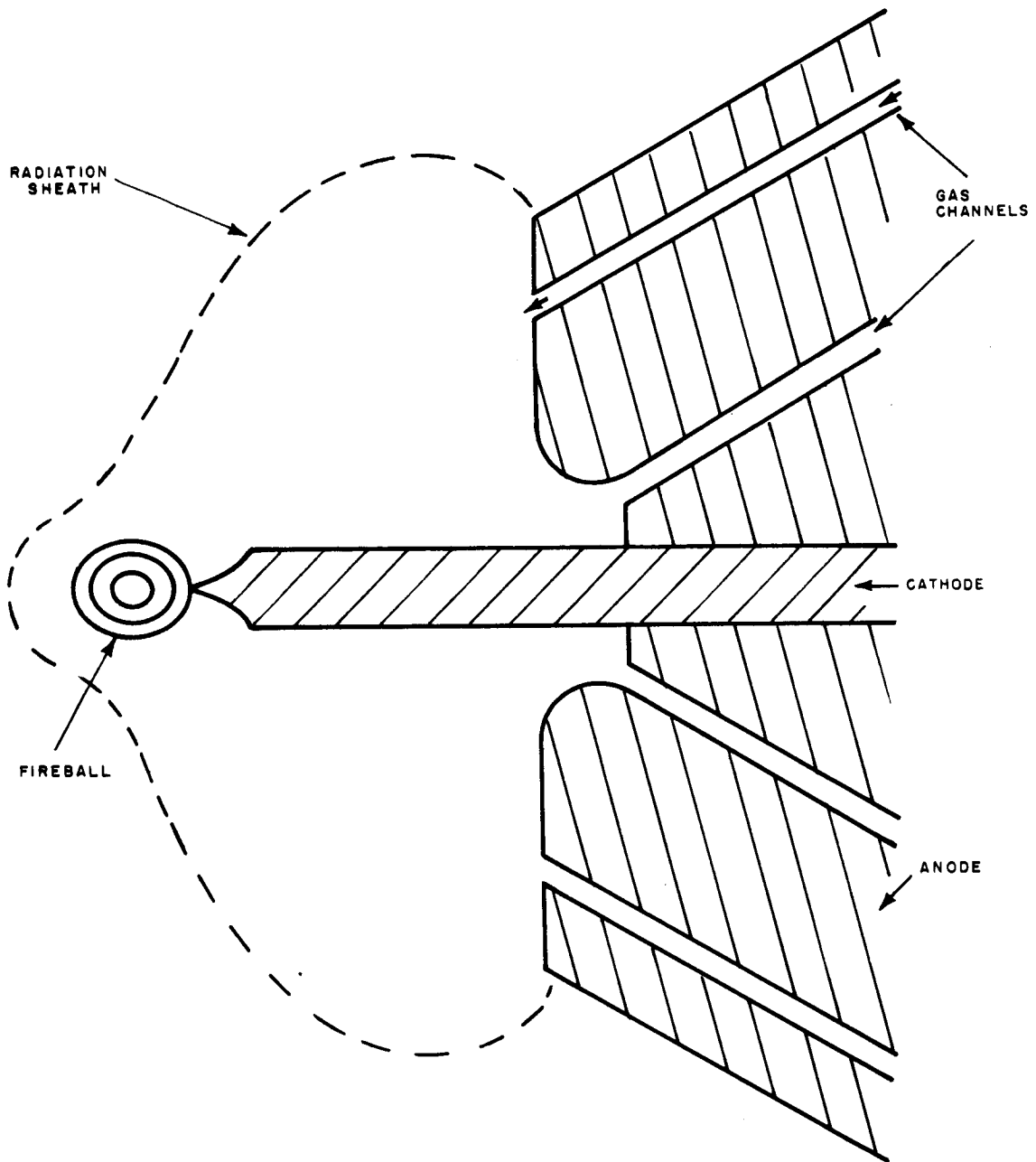
precisely locates the arc column. The total radiant output of a 10-mm x 3-mm arc plasma is reportedly 7.68 kw, with an input of 24.8 kw when operated with argon.

b. A somewhat different approach is utilized in the device shown schematically in figure 25.<sup>45</sup> In most plasma generators the two electrodes are aligned on the axis of the unit. Thus, radiation can emerge only radially, an arrangement disadvantageous for imaging techniques. A single-ended arc is now being operated<sup>45</sup> where a ring-shaped anode surrounds the cathode, which protrudes from the anode plane. The cathode region of the arc at the tip of the cathode is unobstructed over a solid angle of approximately 280 degrees. The reported operating conditions are: Input power 25 KW (units capable of operation at power levels up to 50 KW are under development), 0-300 psig chamber pressure, and a 6-mm diameter luminous sphere with a radiant efficiency of 35 percent when operated with argon at 25 KW.

c. A very useful device that has been used as a combined radiative and convective heating source has been referred to as a modified tandem Gerdien arc.<sup>44</sup> In this source, the test gas, air or other gases of interest, is heated in an arc column which is partially constricted by vortex flow and by mechanical orifices, figure 26.<sup>44</sup> The test model is positioned in close proximity of the arc column which provides the radiant energy. Radiant energy transfer can be changed by varying the distance between this model and the column. Previous column temperature measurements made on an arc of this type indicated peak temperatures between 16,200-18,000 °K.<sup>47</sup>

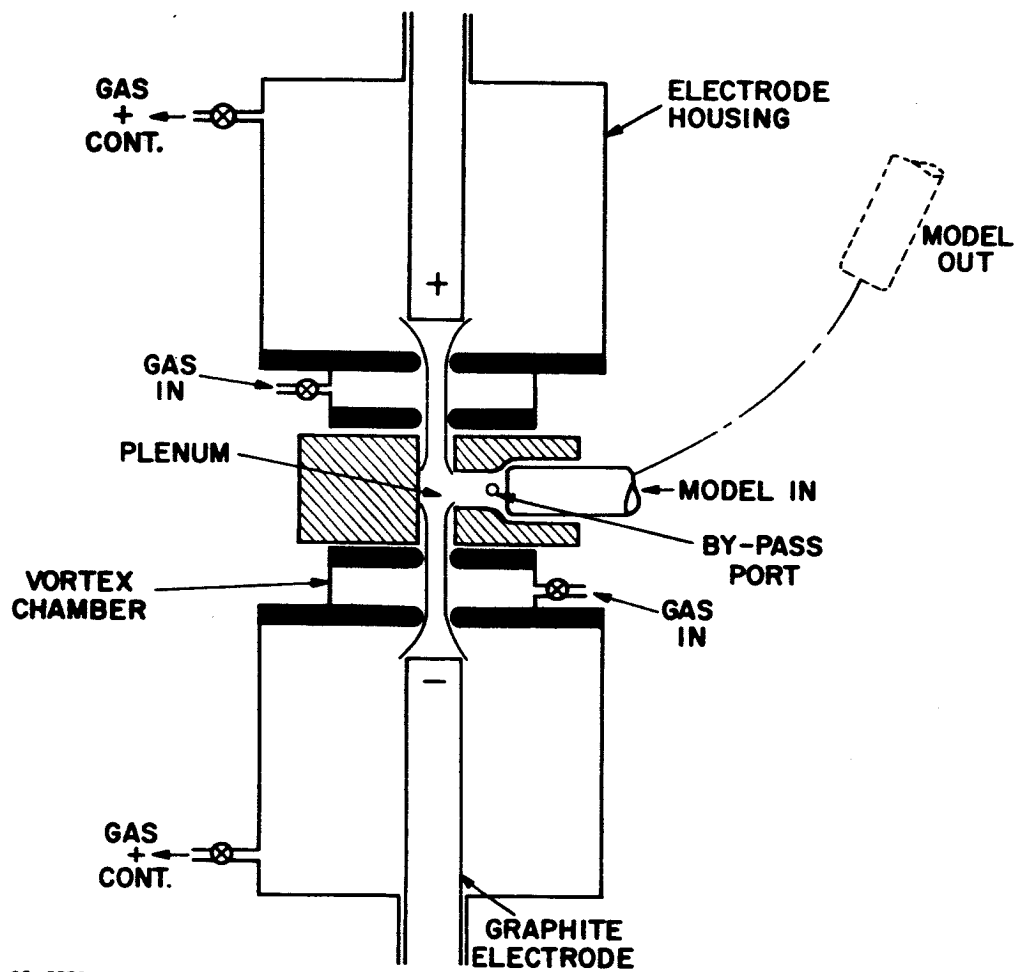
The temperature profile of the column has not been reported. Slightly less than 800 BTU/ft<sup>2</sup>-sec radiative heat transfer from air was measured by a radiation cavity gage at a distance of approximately 1 cm from the column boundary, with an input of 250 KW and one atmosphere chamber pressure. A unit is currently under development which will allow operation at pressures up to 5 atmospheres and permit adjustment of the model effect upon the model performance. Most models tested have been char formers which tend to nullify nonuniformities of the source, thereby allowing this adjustment.

d. The fourth source of this type that is of interest, is similar to that described in section A.<sup>46</sup> The principal differences are in the operating condition, i. e., higher power levels and chamber pressures, and in the associated optics. This device, shown in figure 23, has produced a radiating efficiency of about 35 percent when operated at 100 KW, 25 atmospheres, and 800 amperes. It is expected that this source will produce a usable directed radiation beam which has a high total input power. Four of these sources are being installed in conjunction with a high enthalpy, 2-1/2-megawatt arc heater for a combined variable radiative and convective heating facility (figure 27).



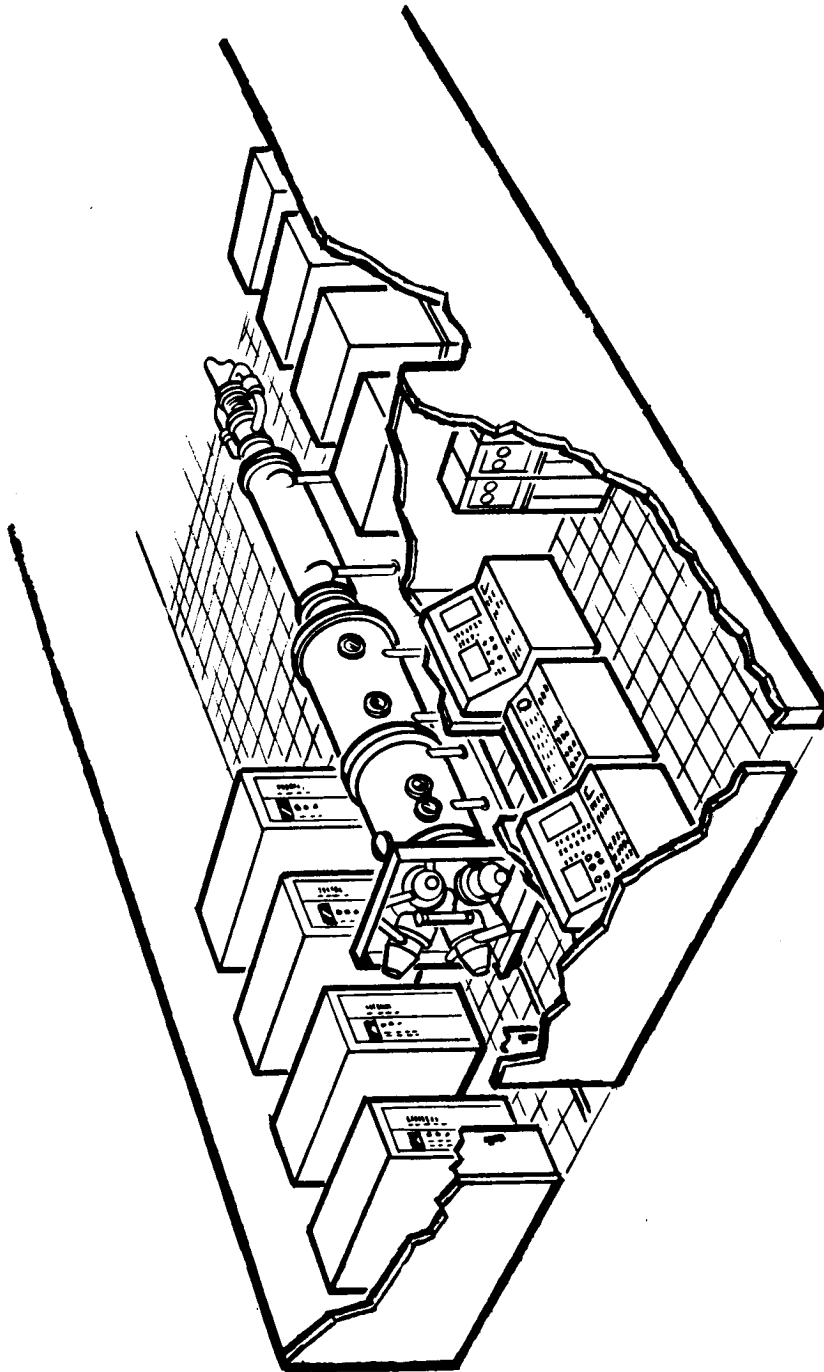
65-5536

Figure 25 VITRO ARC SKETCH



65 - 5536

Figure 26 SCHEMATIC OF MODIFIED TANDEM GERDIEN COMBINED RADIATIVE AND CONVECTIVE HEATING ARC SOURCE



65-5537

Figure 27 ROVERS FACILITY

## 6. Electron-Beam Radiation Sources

Electron beams, consisting of a directed stream of voltage accelerated electrons in a vacuum of pressure less than  $10^{-3}$  or  $10^{-4}$  torr, may be considered as radiation sources, both directly, as in the case of the electron microscopy, or indirectly as a well defined heat source for a primary thermal radiation emitter. All electron beam equipment has certain common elements, however there is a great divergence in size, beam resolution, beam control, and power according to the design application. Common functionally described parts for all systems are:

- a. Electron gun which contains an emitter and some directive provisions. A negative voltage control grid is used in precisely regulated equipment.
- b. High-voltage power supply to accelerate the electrons.
- c. A target area of conductive material.
- d. A sealed chamber with an insulated support for the gun target accesses, a high capacity vacuum pumping equipment capable of  $10^{-3}$  to  $10^{-6}$  torr vacuum, and X-ray shielding.<sup>49</sup>

All beam operations are performed at the low pressure, except some recent in-atmosphere welders, which pass the beam through a series of holes that are pumped to prevent gas from reaching the gun.

Reliable and precise equipment prices start at \$70,000 and up depending upon refinements in the beam controls and accuracy of power measurements. The operating characteristic of this equipment is a capability to focus up to 6 kilowatts into a spot which is 0.003 inches in diameter. At lower power, smaller spots may be obtained. For a lower heat flux, a defocused spot may be used at the sacrifice of spatial distribution uniformity, since the power density is usually described as Gaussian through the spot. A spot diameter is usually defined as the diameter containing one-half the beam power. The voltage is variable up to 150,000 volts and the amperage up to 40 milliamperes in a 6-kw machine. The focussed beam has a long focal length (up to 15 inches): Auxiliary deflection circuits and current modulation circuits can produce uniform power, density patterns, similar to a television screen raster, up to 5 inches. The spatial uniformity is then dependent upon line overlap and lines per inch. Complete feedback voltage and current regulation can be provided which would result in a temporal stable beam. On a swept raster, temporal energy distribution is dependent on the number of lines and the x-y coordinate sweeping frequencies. Instrumentation to measure beam current and voltage can provide control of power to better than 1 percent, and modulation can modify power distribution to compensate for heat loss at edges of thermally conducting targets.

The direct application of electron beams to simulate infrared, visible, or gamma radiation sources for purposes of materials testing is not advised. For example, a beam accelerated by 15,000 volts would provide optical properties of resolution comparable with gamma radiation of 0.1 Å, the radiation intensity would be quite high in comparison with standard optical sources.

Therefore, the application of electron beams to radiation simulating devices is restricted to the application of a heat source for a hot-body radiator. For relatively small targets of several square inches, up to 500 BTU/ft<sup>2</sup>sec could be applied with well controlled distribution to assure spatial uniformity of temperature of the primary radiation source.

The radiation from this source would be temporarily stable after initial heating, but at least one-half of the power would be directed to the reverse side of the target and lost unless a special collector system could be used to collect and redirect some of the reverse transferred energy. The spectral distribution of the electron-beam heated, primary emitter is that of a blackbody at the same temperature, as modified by temperature-dependent spectral emittance coefficients of the target material and any additional windows or optics.

#### 7. Lasers as Radiation Sources

The laser, or optical maser, provides a coherent light output at power levels ranging from watts, for the recently developed continuous-wave gas lasers to gigawatts, for short-pulsed (a few nanoseconds) solid-state optically pumped ruby lasers. Because the light output is coherent, it can be focussed to a diameter approximating the wavelength of light, so that flux levels as high as  $10^{17}$  watts/cm<sup>2</sup> are attainable in principle.

Lasers can therefore provide almost any conceivable radiant flux. Their usefulness as a simulation source, however, is severely limited by the fact that the total output energy, and the duration of the output pulse, are both limited. In addition, the light output is monochromatic.

Since other light sources (arc discharges, for example) can provide radiant fluxes as high as  $10^4$  watts/cm<sup>2</sup>, there appears to be no purpose in the use of lasers for simulation purposes at this and lower flux levels. At higher levels, lasers can serve a useful purpose, but not as a simulation radiation source. This is because the pulse duration of high energy lasers is limited, at the present time, to a few milliseconds. For example, one can obtain, with present ruby laser devices, a total energy output of over 1000 joules, with a pulse duration of about 2 milliseconds. This would provide a radiant flux of  $10^5$  watts/cm<sup>2</sup> on an area of 5 cm<sup>2</sup>, and, by reducing the area, a flux of  $5 \times 10^7$  watts/cm<sup>2</sup> on 1 mm<sup>2</sup>.

The short duration of the pulse makes it unusable for materials testing, as there is insufficient time for the material under investigation to attain quasisteady-state conditions, except at very high flux levels.

The one potential use of lasers appears to be as a means of investigating the basic phenomena that occur at high radiant flux levels. This is particularly the case at flux levels that are higher than those presently attainable with flash tubes.

The laser presents other advantages, for fundamental investigations, in that its output is monochromatic, the output energy and flux are readily controlled, and it is a relatively clean source of radiant energy. Associated electromagnetic noise can be almost completely eliminated, so that measurement techniques requiring sensitive electronic detection are feasible.

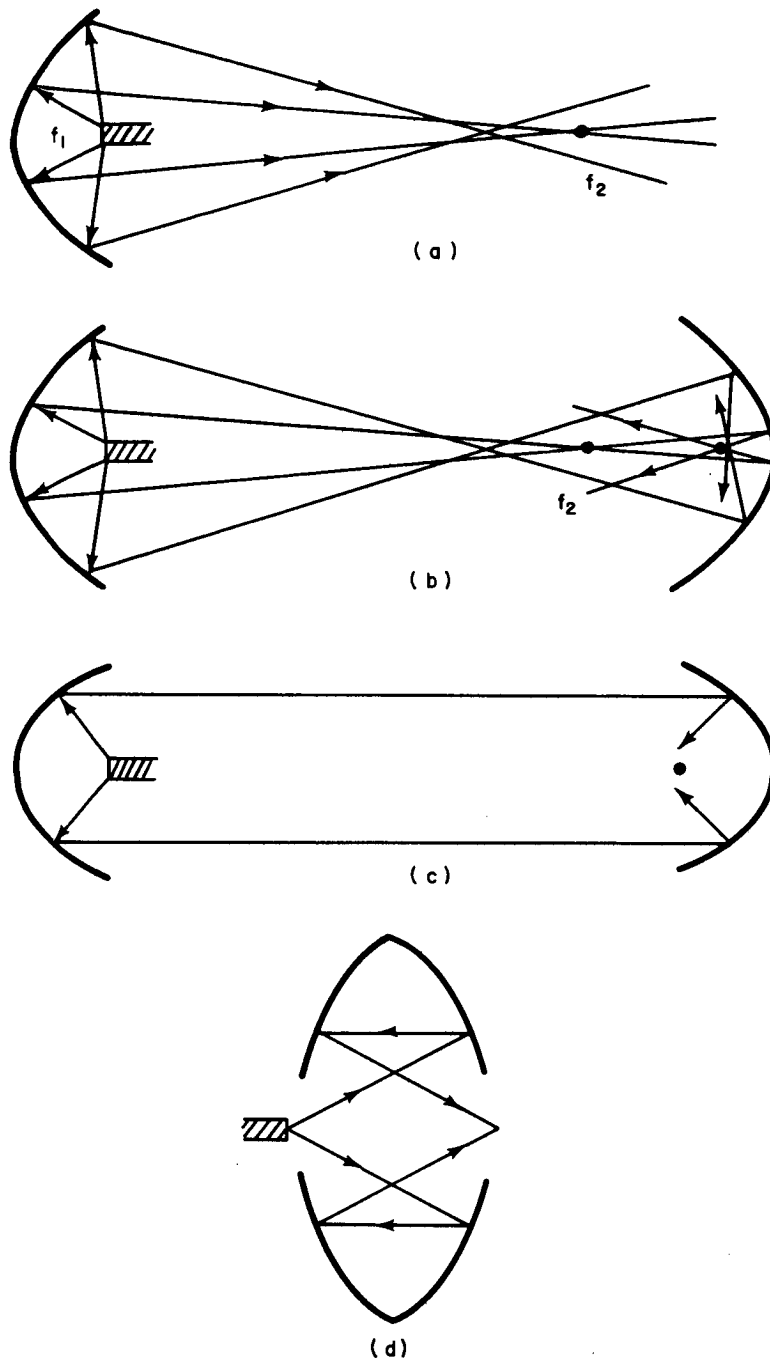
## B. RADIATION SOURCE OPTICS

### 1. Arc Imaging

For many radiation experiments it is an adequate procedure to introduce a test surface into an arc chamber, directly exposing the sample to the radiant flux from the arc source. For some tests, however, this is impossible; in particular this is the case where (a) independent control over the specimen environment (pressure, gas composition, etc.) is desired, or (b) model size is prohibitive, or (c) source uniformity is a requirement. For tests of these types, optical systems are used to collect radiant energy from the arc source, transport it from the source chamber, and concentrate it at the test location.

### 2. Types of Optical Systems

In general, although not necessarily, the optical system used to accomplish these functions consists of at least two elements: the collector and the concentrator. The collector is in every case a mirror which may be spherical, ellipsoidal, or paraboloidal. The concentrator may be either another mirror or a lens, depending upon the geometrical constraints established by the experimental requirements. Figure 28 shows four optical systems which have been used with carbon-arc radiation sources. Figure 28 depicts a single element optical system consisting of an ellipsoidal mirror segment with the source at the primary focus. An image is formed at the secondary focus. In general, such simple systems produce large images with relatively low intensity. The two-mirror system of figure 28b consists of an ellipsoidal collector with a secondary focus which is common to the secondary focus of the ellipsoidal concentrator. The image is formed at the primary of the concentrator. Essentially the same image intensity would be obtained if the arc were placed at the secondary focus of the concentrator, but in this way the distance between the arc and test location is increased.



65-5538

Figure 28 CARBON ARC FURNACES - REFLECTOR SYSTEMS



Paraboloidal mirrors are used in figure 28c, again permitting a large working distance between arc and sample. The paraboloidal mirror produces a parallel outgoing beam if the source is placed at the focus. A variant of this geometry is shown in figure 28d. This "clamshell" construction allows both source and sample to be located outside the optical system.

For plasma-arc sources, as opposed to carbon-arc electrode sources, addition of a third element, the secondary collector, to the system, can improve image brightness. In figure 29 the arc is located at the primary focus of the main ellipsoidal collector. However, many rays which leave the arc at angles not intercepted by the ellipsoid are reflected back by the spherical secondary collector. Thus, a smaller ellipsoidal reflector in combination with a secondary collector can intercept and reflect as much energy as a much larger ellipsoidal reflector. The advantage is lower cost for the smaller mirrors, while the disadvantage is the double reflection with increased losses.

The use of a lens as concentrator offers the further advantage that the light beam is projected completely outside the optical system, offering maximum experimental flexibility. The optical schematic of a radiation lamp developed by Avco RAD is shown in figure 30. This system employs a paraboloidal primary collector, a spherical secondary collector, and a decentered toroidal biconvex concentrating lens. With a 12-inch lens, a 21-inch working distance is obtained between the lens and the test specimen.

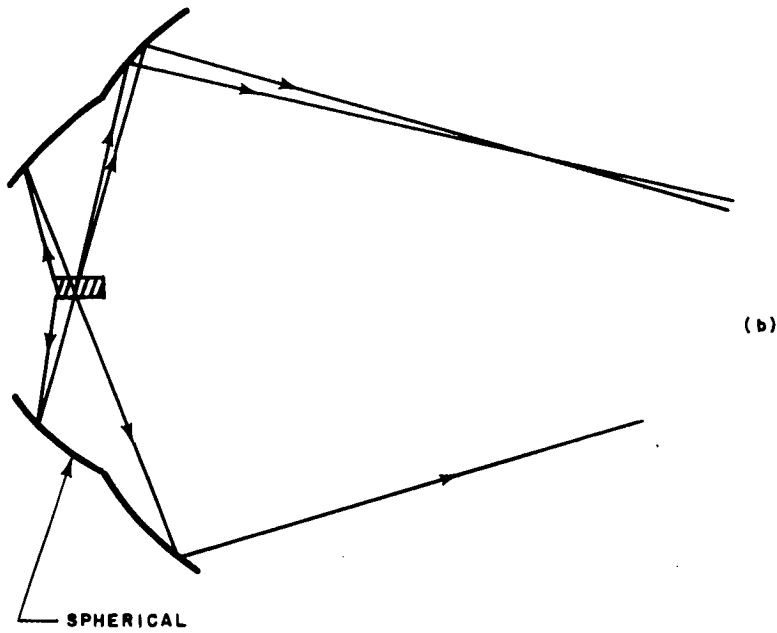
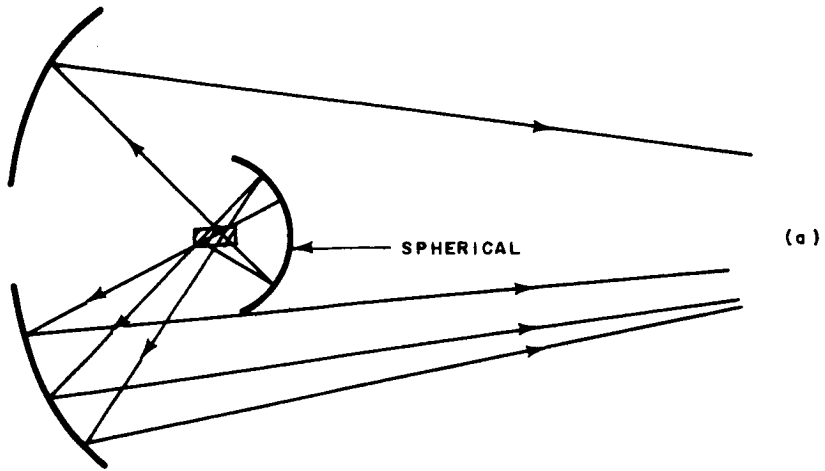
### 3. Imaging System Performance Limitations

The performance of an arc imaging system expressed in terms of the radiant flux delivered to a test sample is dependent upon the following factors:

- a. Source Brightness
- b. Light Collection from Source
- c. Energy Losses in Optical System
- d. Flux Losses in Optical System

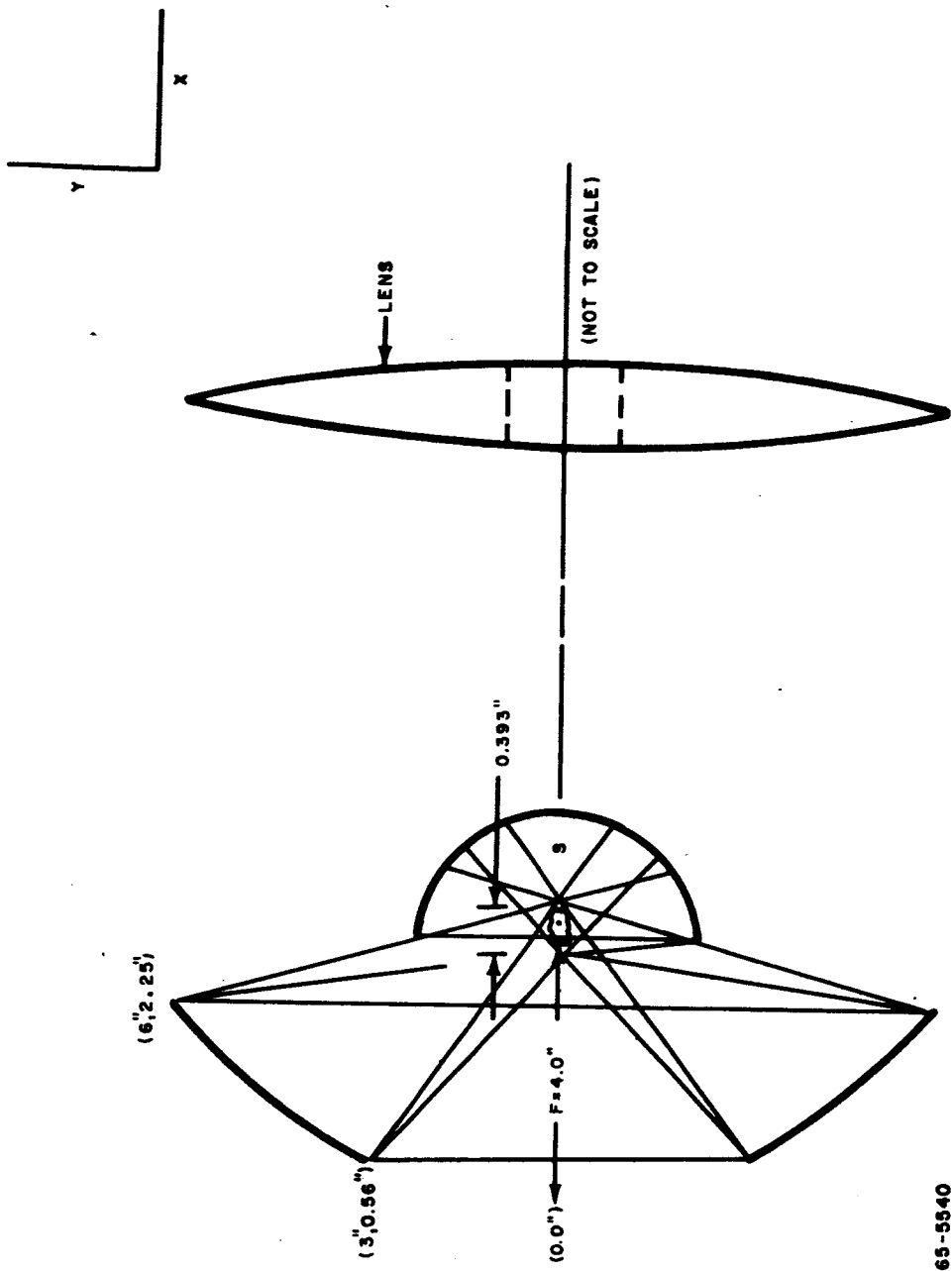
#### 1) Source brightness

For opaque sources obeying Lambert's law in systems where the index of refraction of the medium surrounding the source is the same as that surrounding the test region (e. g. , for any carbon arc), the brightness at the image cannot exceed the brightness of the source. This is a standard result of optics and is demonstrated in many textbooks. Thus, if the emitted flux into a hemisphere



65-5539

Figure 29 USE OF SECONDARY REFLECTORS TO FOLD BACK RAYS



65-5540

Figure 30 PARABOLOID - SPHERICAL REFLECTOR

from the surface of a carbon anode is  $3 \text{ kw/cm}^2$ , the flux received by a sample after imaging cannot exceed this amount and will, in fact, be reduced by any losses.

Some care must be exercised in applying this result to plasma radiation sources if they are operated at pressures such that they are optically thin (for most gases this includes operation at pressures up to several tens of atmospheres for dimensions of the order of centimeters). The plasma becomes opaque to wavelengths corresponding to spectral lines at relatively low pressures, but at higher pressures most of the energy is carried by the continuum radiation, and the plasma will not be opaque to this until extremely high pressures are reached). Transparent, volumetric plasma light sources are not Lambert's law sources and their flux can be increased. For example, figure 31a shows a simple method for doubling the flux from a long, optically thin cylindrical plasma. In figure 31b a method is illustrated for increasing the flux to the blackbody limit at the plasma temperature, given a sufficiently long arc and coaxial mirror.

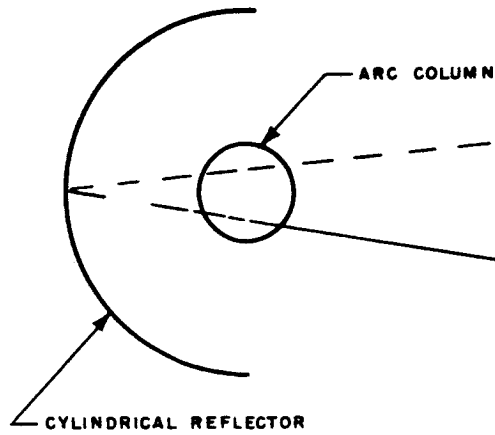
The eventual limit for the plasma radiance is that appropriate to a blackbody at the plasma temperature. However, it should be noted that the plasma temperature is typically of the order of  $15,000 \text{ }^\circ\text{K}$ , and the corresponding flux is  $270 \text{ kw/cm}^2$ .

## 2) Light collection

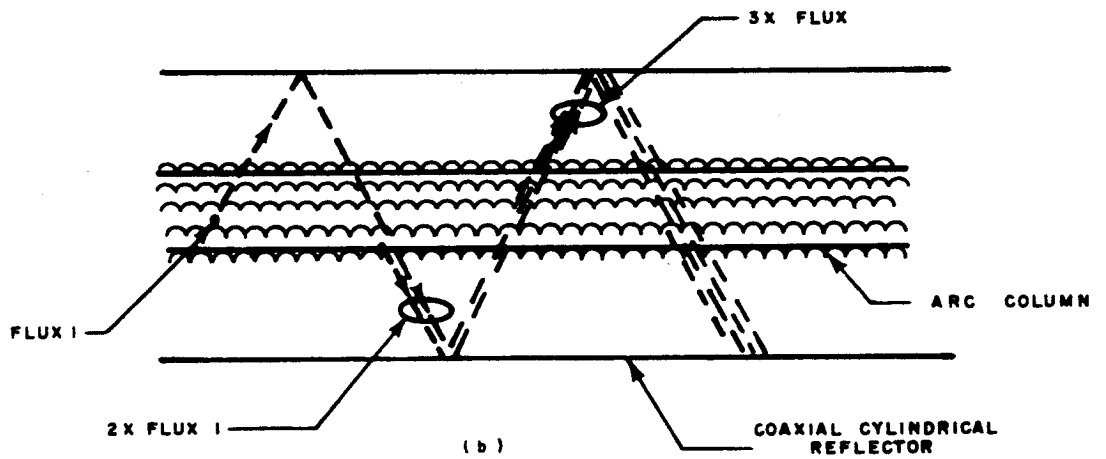
To an approximation of engineering utility, most plasma discharges can be considered as isotropic radiators. Thus, the light-collection efficiency is given by the ratio of the solid angle subtended by the collector(s) to  $4\pi$ . For example, referring to figure 28b, the collection efficiency is approximately 0.5, since all radiation to the left is collected while all to the right is lost. In general, some radiation must be lost; there must be an opening in the system to let the collected beam out, and the electrodes will intercept some radiation. The carbon arc source, in contrast, radiates in general into a hemisphere, with the carbon absorbing the backward radiation.

## 3) Energy losses

Each optical element in the system absorbs some of the incident radiant energy. In general, these losses can be kept small in the visible region of the spectrum, and in the infrared region if the light path does not cross a region which is water-filled. The ultraviolet is more difficult to preserve. In general, reflectances of 0.8 to 0.95 can be obtained for front-surface mirrors and trans-



(a)



(b)

65-8541

Figure 31 FLUX ENHANCEMENT FOR OPTICALLY THIN SOURCES

missions of the same order for quartz lenses. Figure 32 shows the reflectance of a front-surface aluminum mirror as a function of wavelength, and figure 33 shows the transmission of quartz also as a function of wavelength. If the number of optical elements exceeds two or three, these cumulative losses can be quite significant.

#### 4) Flux losses

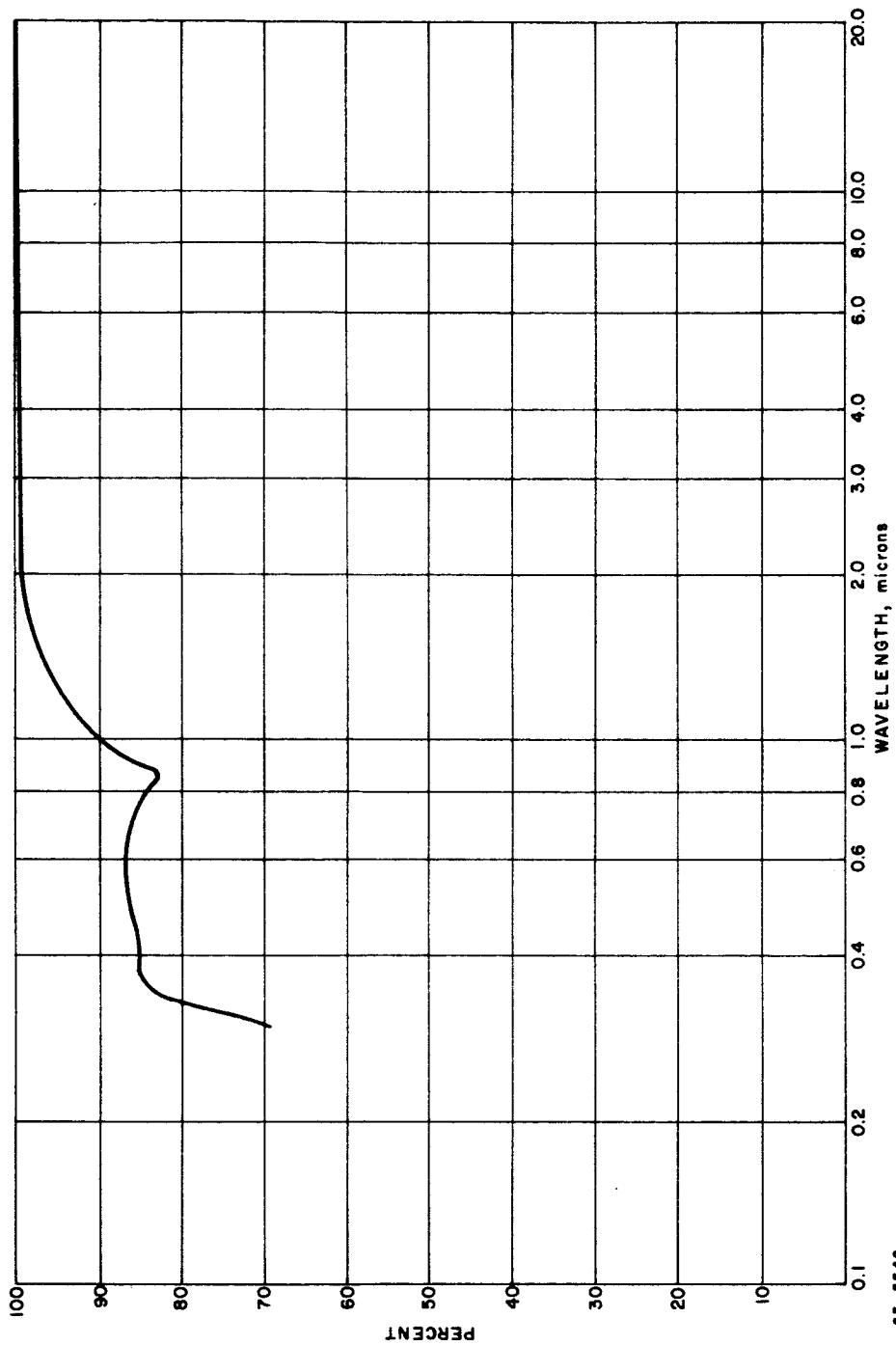
In general, the size of the radiating volume is not negligible compared to the characteristic dimensions of the optics. Also, very large apertures are required to give good radiation collection, and to illuminate the sample from a large solid angle. Thus, depth of field of the optical system is poor, and the image formed will be a distorted one occupying a larger area than the source. This reduces the flux level at the sample. Also, chromatic observations and any optical system imperfections will aggravate this situation.

### C. SPECTRAL RADIANCE OF SOURCES

For comparison purposes the spectral radiance of several gases has been obtained. For the most part this data was obtained in various arc sources in the Avco RAD laboratories except where otherwise noted. Particular attention should be given to figures 34 and 35 which show the dependence of spectral radiance of nitrogen and oxygen on temperature. Nitrogen at 7.7 atmospheres is shown in figure 36; Xenon, reference 50, figure 37; Argon, figure 38; and a carbon arc, reference 51, in figure 39.

When a spectral match has been required, investigations have resorted to the use of one or more filters. Filters have the effect of reducing somewhat the intensity in the desired bands as well as in the undesired bands.

One of the most promising means for enhancement of particular bands of radiation to "fill in" spectral gaps to provide a better match, is to provide additives to the basic radiating (carrier) gas. Several investigations have reported that the spectral distribution of a source, particularly an arc source, can be greatly modified by the addition of powders to the stabilizing gas. 45, 46 This may have an interesting potential. However, it has also been observed that the additives may produce undesirable "side effects", such as damage to the generator source or optics, or lower conversion efficiencies. For example, use of additives with relatively low ionization potentials (e.g., the alkali metals) can be expected to increase infrared radiation (including the continuum). This would be done, however, at the expense of the carrier gas line radiation which may or may not be desirable. Section VI of this report presents a discussion of an approach to the enhancement of spectral radiance.



65-8842

Figure 32 PERCENTAGE REFLECTANCE OF AN ALUMINUM MIRROR

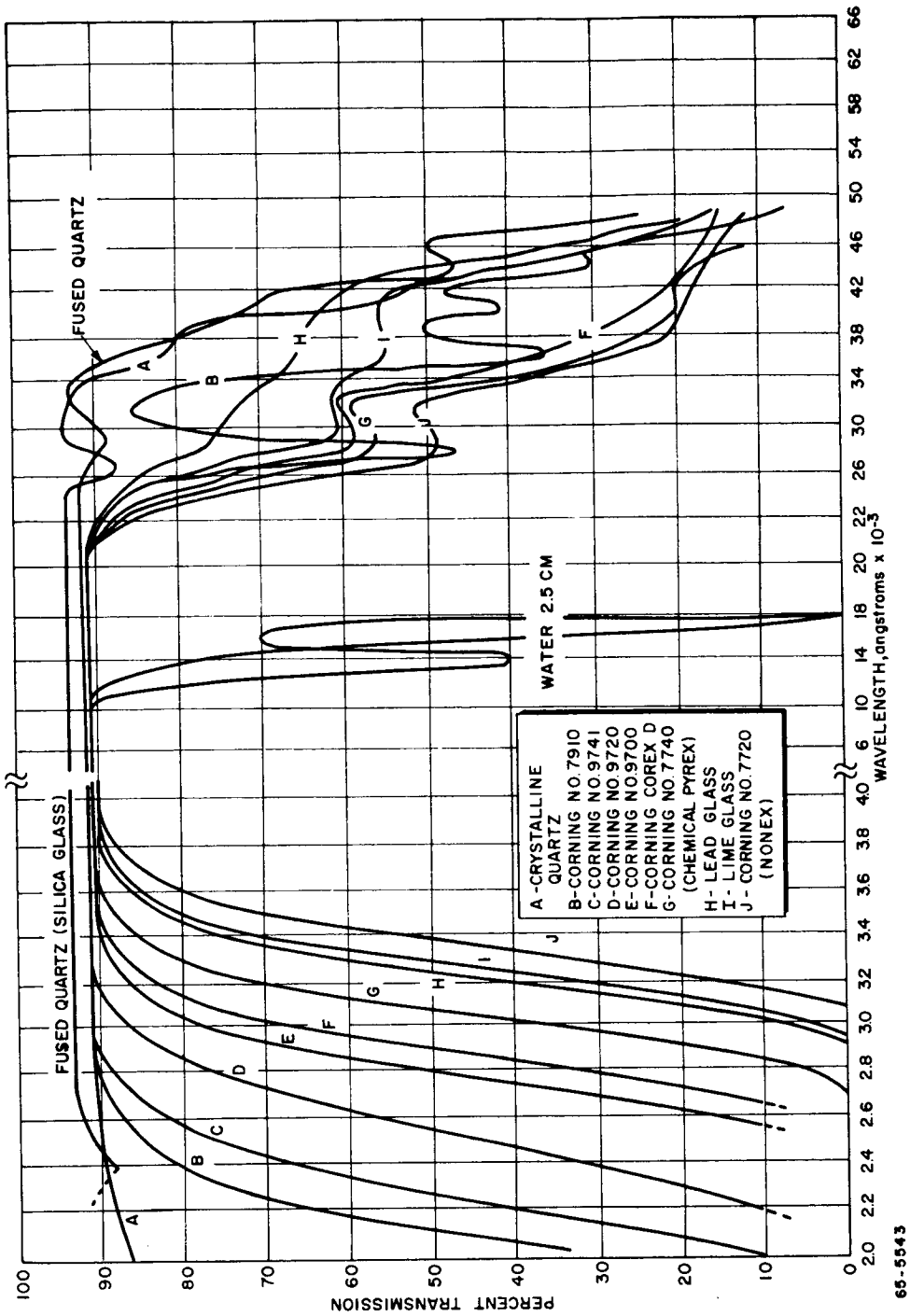
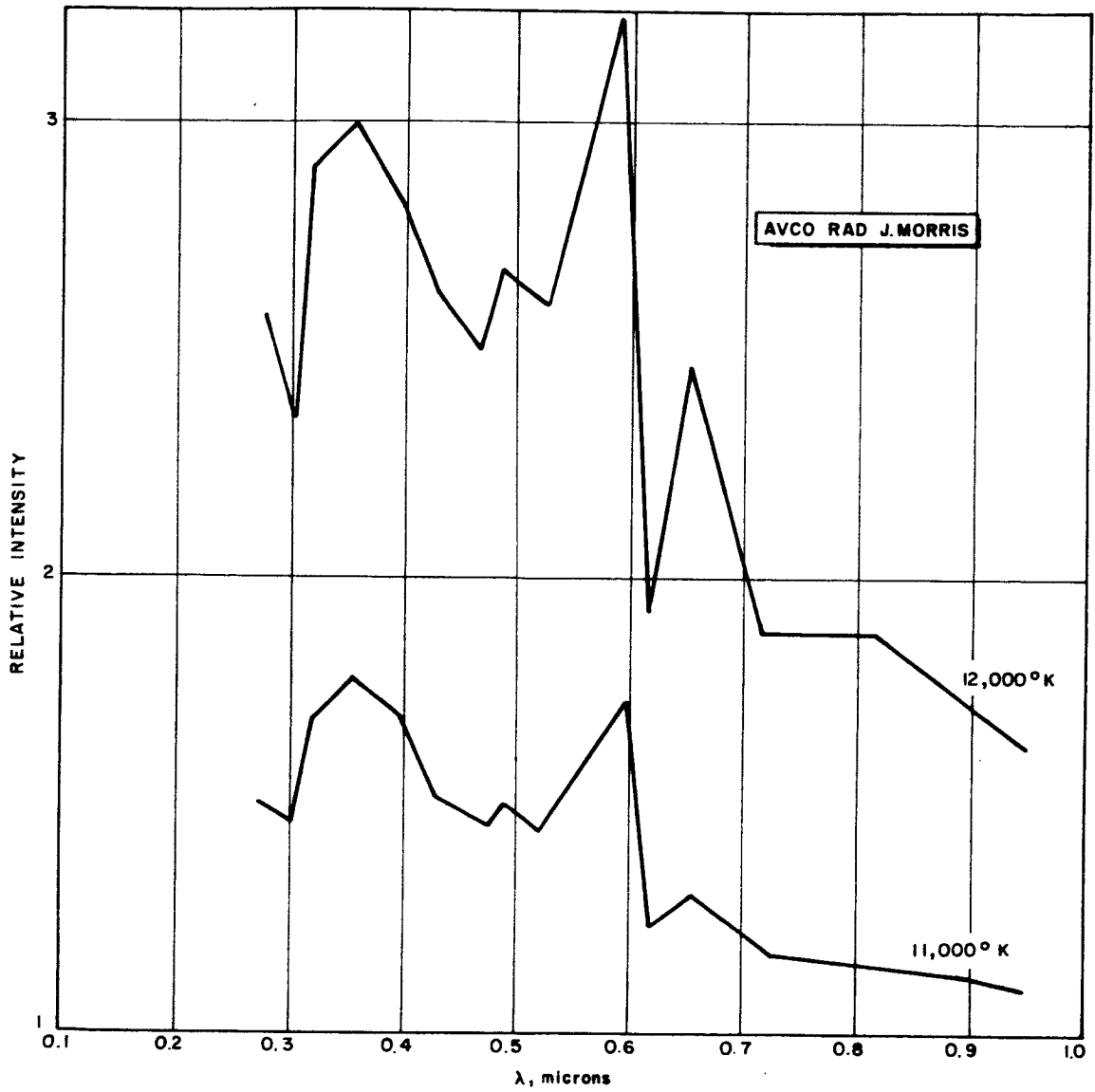


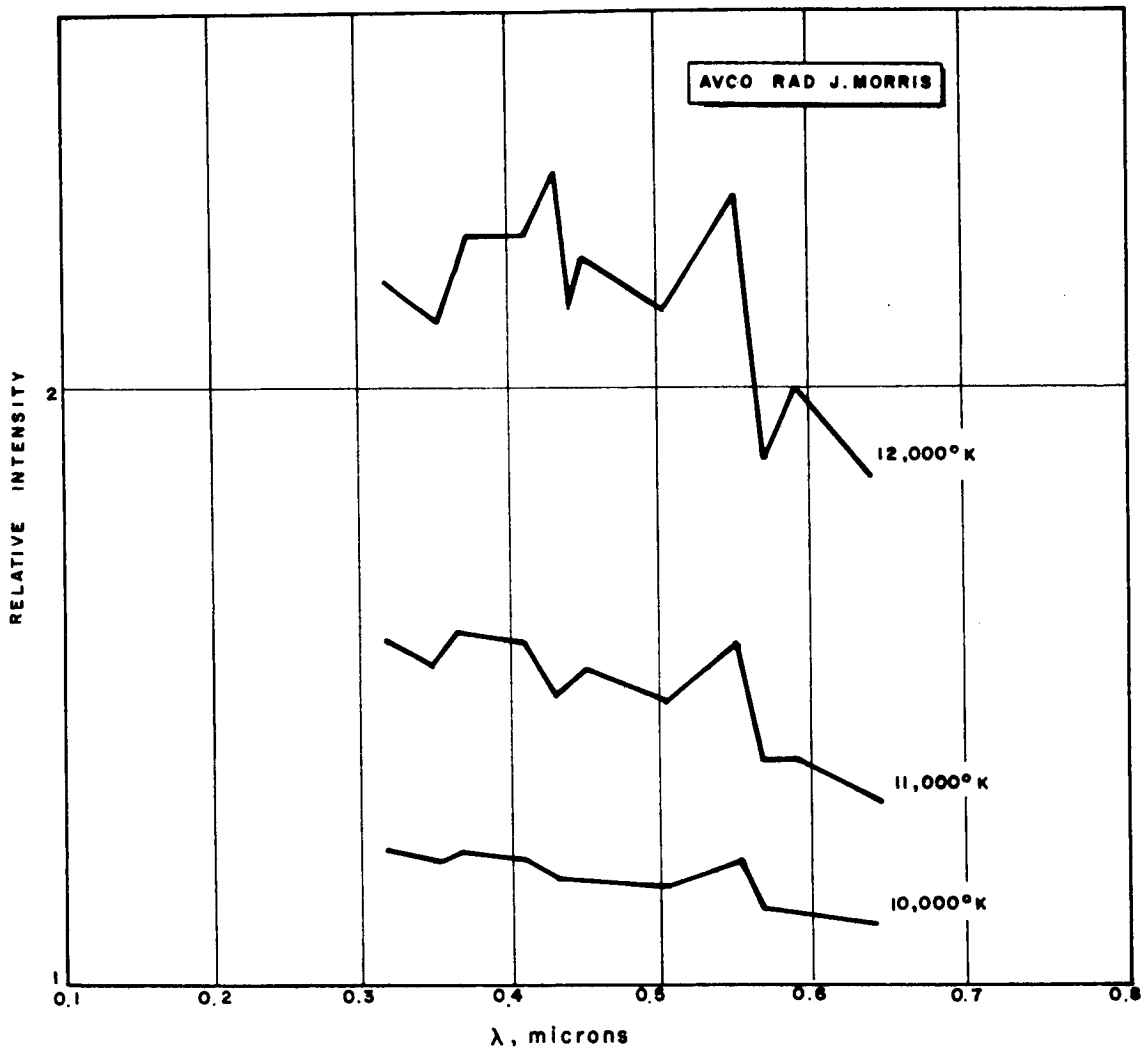
Figure 33 TRANSMISSION CHARACTERISTICS OF QUARTZ, VARIOUS GLASSES, AND WATER





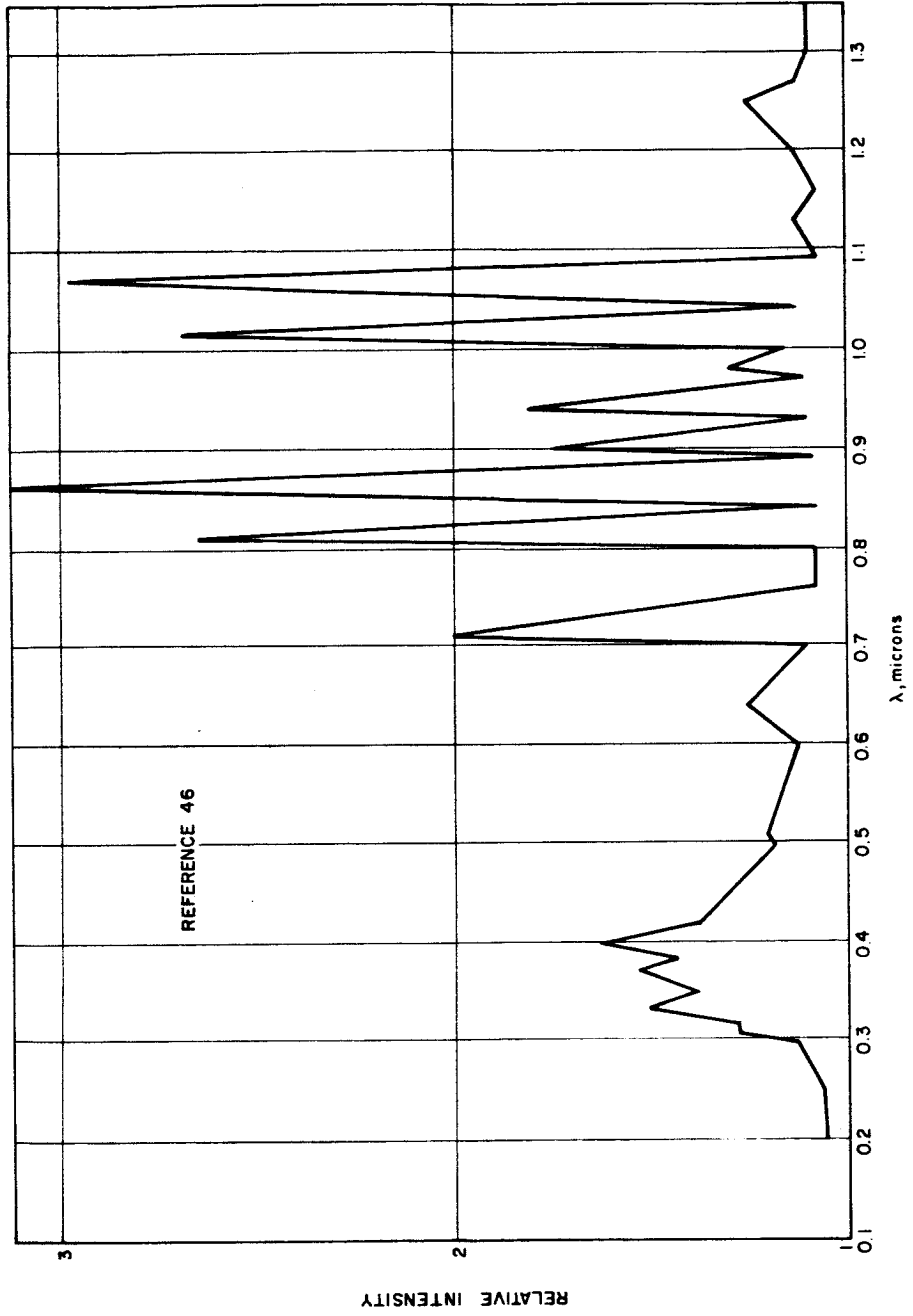
65-5614

Figure 34 SPECTRAL RADIANCE MEASUREMENTS FOR NITROGEN - ONE ATMOSPHERE



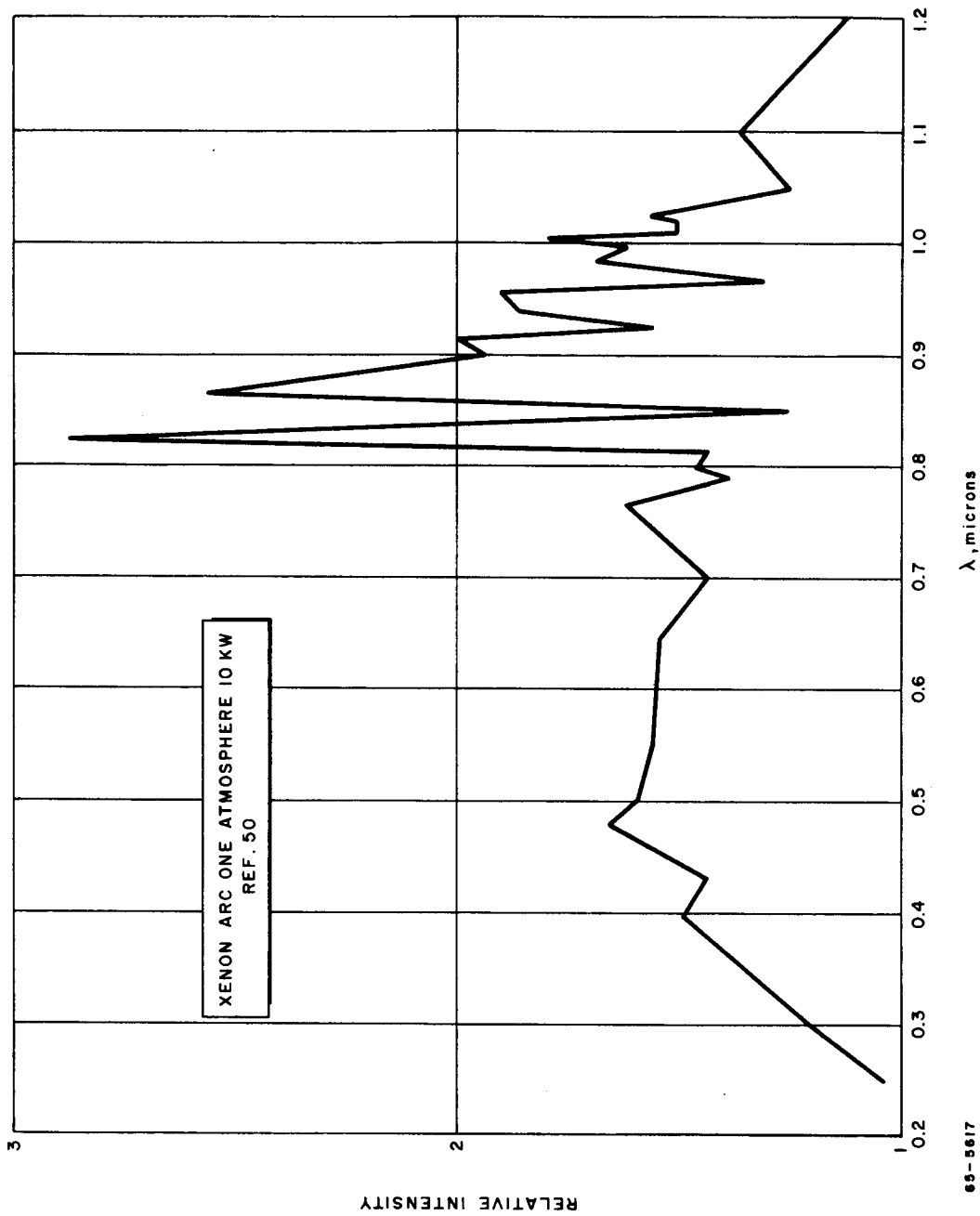
65-5815

Figure 35 SPECTRAL RADIANCE MEASUREMENTS FOR OXYGEN - ONE ATMOSPHERE



65-5616

Figure 36 SPECTRAL RADIANCE MEASUREMENTS FOR NITROGEN -  
7.7 ATMOSPHERES



65-5617

Figure 37 SPECTRAL RADIANCE MEASUREMENTS FOR XENON

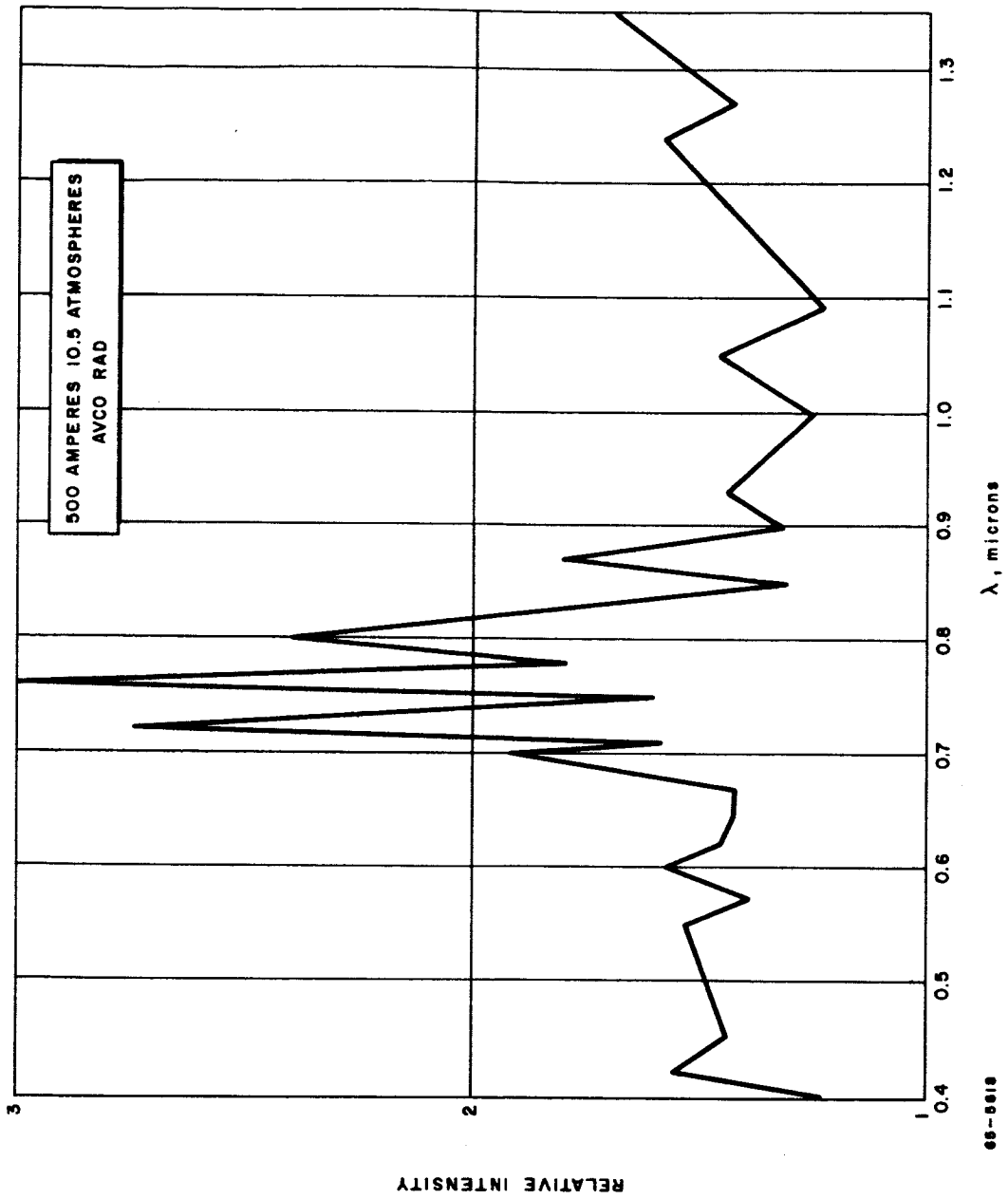
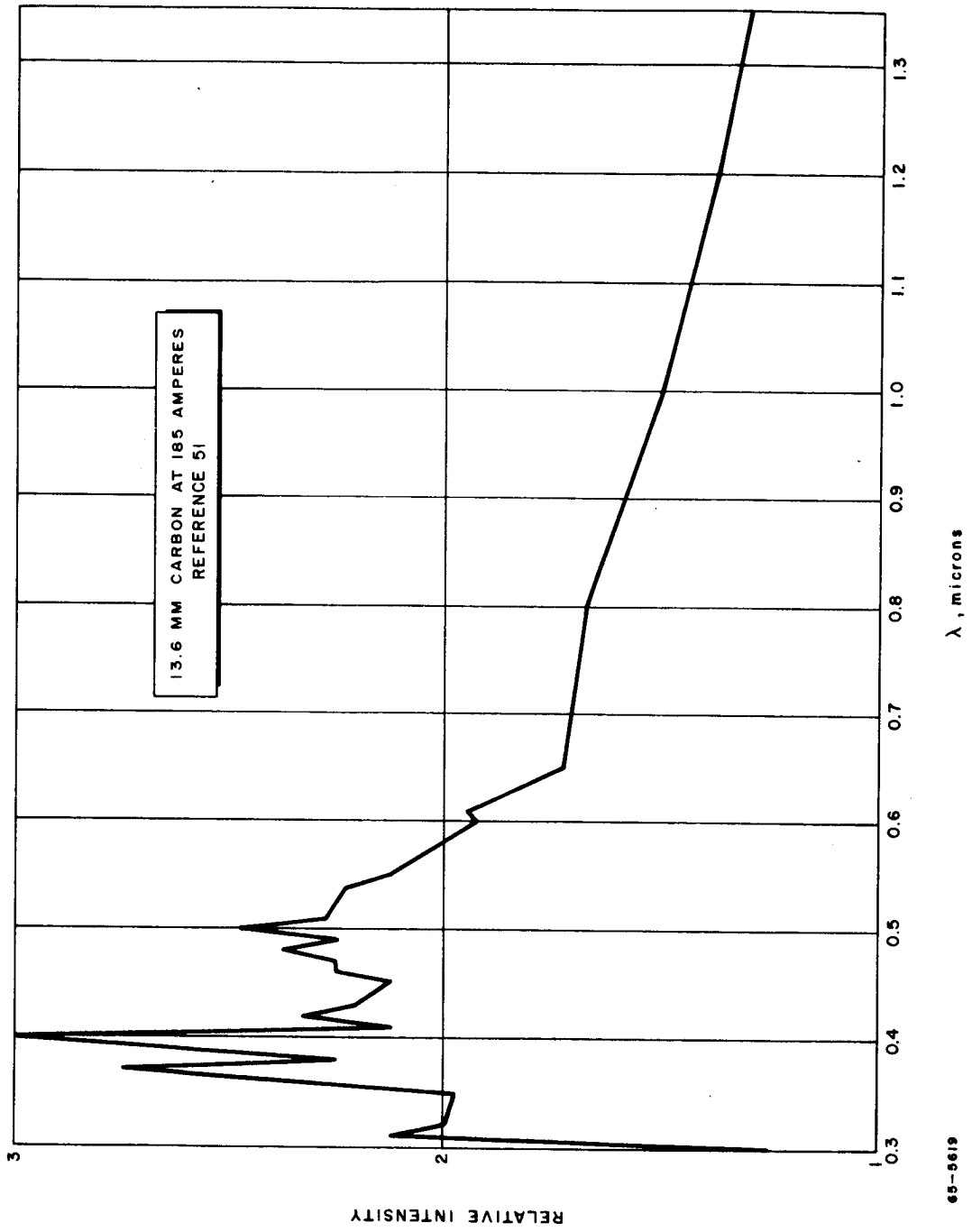


Figure 38 SPECTRAL RADIANCE MEASUREMENTS FOR ARGON



65-5619

Figure 39 SPECTRAL RADIANCE MEASUREMENTS FOR A CARBON ARC

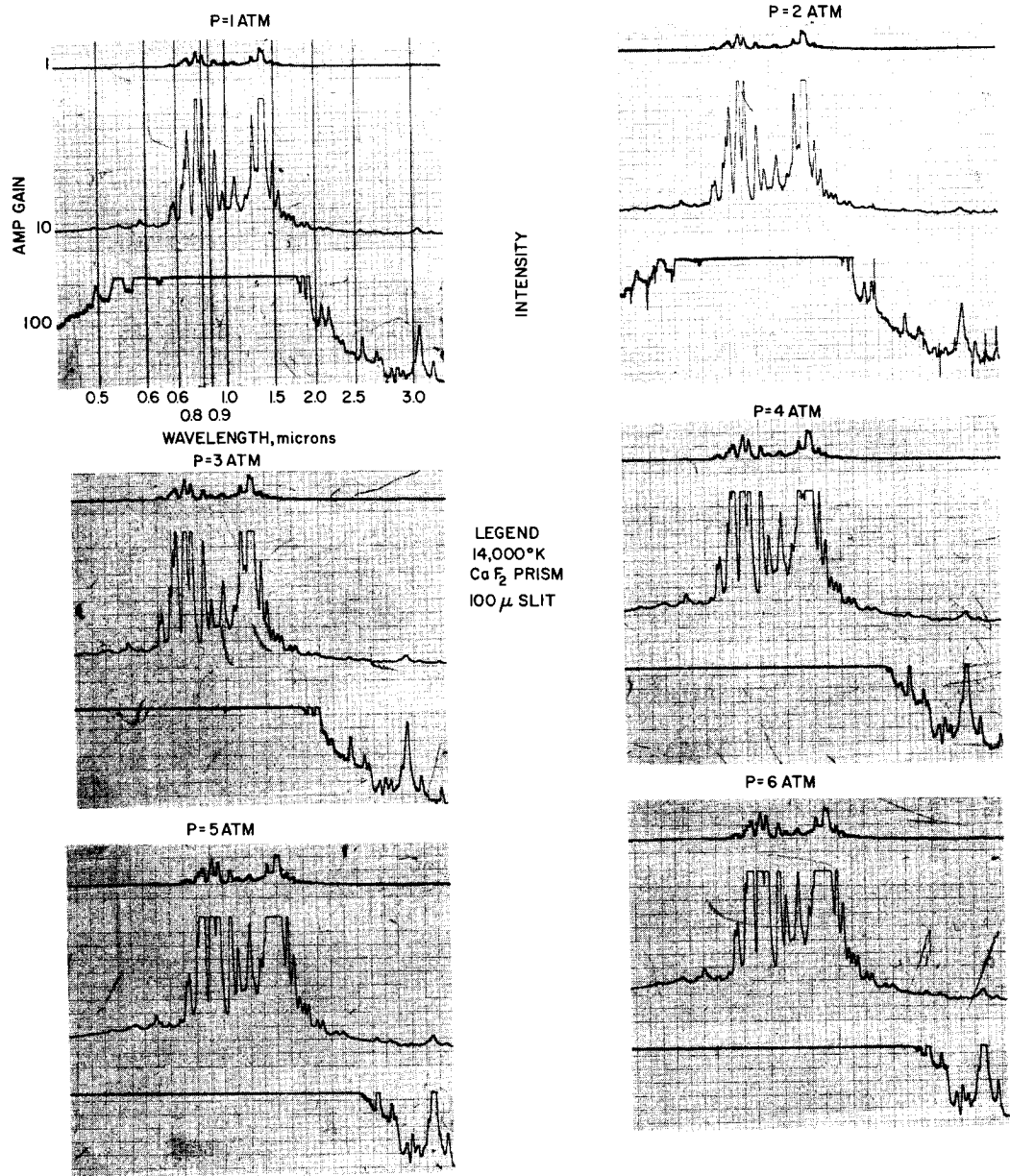
Another possibility is reflected in the data shown in figures 34, 35, 40, and 41. Figures 40 and 41 are spectral scans obtained in a series of tests at low dispersion in the constricted arc described in appendix B. Figure 40 gives the spectral radiance (uncorrected for instrument sensitivity) at 14,000°K and 1 atmosphere pressure for nitrogen, oxygen, and carbon dioxide, and also for a tungsten standard lamp at a true temperature of 2600°K. (The latter curve is used for calibration.) Figure 41 shows six spectral scans for argon at pressures from 1.0 to 6.0 atmospheres, also at 14,000°K. These figures demonstrate the possibilities that may be obtained from source operation temperatures (current), chamber pressure and carrier gas selection with or without additives. Figure 42 shows a spectral scan of this same device with the argon and a small percent of cesium additive.

#### D. SOURCE SELECTION

Selection of a single radiation source to meet all of the requirements established by the manned entry corridor is not possible at the present time. A filtered carbon arc source can provide a fairly well matched spectral distribution which is also fairly efficient. However, the flux levels of such sources are somewhat limited. This limitation is much more severe in a filtered carbon arc source than for the laser and the plasma devices. The laser's potential in this field is however, all but eliminated due to its very short test times. The future of the high pressure compact arc is one of the most difficult to assess. To some extent this type of source is closely related to the plasma generator. In fact, it is believed that a blending of the technology of these two fields will ultimately produce the most satisfactory radiation source. The following is a general performance summary of plasma generators and the carbon arc as imaging systems.

##### 1. Carbon Arc Lamps

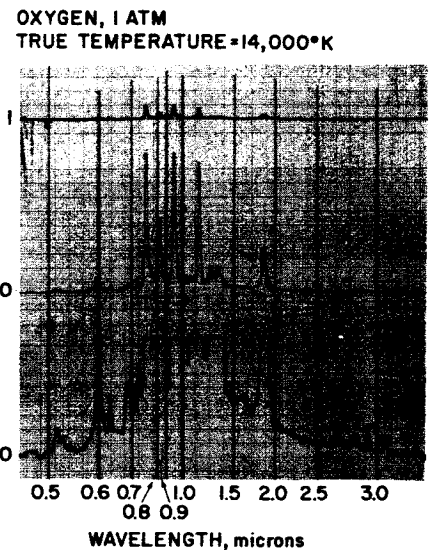
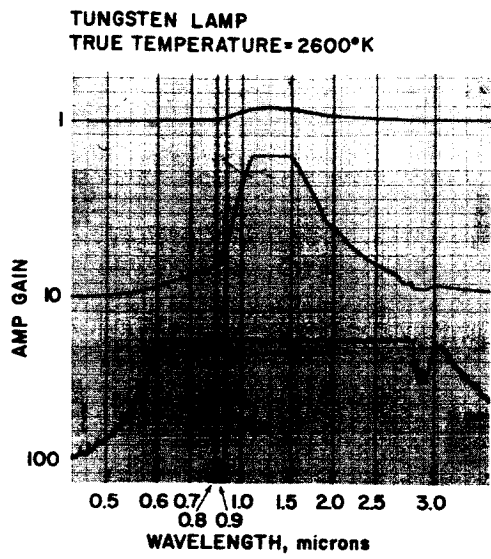
A considerable amount of experience has been accumulated with carbon arc lamps for imaging furnaces, employing single-mirror and double-mirror optics. In general, the single ellipsoidal mirror systems have been unsatisfactory for high-flux applications due to the very small image produced at the primary focus. Double-mirror systems have successfully produced flux levels up to 1.5 kw/cm<sup>2</sup> over spot sizes of the order of 1 cm. Whether ellipsoidal-or paraboloidal-mirror systems have been used appears to be a question of availability and convenience. On purely technical grounds, there seems to be little to choose between them. In general, the optical systems have performed well, to the point that it is unlikely that any substantial flux increase will be produced by an optical refinement. Rather, increases in the source brightness are most likely to yield improved performance.



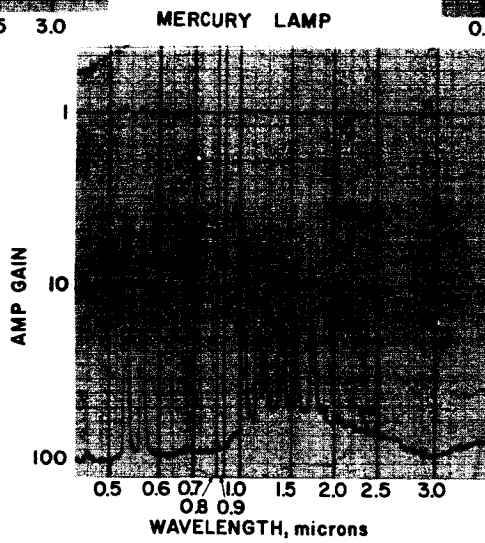
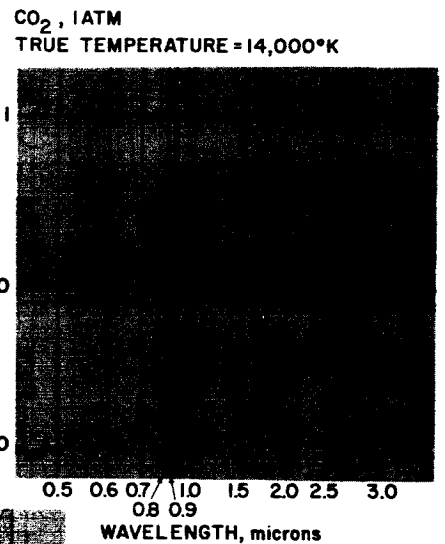
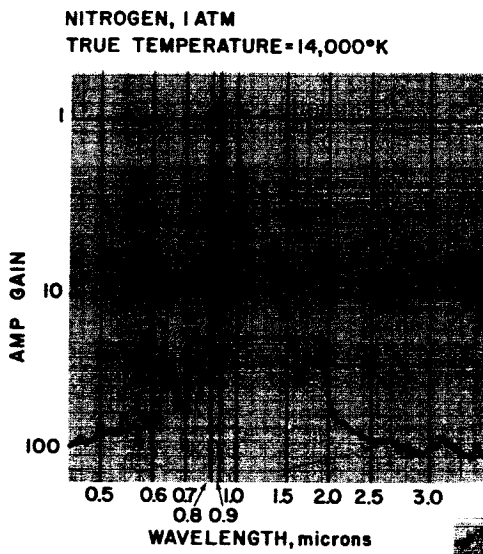
65-5544

Figure 40 SPECTRAL RADIANCE MEASUREMENTS OF VARIOUS GASES



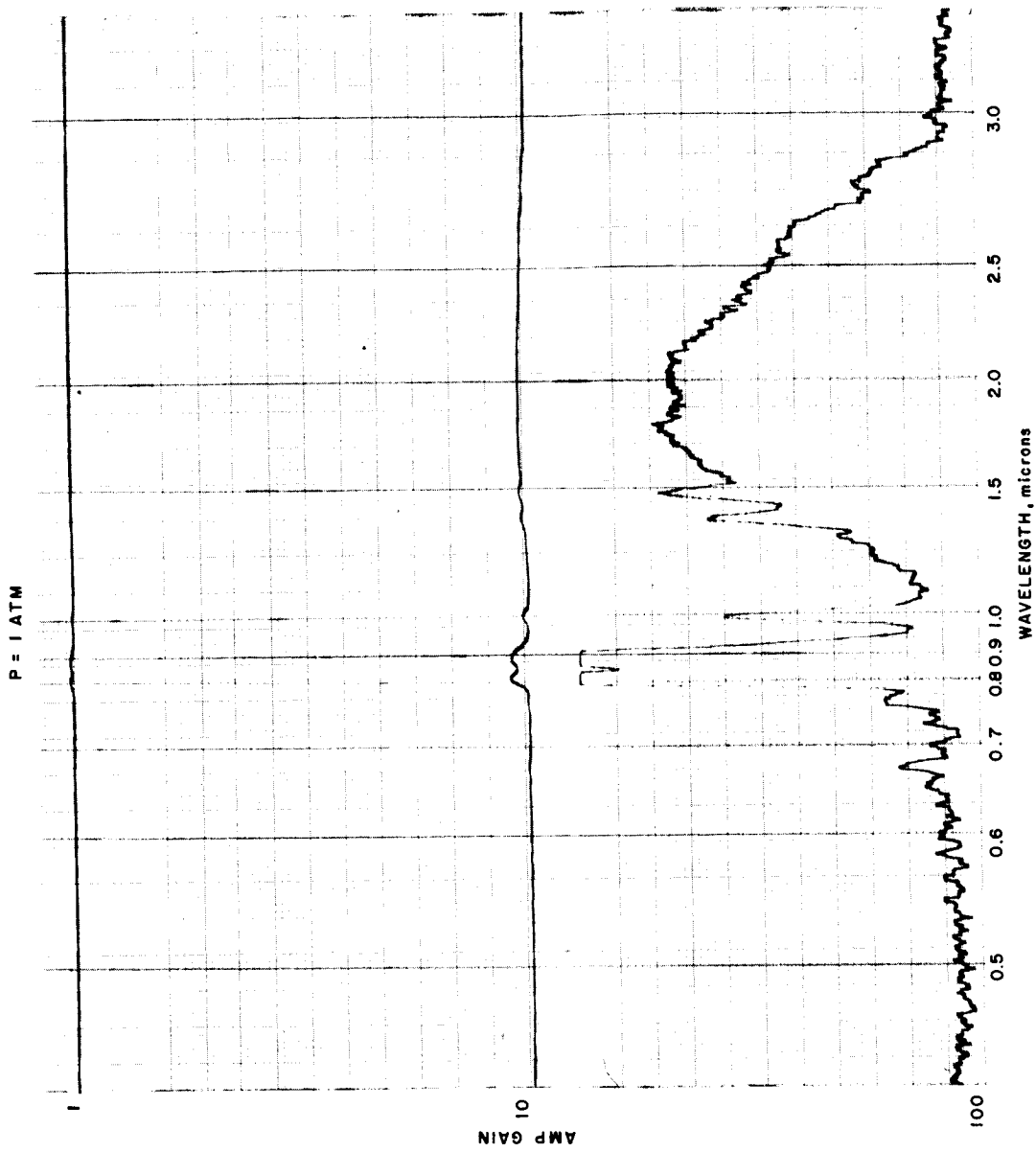


↑  
INTENSITY



65-5545

Figure 41 SPECTRAL RADIANCE OF ARGON AT 14,000°K FOR PRESSURES FROM 1 TO 6 ATMOSPHERES



65-5546

Figure 42 SPECTRAL RADIANCE OF ARGON WITH A TRACE OF CESIUM

## 2. Plasma Arc Lamps

The plasma discharge light source differs from the carbon arc source in that (a) it is, in general, of very high temperature and low emissivity, as compared to the low temperature and high emissivity of the carbon arc, and (b) it offers the possibility of additional light collection or flux enhancement owing to its transparency. Apart from these characteristics of the source, the optical considerations are little different from those which affect the carbon arc. Four specific plasma radiation sources were discussed in the source portion of this section.

The source, (V. A. 5. a) shown in figure 24, employs a spherical secondary collector and a paraboloidal primary collector. Thus, the exit beam will be mostly parallel rays with a diameter equal to the paraboloidal diameter. (Finite source size will introduce some convergence and divergence.) No concentrator is specified, although it would be either a second paraboloid or a lens. In the first case, higher flux would be obtained at the expense of experimental flexibility. The light-collection efficiency appears to be  $\sim 0.6$ , and the transmission efficiency is  $\sim 0.7$  for the specified elements. A concentrator will reduce this somewhat. The flux delivered to a sample will depend upon the concentrator chosen and will be a function of the desired working distance; however, we estimate it to be up to  $2 \text{ kw/cm}^2$  for sufficiently short working distances.

The arc system (V. A. 5. b) figures 25, specified no optics. However, it should be noted that it differs from the previous system (optically) only by having the anode on the same side as the cathode. Apart from effects this may have on the intrinsic source brightness, we see no clear optical advantage or drawback to this arrangement. Roughly, the fraction of the radiation intercepted by the electrodes is the same.

The device (V. A. 5. c) shown in figure 26 does not appear to be well suited for imaging without further arc development. The operation of the device requires the proximity of the envelope to the arc, and a large fraction of the radiation would thus be intercepted. This source is of particular value in that the spectral distribution and flux can be made to match the gas and flight conditions of interest. It does, however, limit model size and is somewhat nonuniform.

Finally, the unit (V. A. 5. d) shown in figure 23, is expected to deliver approximately  $1 \text{ kw/cm}^2$  (normal incidence) to a target with a working distance between the target and the final optical element of 21 inches. This large working distance makes it useful for combination with an arc-plasma generator to produce simultaneous convective heating. Alternatively, by replacing the lens with a second paraboloidal mirror and thus shortening the working distance considerably, a flux of up to  $4 \text{ kw/cm}^2$  may be achieved.

A general summary of the performance characteristics of the sources with respect to the attaining of the fluxes of the manned entry corridor, spatial uniformity, temporal uniformity, spectral distribution as compared to air, compatibility with a convection heating source, operation characteristics and equipment cost are all shown in table III.

TABLE III  
SOURCE EVALUATION SUMMARY

Source	Flux-Max	Size Limit (inches)	Uniformity	Time Stability	Spectral Match With Air	Compatibility with Convective Source	Remarks
Sun	3660 BTU/ft <sup>2</sup> sec	~ 1	Poor	Good	Fair	Fair	Cost moderate to high. Not available at Wilmington
Carbon Arc	915 BTU/ft <sup>2</sup> sec (3660 under pressure)	1/3	Poor	Poor	Fair	Fair to good	Cost low to moderate. Short-time operation.
Carbon Vapor Lamp	Unknown	~ 1/2	Poor	Medium	Poor to fair	Fair to good	Not in hardware stage
Electrical Resistors	300	Dependent only on size of power supply	Excellent	Excellent	Poor to fair	Fair to good	Low Cost - Great flexibility in size and shape.
High Pressure Compact Arcs	100-500	1-1/2	Poor	Good	Poor	Fair to good	Moderate to high cost. Continuous operation possible
Plasma Generator (Plasmadyne Type)	Good*	*	Poor to fair	Good	Poor to fair	Good*	Moderate to high cost. Continuous operation
Plasma Generator (Vitro Type)	Good*	*	Poor to fair	Good	Poor to fair	Good*	Moderate to high cost. Continuous operation
Plasma Generator (G. E. Tandem Gerdien)	1000 BTU/ft <sup>2</sup> sec	3/4	Poor to fair	Good	Good	Good but limited Model size	Moderate to high cost. Continuous operation
Plasma Generator (Avco RAD Type)	1000-4000 BTU/ft <sup>2</sup> sec	2 at maximum flux. Larger size with reduced flux	Poor to fair	Good	Poor to fair	Good	Moderate to high cost. Continuous operation
Electron Beam Laser	100 BTU/ft <sup>2</sup> sec 100,000 BTU/ft <sup>2</sup> sec for a 3/4-inch Model	2 3/4	Good Poor to fair	Good None	Poor to fair None	Poor Good	High Cost Moderate to high cost. Test time 2 x 10 <sup>-3</sup> sec.

See appropriate remarks in source description section for operational parameters.

\*Devices have not as yet been coupled with Optimum Optics, therefore performance not fully established.

## VI. RECOMMENDATIONS FOR FUTURE RESEARCH

The major problem observed during the study was the great void of information or data still needed to establish the relative importance of the flight parameters in simulation. This was not surprising as there is still considerable dispute as to the relative importance of the parameters present in flights that have only convective heating. Even though this problem has not been answered completely for convective heating, an attempt should be made to evaluate these requirements. As a first order, one relies on the experience gained from the extensive convective-heating testing that has been done. This experience would indicate that one should pay particular attention to the total flux (both convective and radiative), run time sufficient to obtain a steady-state performance, model size and source uniformity adequate to isolate material or heat-protection system performance, and enthalpy and radiant fluxes matched to the flight regime. The importance of flow chemistry, shear source spectral distribution, variation of conditions during run-matching total run time, and parameter variation may or may not be important, dependent on the particular trajectory and specific material under investigation. These are conclusions that one might make based on past experience in simulation testing. To establish their validity or to establish the actual importance of the several parameters requires additional information not presently available. To obtain this information, a study is recommended which could accomplish the following:

1. Determine the importance of matching the convective and radiative heat fluxes for the principal classes of heat-protection materials.
2. Establish the importance of spectral distribution of the radiative source on material performance.

Item 1 is undoubtedly the most complex of the two, as it would involve an evaluation of material emissivity, reflectance and opacity, surface conditions, boundary-layer blocking, etc. It also requires a rather flexible facility which can provide the required environments. Item 2 is somewhat less involved in that a single source which can operate on several different gases to produce several differing spectral distributions, all of which would have comparable total fluxes, would be used to test principal classes of heat-protection materials. If the latter study establishes the need to match the spectral distribution, a third program should be instituted. This program would investigate the selection of additives and source optimization for plasma arc devices. A suggested technical approach to this would comprise four phases. These are: (a) Choice of potential additives on analytical grounds, utilizing the known additive spectral properties and considering also the material compatibility for the final application; (b) measurement in a recently developed standard wall, stabilized constricted arc of the spectral radiation of those carrier-additive mixtures which appear most

promising, as a function of temperature and pressure; (c) calculation, using existing techniques and computer programs, of the arc parameters (current, dimensions, heat-removal rate, etc.,) required to produce the desired temperature-pressure conditions in a prototype compact arc infrared source; and, (d) design, manufacture and test of a prototype source using the results of the first three phases.

These programs, however, will require some time to pursue and complete, therefore, due to the immediate requirement for radiation simulation in this entry corridor, it is recommended that NASA - MSC obtain plasma generator radiation sources suitable for imaging on models being tested in the NASA - MSC 10-megawatt facility now under development. This type of source could be utilized in conjunction with the smaller arcs and facilities now present or being installed in the MSC laboratories; or even as a separate radiation facility until the larger arc facility is available.

APPENDIXES

- A. EXPERIMENTAL RADIATION MEASUREMENTS FROM SHOCK-HEATED FACILITIES
- B. ESTIMATES OF CONTINUUM RADIATION BASED ON EXPERIMENTAL RESULTS FROM AN ARC-HEATED PLASMA
- C. EVALUATION OF EXPERIMENTAL RESULTS OF A MATERIAL SUBJECT TO RADIATIVE HEATING
- D. THE EFFECT OF ELECTROMAGNETIC RADIATION ON SOLIDS
- E. REFERENCES



## APPENDIX A

### EXPERIMENTAL RADIATION MEASUREMENTS FROM SHOCK-HEATED FACILITIES

Comparison studies have been made of the radiation data obtained experimentally from shock-heated gas. Graphical representation of these data are shown in figures A-1 through A-4 for air as a function of flight velocity.

Figures A-1 through A-4 present shock-tube data for total stagnation-point-region equilibrium-radiation measured independently by four investigators (references 1, 6, 52-54) utilizing different measurement techniques. For convenience of comparison the stagnation-point region volumetric radiation was normalized using the relationship

$$E_t \propto (\rho/\rho_0)^{1.7} \cdot f(V_\infty) \quad (A-1)$$

where the above equation was suggested by reference 54 and 7. Figure A-5 is a composite comparison of the equilibrium data presented in figures A-1 through A-4. As will be subsequently pointed out in the following section, erroneous results were found in the data of references 53 and 6; however, figures A-1 through A-4 present these data in the corrected form.

#### 1. REDUCTION OF SHOCK-TUBE DATA

In the reduction of shock-tube data, heating rates of test surfaces, due to radiation from shock-heated gas, are distinguished from heating rates due to convective heat transfer by several means. For example, when the test probes have large nose radii, the radiative contribution at the stagnation point region is large enough to become the dominant mode of heat transfer, and direct measurements of radiation can be made using thin-film resistance thermometers or thick-film calorimeter gages (see reference 52). Another method is by means of locating on the test probe a transparent window through which incident radiant energy from the shock-heated gas cap is transmitted and collected by a thin-film radiative heat transfer gage. This latter technique was utilized by references 1, 6, and 53; however, references 1 and 53 used a hemispherical-faced probe while reference 6 used a blunt-faced probe. Finally, as was performed by reference 54, measurements utilizing photomultiplier tubes may be made of the total radiation from shock layers of gun-launched models flying in still air or moving upstream in the test section of a shock tunnel.

Once the above data is obtained, its reduction into terms of total radiation emitted from the stagnation point region requires further analysis. The first, and probably most important analysis, is determining whether the radiant energy so collected and measured is due primarily to nonequilibrium conditions, equilibrium conditions, or a combination of both in the shock-heated gas cap.

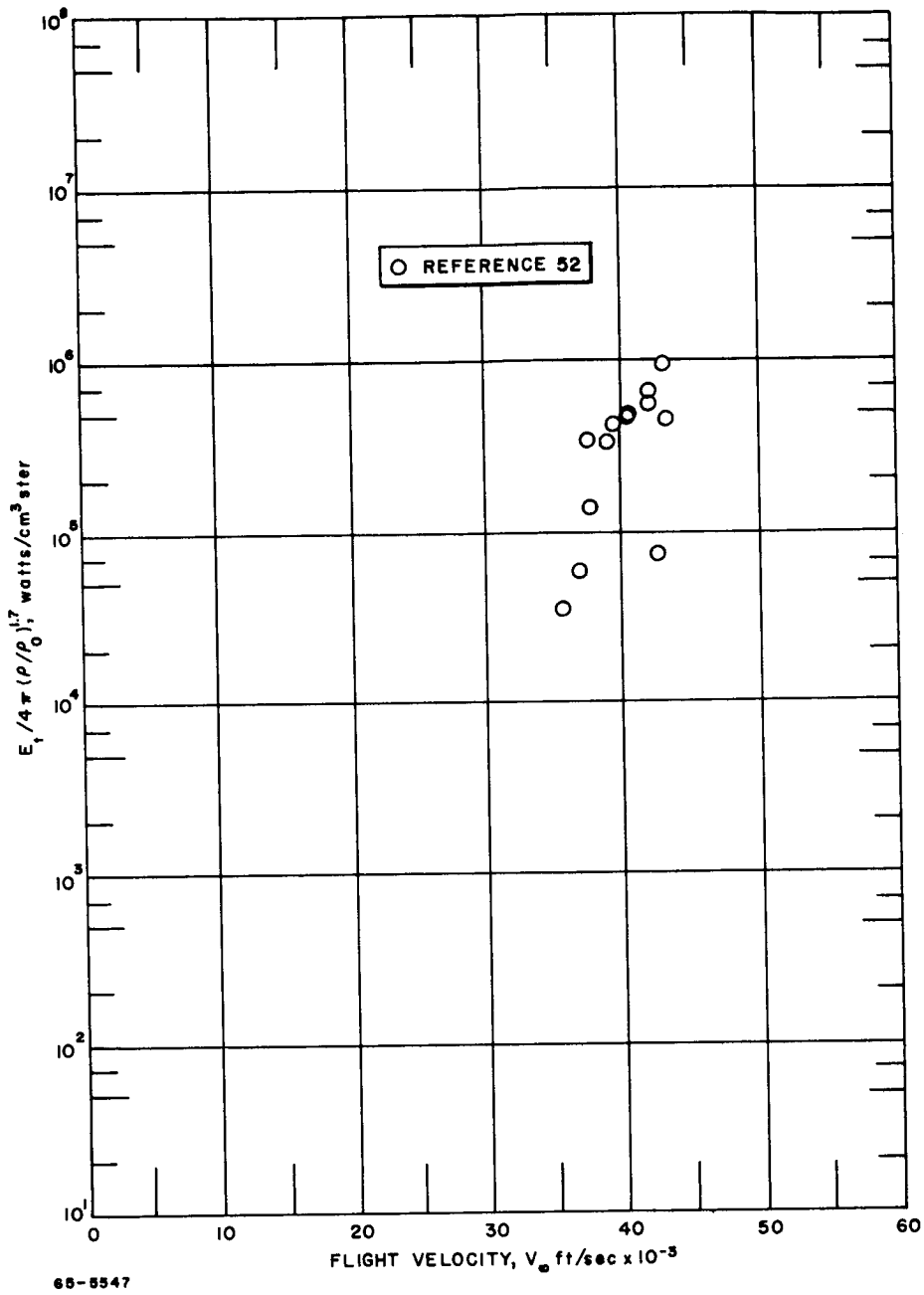


Figure A-1 NORMALIZED EQUILIBRIUM RADIATION DATA OF AIR VERSUS FLIGHT VELOCITY

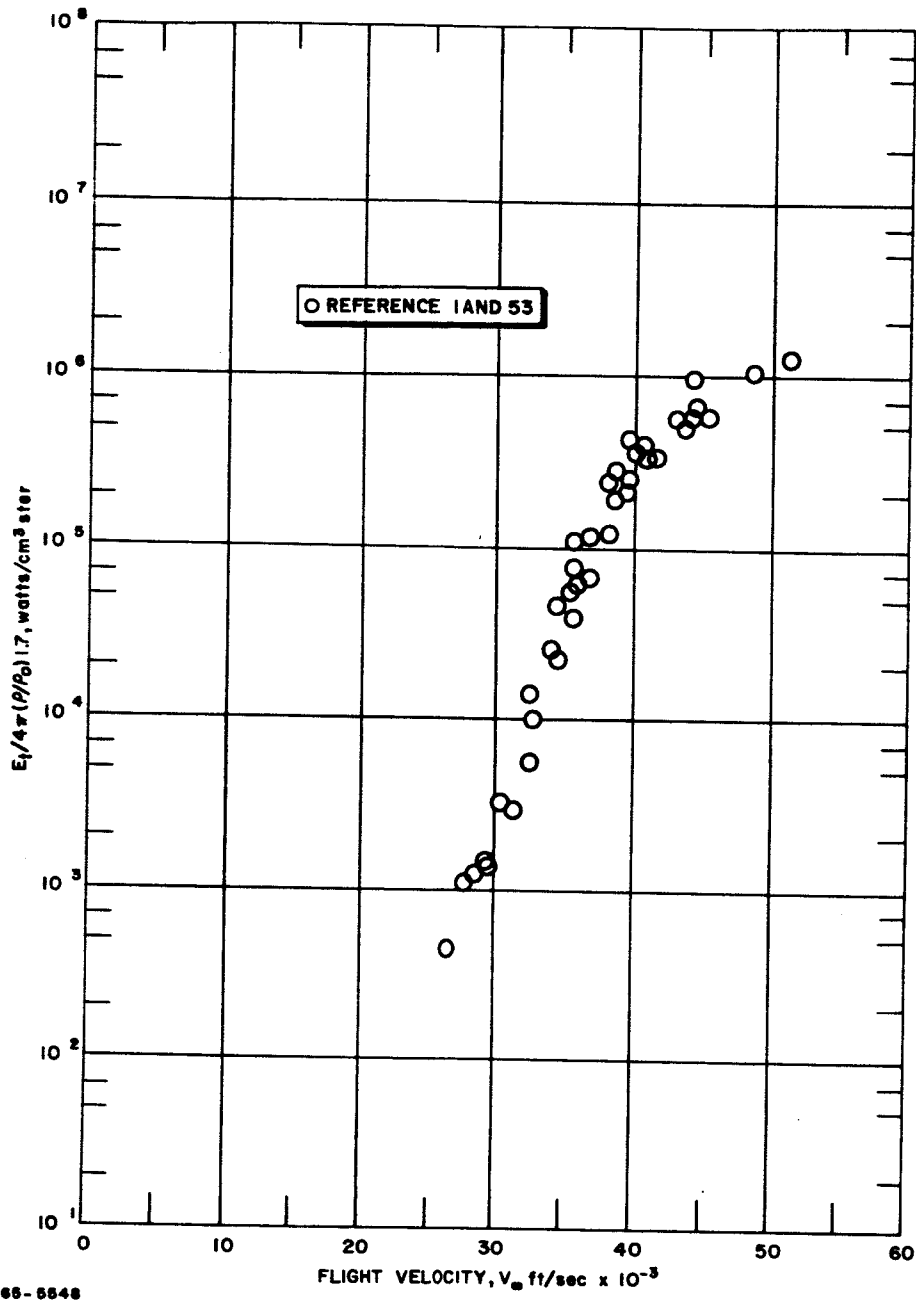


Figure A-2 NORMALIZED EQUILIBRIUM RADIATION DATA OF AIR VERSUS FLIGHT VELOCITY

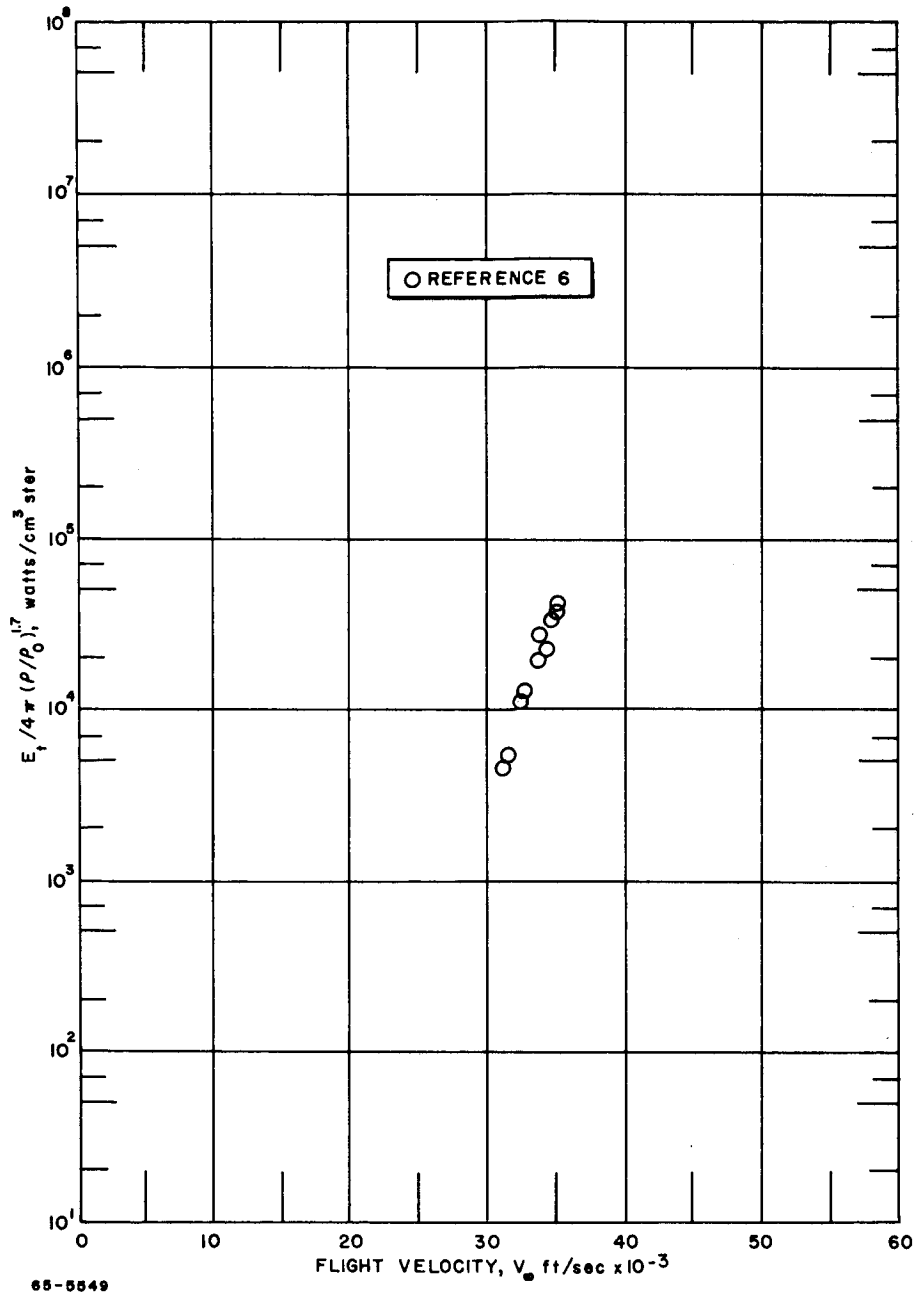


Figure A-3 NORMALIZED EQUILIBRIUM RADIATION DATA OF AIR VERSUS FLIGHT VELOCITY

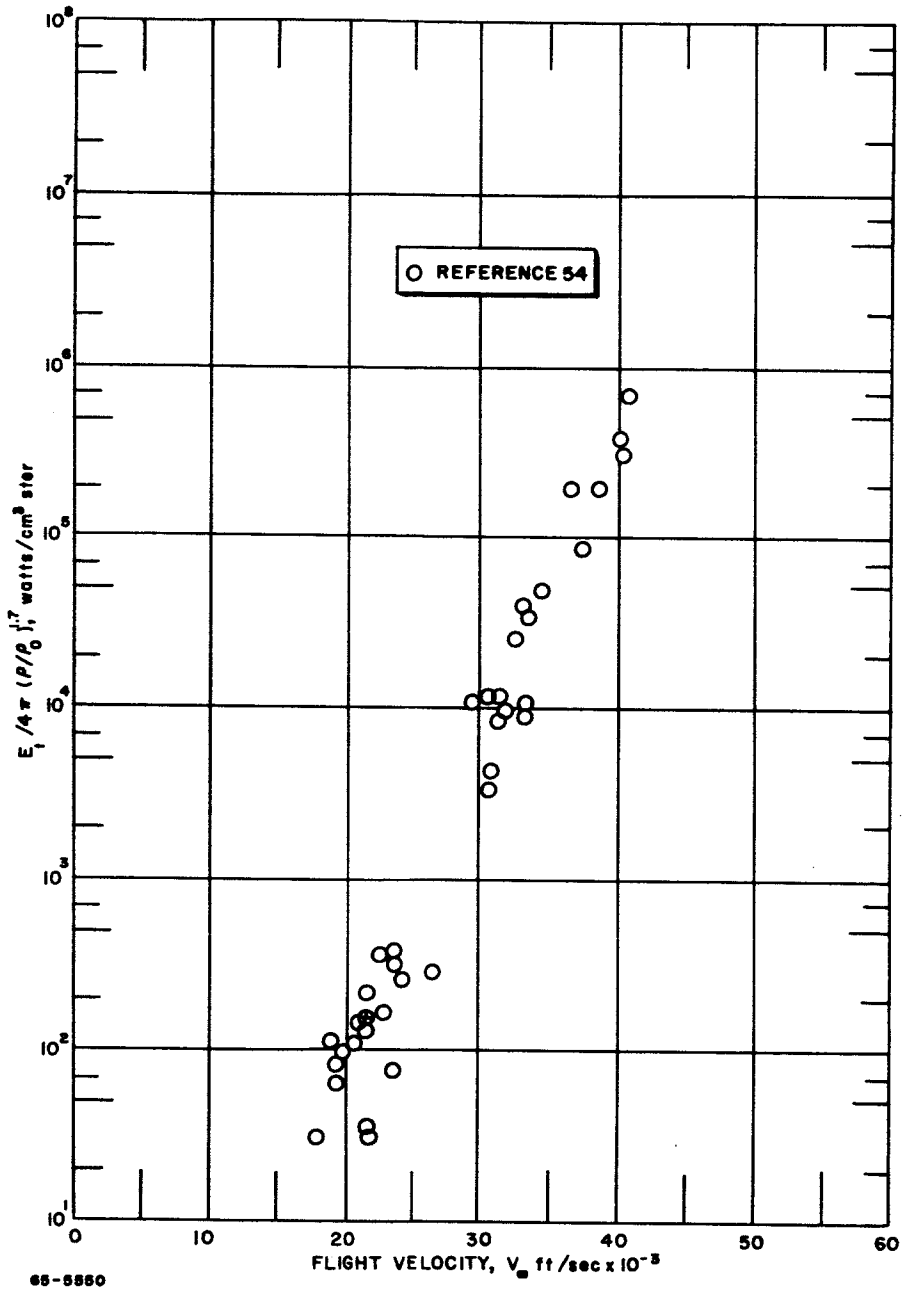


Figure A-4 NORMALIZED EQUILIBRIUM RADIATION DATA OF AIR VERSUS FLIGHT VELOCITY

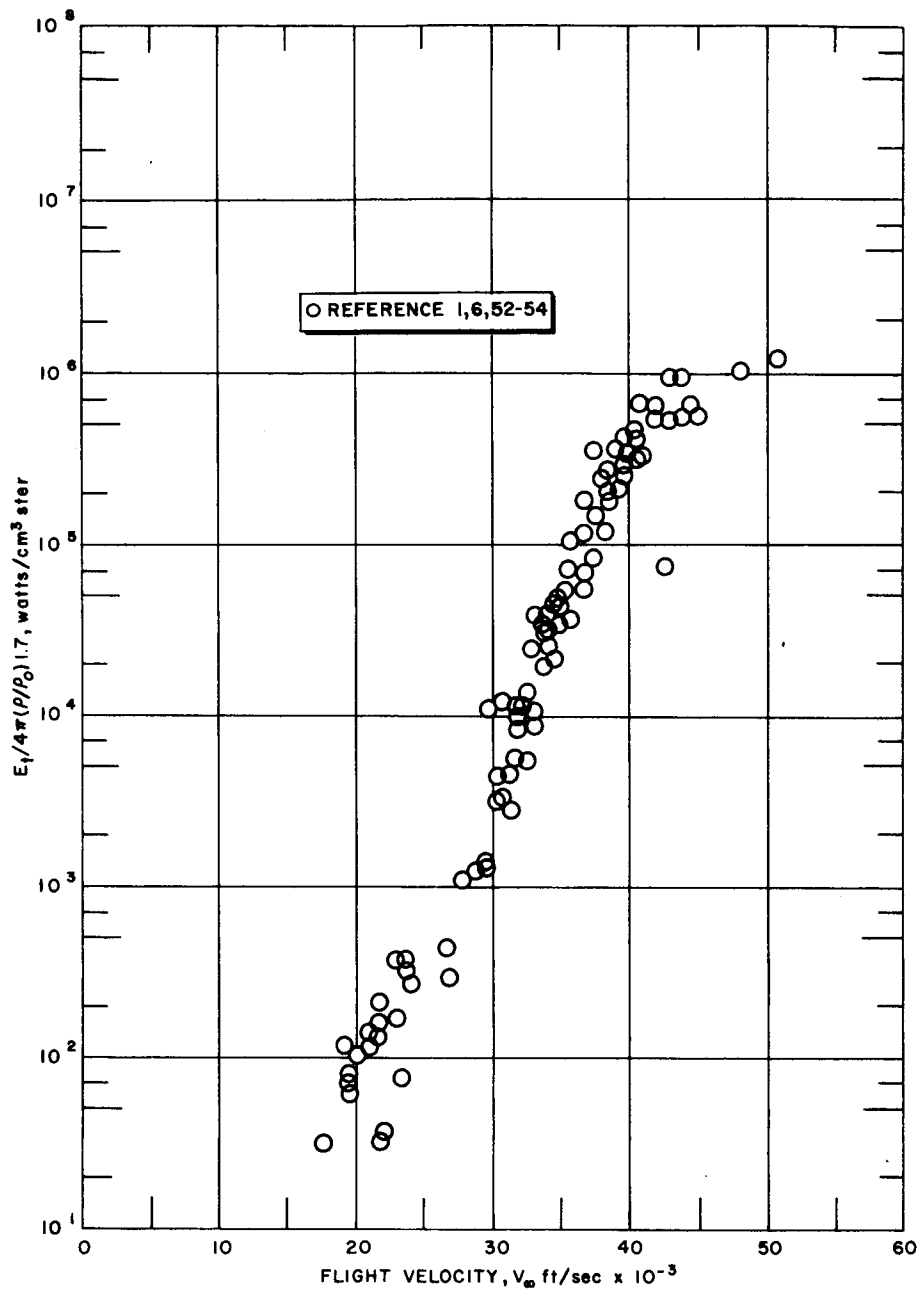


Figure A-5 COMPOSITE OF NORMALIZED EQUILIBRIUM RADIATION DATA OF AIR VERSUS FLIGHT VELOCITY

When equilibrium conditions are known to prevail and direct radiation measurements can be made, the total equilibrium radiation,  $E_t$ , at the stagnation point region, may be calculated from the following semi-empirical equation:

$$E_t = 2 \dot{q}_{\text{rad, stag. pt.}} / \delta F_1 \quad (\text{A-2})$$

where  $\dot{q}_{\text{rad, stag. pt.}}$  is the radiative power flux measured at the stagnation point region of the probe,  $\delta$  is the shock detachment distance and  $F_1$  is a correction factor taking into account the shape of the shock front and thermodynamic variations therein. It was reported by Nerem (references 1 and 53), who in turn referenced Wick<sup>55</sup>, that  $F_1$  is approximately 0.84, and the ratio  $\delta/R_N$  is approximately 0.045 for a probe of hemispherical-nose radius  $R_N$  in the flight-velocity range of  $20 \times 10^3$  to  $60 \times 10^3$  ft/sec and at simulated altitudes of  $100 \times 10^3$  to  $240 \times 10^3$  feet. In addition, it was reported Page<sup>54</sup> that the ratio  $\delta/R_N$  could also be closely approximated in the above flight range by the relationship

$$\delta/R_N = \frac{3}{4} \frac{\rho_\infty}{\rho} \quad (\text{A-3})$$

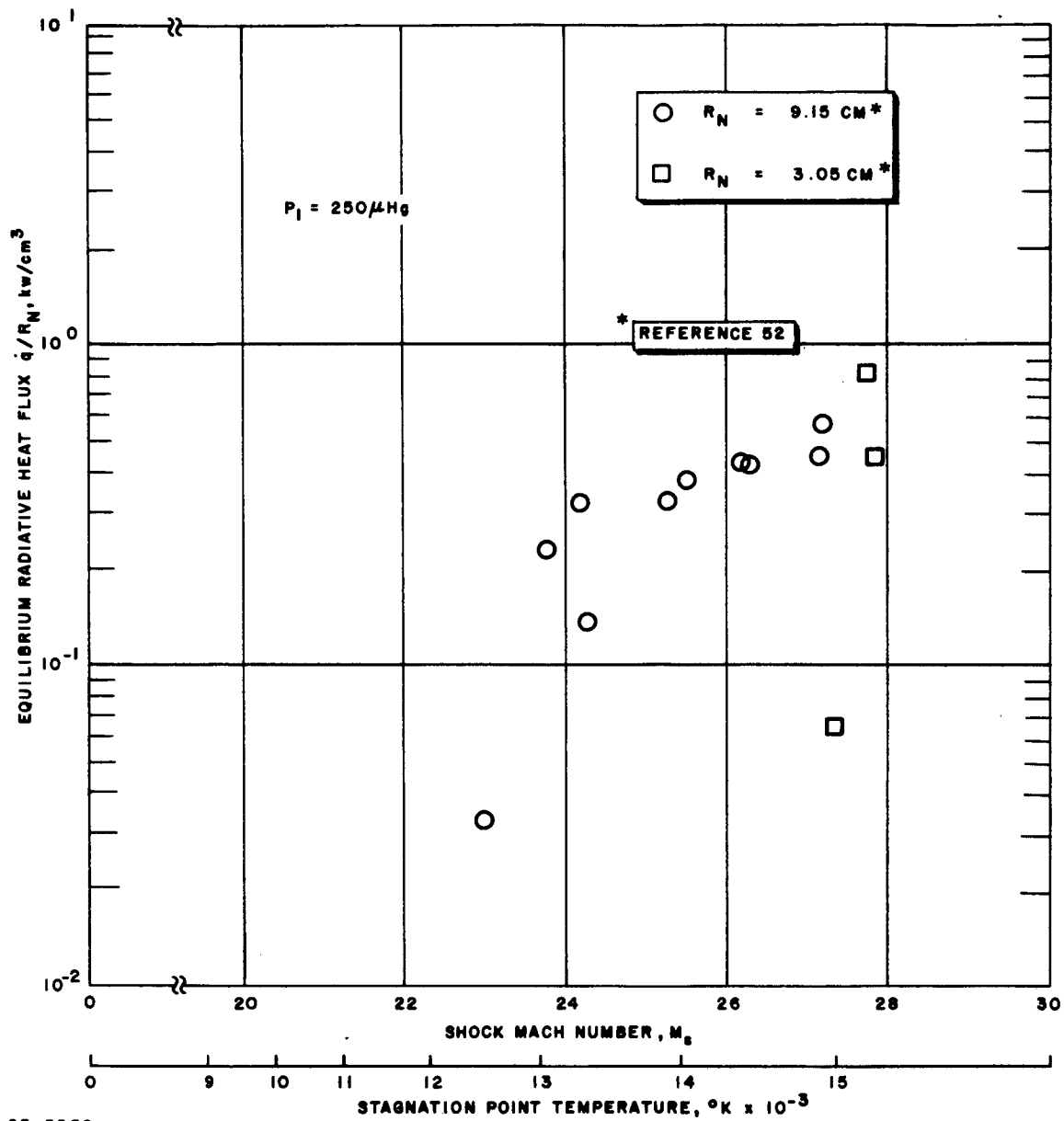
For test probes utilizing transparent windows, the total equilibrium radiation,  $E_t$ , may be calculated from a semi-empirical relation having the form:

$$E_t = 2 \dot{q}_{\text{rad, gage}} / \delta F_1 F_2(T) a_g \quad (\text{A-4})$$

where  $\dot{q}_{\text{rad, gage}}$  is the radiative power flux seen by the collector gage,  $F_2$  being its view factor and  $a_g$  its absorptivity.  $T$  is the transmission coefficient of the transparent window.  $F_1$  and  $\delta$  are as described above.

## 2. REDUCTION OF FLAGG'S DATA<sup>52</sup>

Flagg's data<sup>52</sup> were obtained in the form of figure A-6. It was necessary to correct his ratio  $\dot{q}/R_N$  into total equilibrium radiation,  $E_t$ , emitted from the stagnation point region. This was accomplished utilizing equation A-2. The choice of  $F_1$  and  $\delta$  values were those suggested by Wick<sup>55</sup>, since it was determined that Flagg's data simulated flight velocities and altitudes where Nerem<sup>1,53</sup> stated  $F_1 = 0.84$  and  $\delta/R_N = 0.045$ . Flagg's stagnation density ratios  $\rho/\rho_0$  and simulated flight velocities were determined using shock-tube gas dynamic charts.<sup>56</sup> By use of reference 56, all flight conditions for Flagg's data were known. Therefore it was of interest to compare Wick's<sup>55</sup> approximation of the ratio  $\delta/R_N$  against Page's<sup>54</sup> (equation A-3). Page's approximation<sup>54</sup> yields values of  $\delta/R_N$  for Flagg's data from  $\delta/R_N = 0.0625$  to  $0.0595$  (a discrepancy of approximately 30 percent). Hence, the shock-tube data so plotted in figure A-1 is questionable.



65-5552

Figure A-6 SHOCK-TUBE DATA REPORTED BY FLAGG



### 3. REDUCTION OF NEREM'S DATA 1, 53

Nerem 1, 53 published all of his data in a tabulated form giving initial shock-tube driven pressures,  $P_1$ , shock velocities,  $V_s$ , simulated flight velocity,  $V_\infty$ , stagnation density ratios,  $\rho/\rho_0$  etc. Thus no reduction of his data was necessary. However, by examining Nerem's data reduction procedure, it was established that he used shock-tube gas dynamic charts published by Ziemer<sup>57</sup>. Since Nerem's tabulated data gave adequate parameters, a comparison was made against the shock-tube gas dynamic charts published by Laird, J. D. and K. Heron.<sup>56</sup> Several discrepancies were found. Differences up to 25 percent was found in stagnation density ratios (Nerem's values being high). Nerem's calculated results indicating a constant stagnation density ratio  $\rho/\rho_0$  for a constant initial pressure  $P_1$  was also in disagreement with reference<sup>56</sup>. It was also established that Nerem overestimated his flight velocities,  $V_\infty$ , by 3 percent. Although these errors are comparable to shock-tube experimental scatter, the data so presented in figures A-1 through A-5 are very sensitive to density and flight velocity, and the magnification of the already present experimental scatter makes direct comparisons difficult. Nerem's density values were corrected using reference 56, and this data is shown in figures A-2 and A-5.

Another disturbing feature, brought out by the above discrepancies, is the shock-detachment distances,  $\delta$ , calculated by Nerem in his data reduction (see equations A-3 and A-4). The means used by Nerem to determine his shock-detachment distance,  $\delta$ , is not known at this time. However, if it were calculated from equation (A-3), then his detachment distances are questionable (upward to 25 percent) also. Therefore, the reliability of Nerem's data as shown in figures A-2 is questionable.\*

### 4. REDUCTION OF HOSHIZAKI DATA<sup>6</sup>

Hoshizaki's<sup>6</sup> results were presented in his report in the form of figure A-7. As seen in figure A-7, Hoshizaki's data was calculated to have a stagnation density ratio of .193 for an initial pressure  $P_1 = 1.16$  mm Hg.\*\*

An investigation of the data was made utilizing the shock-tube gas dynamic charts of reference<sup>56</sup>. A discrepancy of 25 percent in stagnation density ratio was found (Hoshizaki's value being high). Hoshizaki did not reference use of any gas dynamic charts; however, it was learned<sup>58</sup> that Hoshizaki used Ziemer's<sup>57</sup> charts and, after publication, was aware that Ziemer's charts were outdated. No further investigation was made into the reduction procedures used by Hoshizaki. As presented in figures A-3 and A-5, his data has been corrected using reference 56.

\* Prior to publication of this report, a telephone conversation with R. Nerem revealed that he was aware, after his publication, that the Ziemer charts<sup>57</sup> were outdated. However Nerem stated that his shock detachment distances were obtained experimentally and were not dependent on the density relation given in equation (A-3).

\*\* It is of interest to note that Nerem<sup>1</sup> and<sup>53</sup> reported this same data in his report as  $\rho/\rho_0 = 0.16$  and  $P_1 = 1.0$  mm Hg.

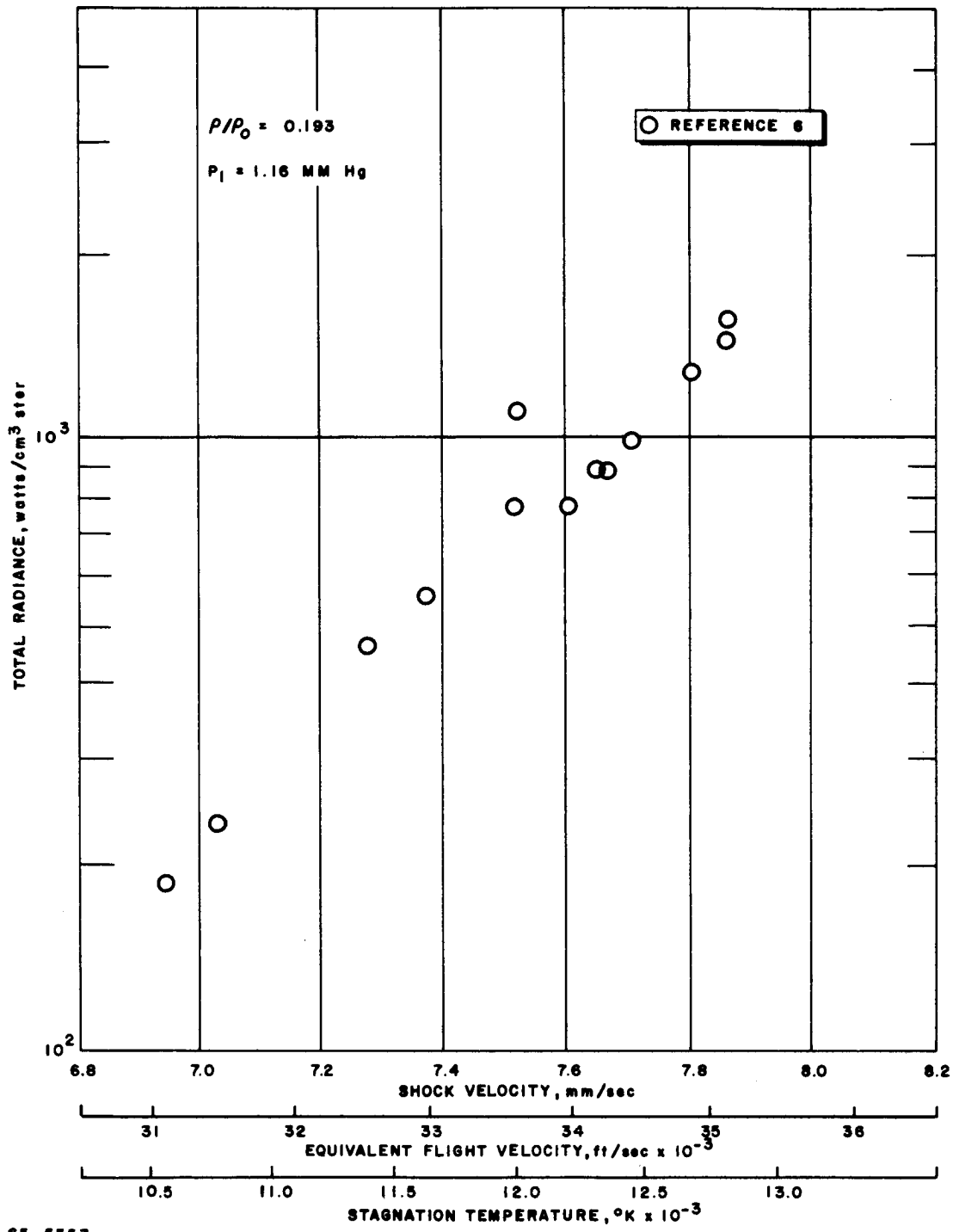


Figure A-7 SHOCK-TUBE DATA REPORTED BY HOSHIZAKI

## 5. REDUCTION OF PAGE'S DATA<sup>54</sup>

Page, W. A., et al<sup>54</sup> tabulated his experimental results in a form where no reduction of his data was necessary. His equilibrium radiation data are plotted in figures A-4 and A-5.

Though Page et al<sup>54</sup> cited Ziemer's gas dynamic charts, it is not clear as to the extent they were used as Feldman's charts<sup>59</sup> were also cited. If Ziemer's were used, the calculated density ratios should be questioned.\* As was noticed in the data of Nerem<sup>1, 53</sup> and Hoshizaki<sup>6</sup>, Ziemer's charts tend to overestimate these ratios for a given set of initial shock-tube conditions with the discrepancies being more pronounced at the higher density values. Therefore, it must be concluded that Page's data so plotted in figures A-4 and A-5 are also questionable in excess of their exhibited experimental scatter.

## 6. CONCLUSIONS AND GENERAL REMARKS

As pointed out in the preceding sections, published radiation data obtained via shock-heated gas experiments is questionable as it is greatly influenced by the reliability of gas dynamic charts and theoretical models used in describing the gas cap. However, it must be argued that the above described means for obtaining radiative data are representative of each other within approximately a factor of 2 (see figure A-5).

---

\*It should be noted here that until recent time, gas dynamic charts by Feldman<sup>59</sup> have been widely used in shock-tube work. Feldman's charts were recently expanded in terms of flight conditions and are represented by reference 56. It is generally accepted that reference 56 represents the present state-of-the-art in shock-tube gas dynamic charts.

## APPENDIX B

### ESTIMATES OF CONTINUUM RADIATION BASED ON EXPERIMENTAL FROM AN ARC-HEATED PLASMA

The purpose of this section is to present estimates of the continuous spectrum from free-free and free-bound transitions of electrons in the field of ions and neutral atoms from high temperature air based on preliminary analysis of experimental results which were obtained spectroscopically from arc-heated plasmas. Comparison of these estimates are made with theory and shock-tube data. Estimates of vacuum UV radiation are also presented.

#### 1. ESTIMATES OF THE CONTINUOUS SPECTRUM

Utilizing a mechanically constricted arc technique, Morris et al<sup>60</sup> have obtained continuum radiation data of high temperature oxygen and nitrogen gases at atmospheric pressure for equilibrium gas temperatures of 9,000 to 14,000°K over the 0.25 $\mu$  to 2.5 $\mu$  spectral range.

The plasma diagnostic techniques and experimental apparatus used by Morris<sup>60</sup> are described in last portion of this appendix.

These experimental data were curve-fitted into expressions similar to Kramers' Unsold semiclassical approximation<sup>61</sup> as:

$$E_c^{(a)} = 1.425 \times 10^{-34} T^{1/2} n_e \sum_i \gamma_i n_i \text{ watts/cm}^3 \quad (\text{B-1})$$

where  $E_c^{(a)}$  is the continuum radiation per unit gas volume of chemical species, a, at Kelvin temperature T;  $\gamma_i$  is a variable coefficient dependent upon the number density,  $n_i$ , of the *i*th constituent; and  $n_e$ , is the total electron number density of the gas.

The total continuum radiation,  $E_c$ , from air was then estimated by the relation

$$E_c = \sum_a E_c^{(a)} \quad (\text{B-2})$$

Since equation (B-2) depends only on temperature and number densities of given chemical species, extension of Morris<sup>60</sup> original data was made for air at various pressure levels utilizing gas compositions of Burhorn and Wienecke<sup>62</sup> and Flinn.<sup>63</sup> The results of these calculations are presented in table B-I at pressure levels of 0.1, 0.3, 1.0, 3.0, 10, and 30 atmospheres and at equilibrium gas temperatures ranging from 9,000 to 20,000°K. For convenience, tabulated values of enthalpy,<sup>62,63</sup> density ratios,<sup>62,63</sup> and simulated flight velocities are also presented.

TABLE B-I

CONTINUUM RADIATION DATA OF AIR

(0.25 $\mu$  - 2.50 $\mu$ )

Pressure P Atmosphere	Temperature T °Kelvin	Radiation $E_c/4\pi$ watts/cm <sup>3</sup> ster	Density Ratio $\rho/\rho_0$	Enthalpy $h$ ergrs/gram	Flight Velocity $V_{\infty}$ feet/sec
1.0 E-1	9 E3	4.68 E-2	1.48 E-3	4.68 E11	3.17 E4
1.0 E-1	10 E3	1.63 E-1	1.27 E-3	5.43 E11	3.41 E4
1.0 E-1	12 E3	1.10 E-0	8.42 E-4	8.91 E11	4.37 E4
1.0 E-1	14 E3	2.24 E-0	5.52 E-4	1.41 E12	5.50 E4
1.0 E-1	16 E3	2.29 E-0	4.39 E-4	1.67 E12	6.00 E4
1.0 E-1	18 E3	1.99 E-0	3.82 E-4	1.79 E12	6.20 E4
1.0 E-1	20 E3	1.70 E-0	3.40 E-4	1.89 E12	6.37 E4
3.0 E-1	9 E3	2.16 E-1	4.48 E-3	4.54 E11	3.12 E4
3.0 E-1	10 E3	6.87 E-1	3.91 E-3	5.07 E11	3.29 E4
3.0 E-1	12 E3	4.91 E-0	2.80 E-3	7.36 E11	3.97 E4
3.0 E-1	14 E3	1.44 E+1	1.86 E-3	1.18 E12	5.05 E4
3.0 E-1	16 E3	1.87 E+1	1.37 E-3	1.57 E12	5.82 E4
3.0 E-1	18 E3	1.75 E+1	1.16 E-3	1.75 E12	6.14 E4
3.0 E-1	20 E3	1.53 E+1	1.02 E-3	1.86 E12	6.33 E4
1.0 E-0	9 E3	1.27 E-0	1.52 E-2	4.25 E11	3.02 E4
1.0 E-0	10 E3	3.94 E-0	1.33 E-2	4.65 E11	3.16 E4
1.0 E-0	12 E3	2.77 E+1	9.86 E-3	6.18 E11	3.64 E4
1.0 E-0	14 E3	1.03 E+2	6.86 E-3	9.54 E11	4.53 E4
1.0 E-0	16 E3	1.70 E+2	4.88 E-3	1.37 E12	5.42 E4
1.0 E-0	18 E3	1.84 E+2	3.94 E-3	1.63 E12	5.91 E4
1.0 E-0	20 E3	1.64 E+2	3.43 E-3	1.76 E12	6.15 E4
3.0 E-0	9 E3	6.21 E-0	4.70 E-2	4.07 E11	2.96 E4
3.0 E-0	10 E3	1.85 E+1	4.08 E-2	4.48 E11	3.10 E4
3.0 E-0	12 E3	1.26 E+2	3.10 E-2	5.59 E11	3.47 E4
3.0 E-0	14 E3	5.17 E+2	2.28 E-2	7.93 E11	4.13 E4
3.0 E-0	16 E3	1.11 E+3	1.63 E-2	1.16 E12	4.99 E4
3.0 E-0	18 E3	1.40 E+3	1.26 E-2	1.49 E12	5.66 E4
3.0 E-0	20 E3	1.38 E+3	1.06 E-2	1.69 E12	6.03 E4
1.0 E+1	9 E3	3.40 E+1	1.66 E-1	3.66 E11	2.80 E4
1.0 E+1	10 E3	9.20 E+1	1.40 E-1	4.27 E11	3.08 E4
1.0 E+1	12 E3	6.49 E+2	1.07 E-1	5.20 E11	3.34 E4
1.0 E+1	14 E3	2.76 E+3	8.30 E-2	6.72 E11	3.81 E4
1.0 E+1	16 E3	7.26 E+3	6.17 E-2	9.37 E11	4.49 E4
1.0 E+1	18 E3	1.16 E+4	4.65 E-2	1.26 E12	5.20 E4
1.0 E+1	20 E3	1.33 E+4	3.76 E-2	1.53 E12	5.73 E4
3.0 E+1	9 E3	1.49 E+2	5.48 E-1	3.12 E11	2.59 E4
3.0 E+1	10 E3	4.93 E+2	4.41 E-1	3.94 E11	2.91 E4
3.0 E+1	12 E3	3.05 E+3	3.28 E-1	4.99 E11	3.27 E4
3.0 E+1	14 E3	1.28 E+4	2.62 E-1	6.06 E11	3.60 E4
3.0 E+1	16 E3	3.76 E+4	2.03 E-1	7.96 E11	4.13 E4
3.0 E+1	18 E3	7.12 E+4	1.55 E-1	1.06 E12	4.77 E4
3.0 E+1	20 E3	9.59 E+4	1.23 E-1	1.39 E12	5.39 E4

The simulated flight velocities,  $V_\infty$ , were calculated via the conservation of energy law as:

$$V_\infty \approx \sqrt{2h_s}$$

$$h_s \gg h_\infty \tag{B-3}$$

where, for normal shock solutions, the thermodynamic conditions of state listed in table B-1 are considered to be those of the gas cap's stagnation region.

Figures B-1 through B-4 are graphical plots of the tabulated values presented in table B-1. Figure B-5 is a cross plot of figure B-2. In figure B-5, a dashed curve representing the 30-atmosphere level was generated to provide somewhat of an upper bound for equations (B-1) and (B-2) since the original data were obtained at one atmosphere.

## 2. COMPARISON WITH THEORY

Figure B-6 presents for comparison purposes theoretical predictions of total equilibrium air radiation,  $E_t$ .<sup>16, 17</sup> Superimposed on figure B-6 are the extended estimates of continuum radiation,  $E_c$ , based on Morris et al<sup>60</sup> data. As seen, agreement with theory is only favorable at density ratios of about  $10^{-1}$ . This difference may be explained by the following: The theories of references 16 and 17 are considered for the spectral range in question to represent the total equilibrium radiation. Their approximate theoretical treatments, whose accuracy is not definitely known, was based on rather indirect and somewhat uncertain comparisons with a few experimental observations. Their treatments do not include atomic- and ionic-line radiation. Preliminary measurements by Morris et al<sup>60</sup> have indicated that these latter radiative mechanisms at atmospheric pressure, both in the case of nitrogen and oxygen, are comparable to that measured for continuum. \*\* Hence in terms of total radiation,  $E_t$ , Morris et al<sup>60</sup> continuum data,  $E_c$ , should be multiplied by approximately a factor of 2. This then makes a favorable comparison with the magnitudes of the above theories at the  $10^{-3}$  and  $10^{-2}$  density ratios.

## 3. COMPARISON WITH-SHOCK TUBE DATA

Total equilibrium radiation data of air obtained via shock tube analysis<sup>1,6,52-54</sup> have been compiled and reported in appendix A. A comparison of these data was made with the above estimates obtained via arc heated plasma columns. Figure 9 presents the shock tube data normalized by the relation.

$$E_t / (\rho / \rho_0)^{1.7} \text{ af } (V_\infty) \tag{B-4}$$

\* These theories were particularly chosen for the comparison, as they in general cover the same spectral range as the present estimates.

\*\* Measured between 9,000 to 14,000°K.

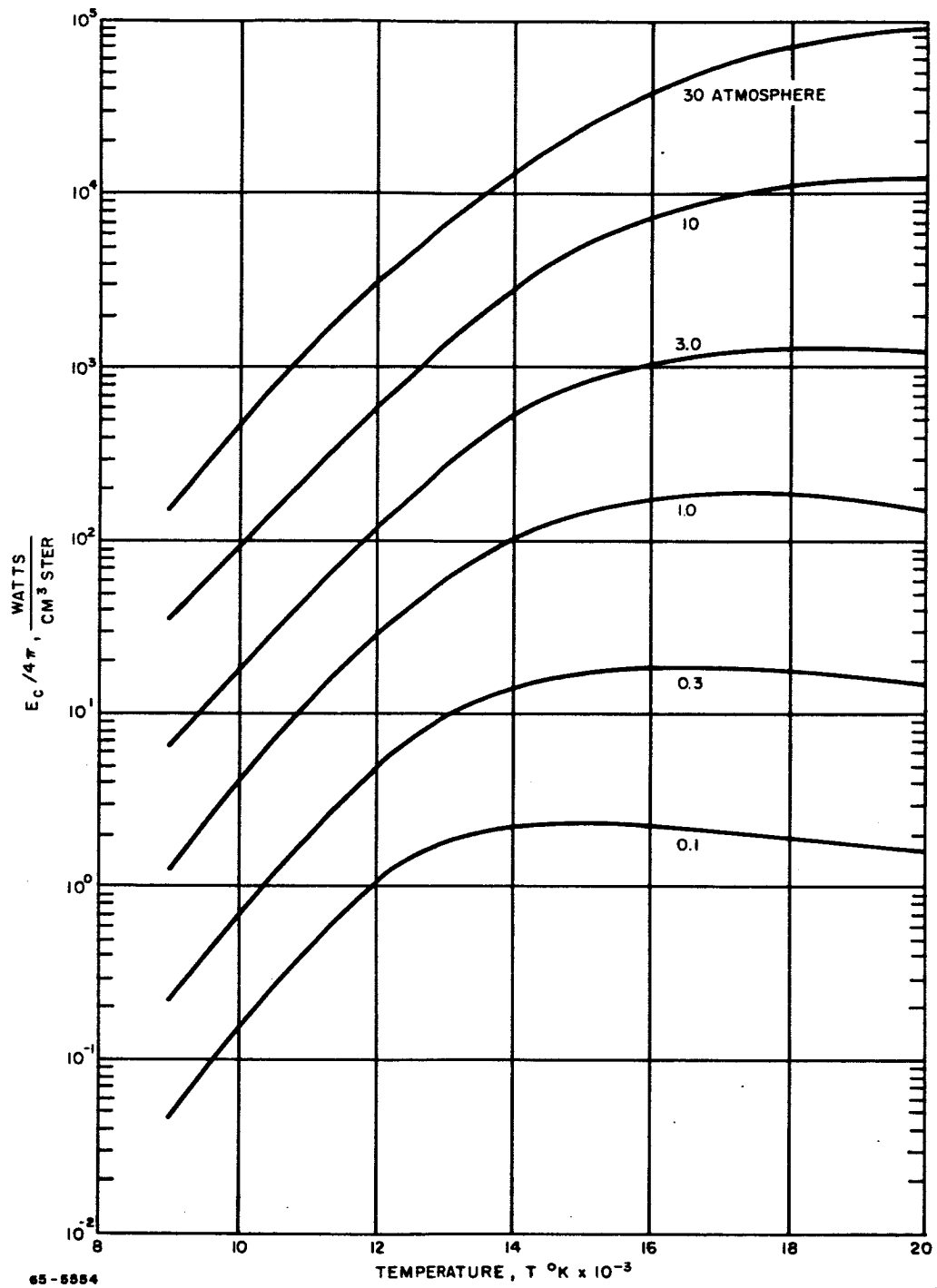
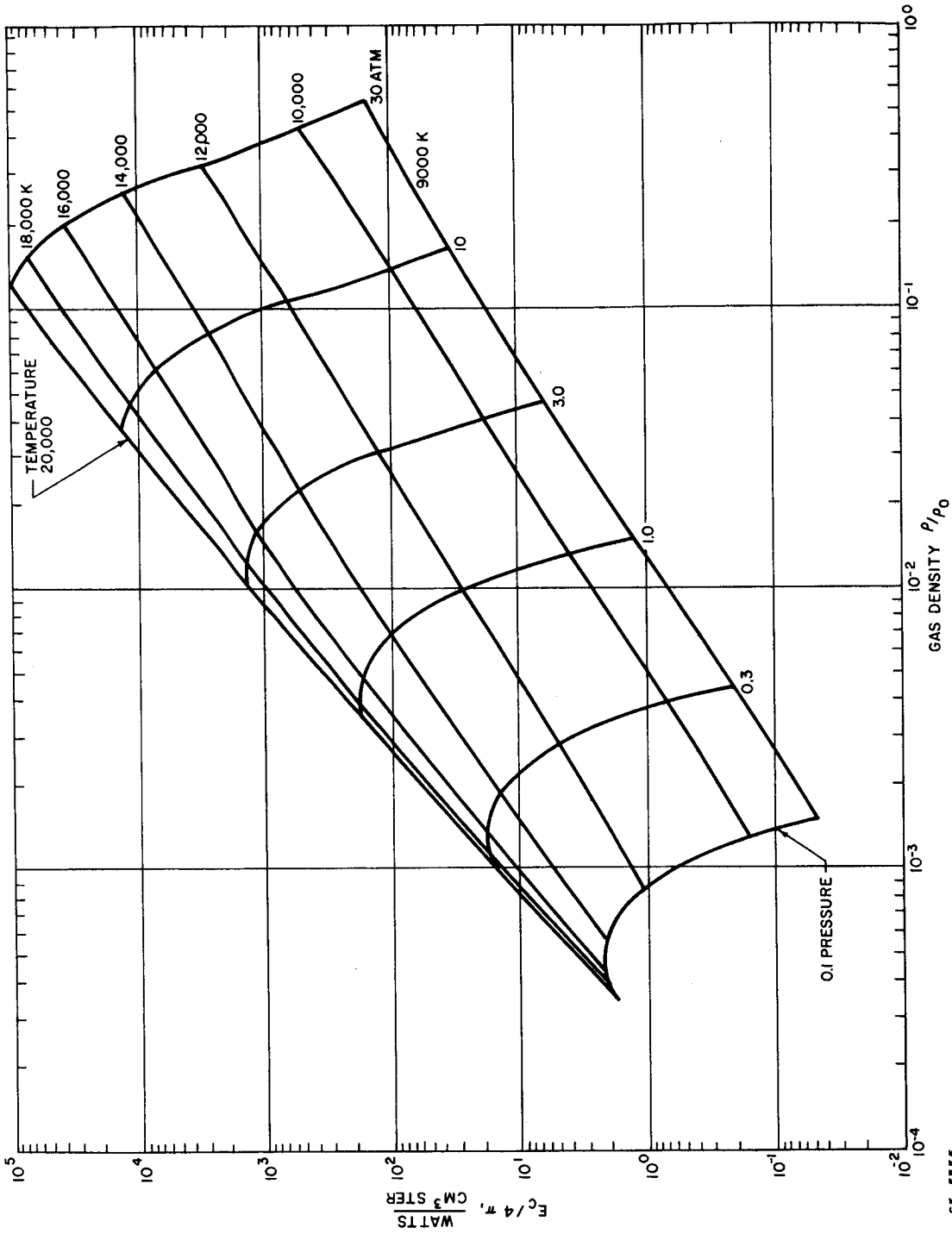


Figure B-1 CONTINUUM RADIATION OF AIR VERSUS TEMPERATURE AT CONSTANT PRESSURES



65-5555

Figure B-2 CONTINUUM RADIATION OF AIR VERSUS DENSITY AT CONSTANT PRESSURES AND TEMPERATURES



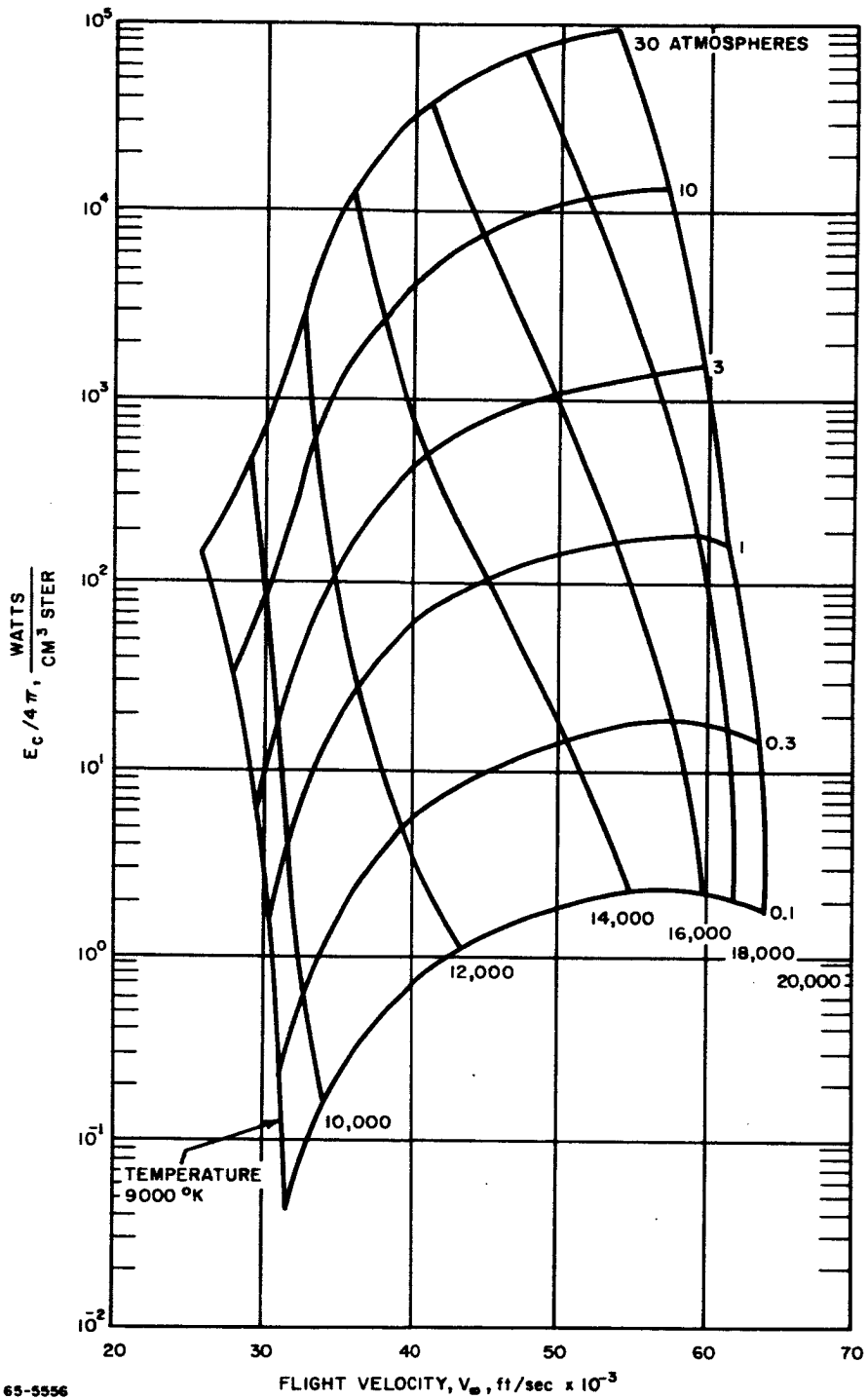


Figure B-3 CONTINUUM RADIATION OF AIR VERSUS FLIGHT VELOCITY AT CONSTANT PRESSURES AND TEMPERATURES

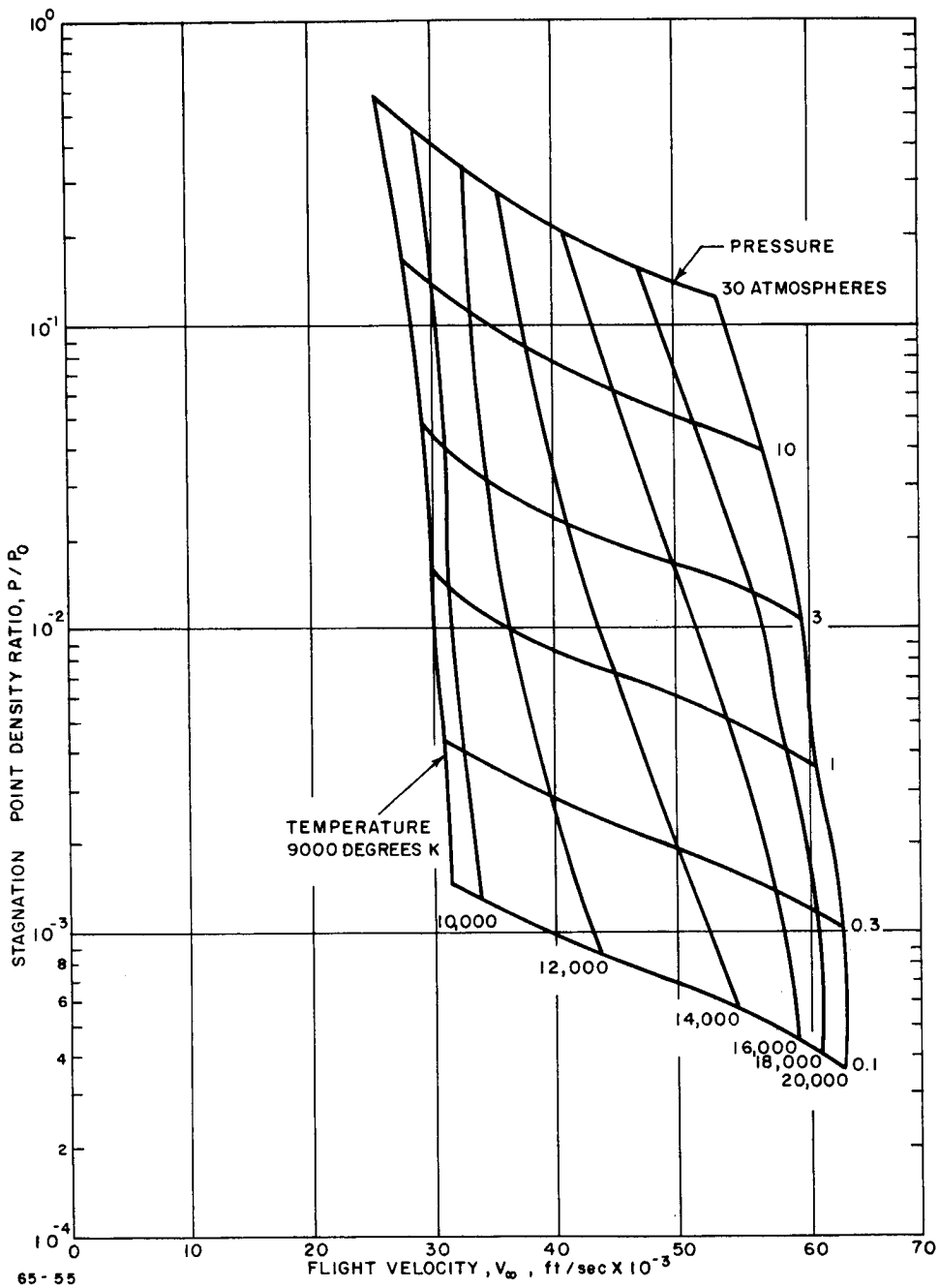


Figure B-4 DENSITY OF AIR VERSUS FLIGHT VELOCITY AT CONSTANT PRESSURES AND TEMPERATURES

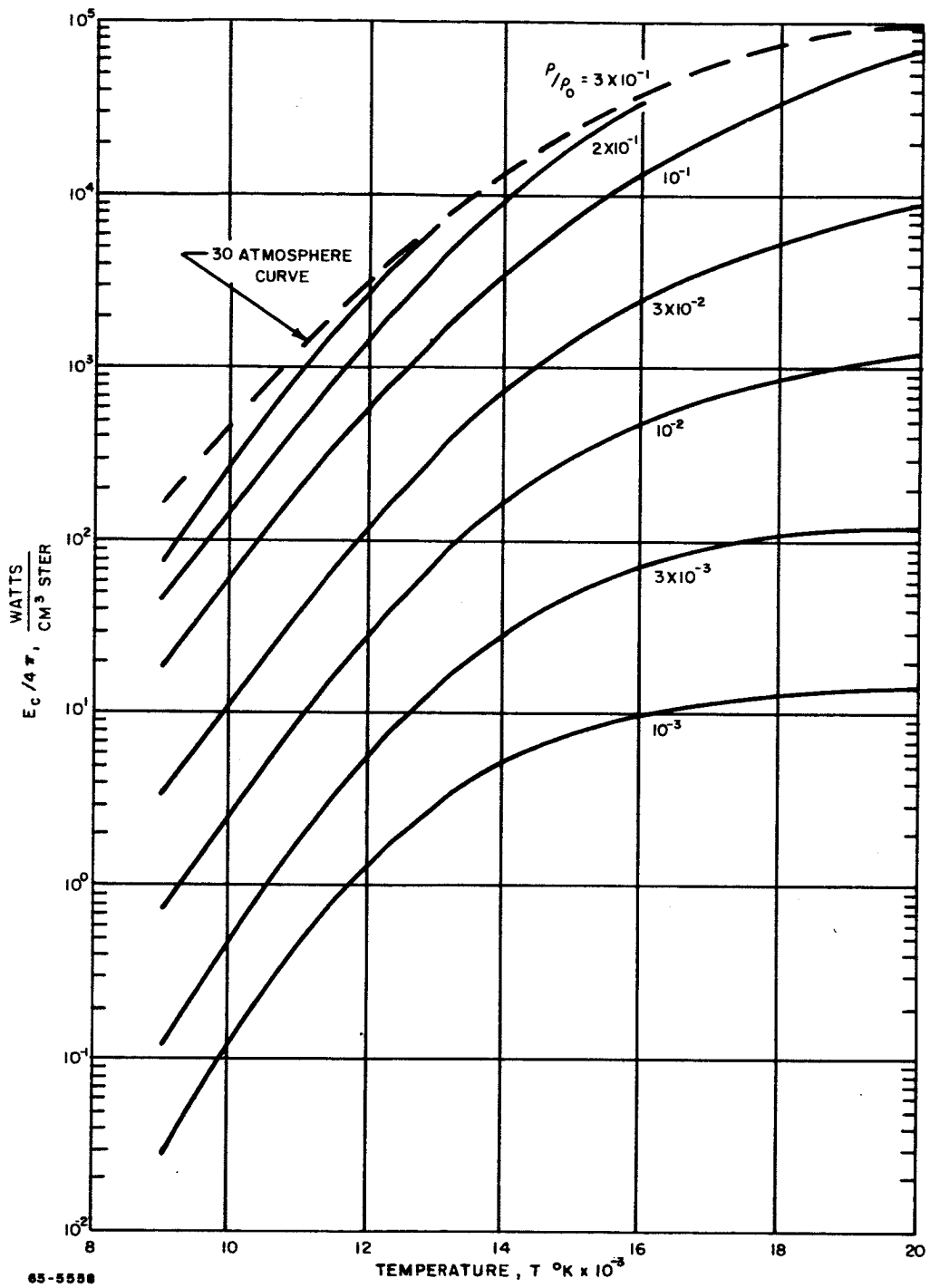


Figure B-5 CONTINUUM RADIATION OF AIR VERSUS TEMPERATURE AT CONSTANT DENSITY

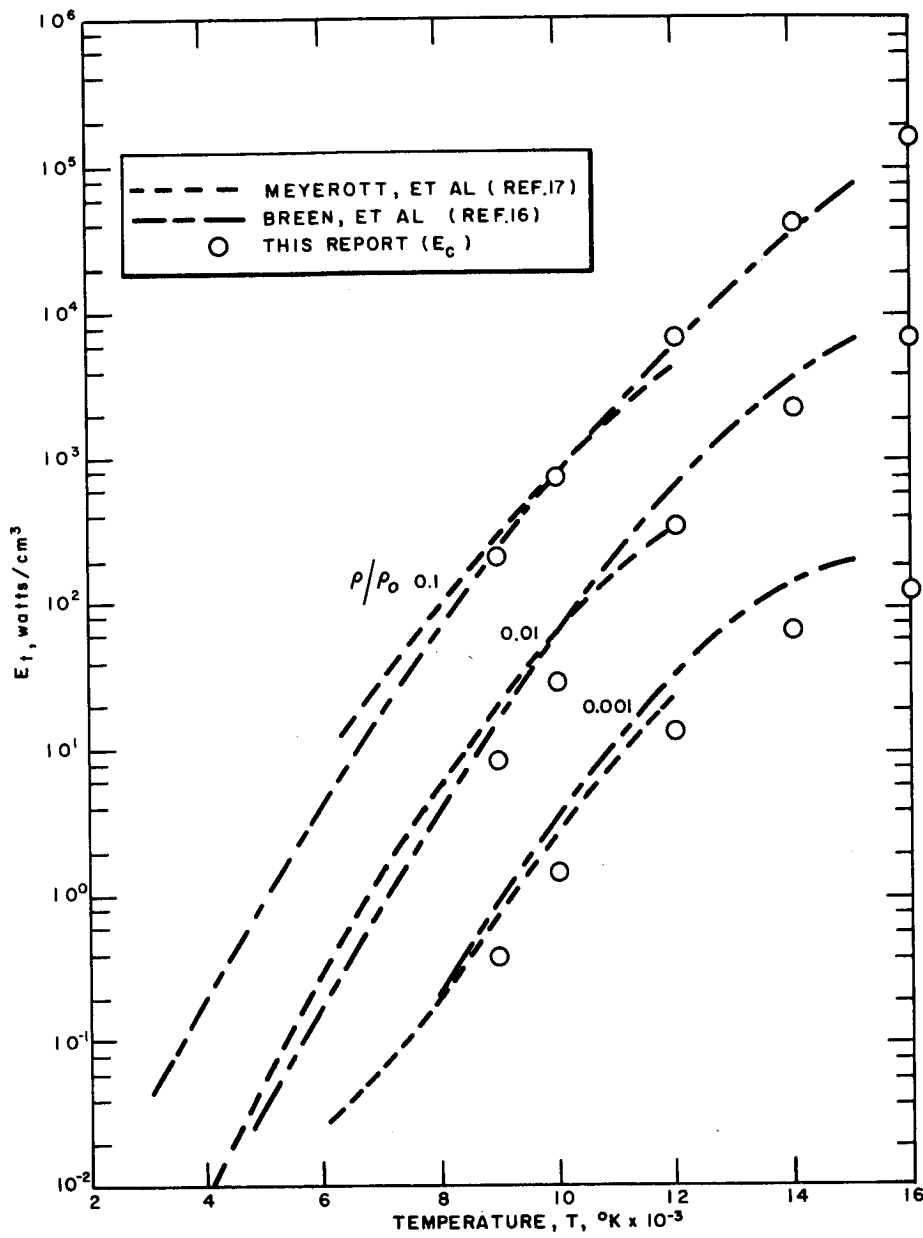


Figure B-6 TOTAL EQUILIBRIUM AIR RADIATION VERSUS TEMPERATURE AT CONSTANT DENSITY RATIOS (THEORY VERSUS EXTENDED DATA)

where the above normalization was suggested by references 54 and 7.\* Superimposed on figure 9 are equilibrium air-radiation estimates  $E_c$  and  $E_t$  of Morris. As demonstrated favorable agreement is made with these shock-tube data.\*\*

#### 4. UV-RADIATION

As mentioned previously the above estimates represent the near UV, visible and near IR-regions of the spectrum. Current theories<sup>2, 15</sup> however, indicate that at the higher temperatures of interest the integrated continuum spectrum of the vacuum UV-region is of the same magnitude as the total value previously predicted<sup>16, 17</sup> from the near UV, visible and the near IR-regions of the spectrum. Therefore an attempt has been made to calculate this UV-radiation and make some comparison.

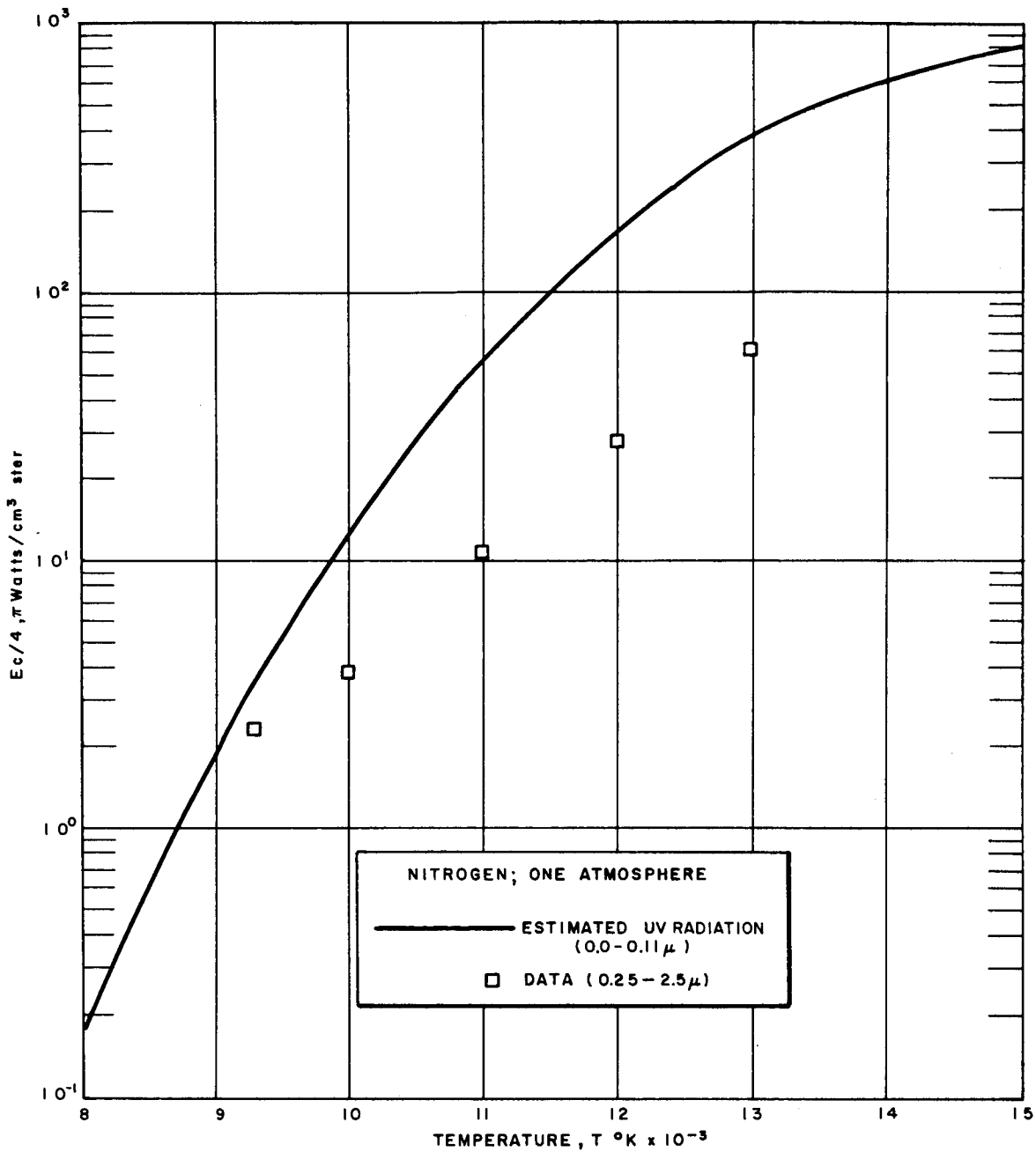
As the composition of air is mainly that of nitrogen, only the UV-region of this gas was investigated.

Utilizing expressions given by Burgess and Seaton,<sup>64</sup> the photoionization cross sections at the absorption edges of the  $2p^3 2p^0$ ,  $2p^3 2D^0$ , and  $2p^3 4S^0$  configurations for atomic nitrogen were estimated. Following suggestions given by Bethe and Salpeter,<sup>65</sup> and Lindenmeier,<sup>66</sup> an average oscillator strength of the above configurations was calculated. Using formulations given by Griem,<sup>67</sup> the emission coefficients and hence UV-spectral distributions were estimated at numerous temperatures. The integrated spectrum results are shown in figure B-7.

In figure B-7, the original nitrogen continuum data of Morris<sup>60</sup> are also presented. As illustrated, the 0-0.1  $\mu$  estimates exceed the 0.25-2.5  $\mu$  data at the higher temperatures. The deviation in temperature dependence of the data is accounted in part by photon emission due to electron attachment to neutral atoms.\*\*\*<sup>68, 69, 70</sup> This radiation mechanism is more prominent at the lower temperatures.

It should be pointed out that the above UV-estimates made the normal assumption of an optically thin gas and placed no blackbody ceiling on the spectrum. The values of these estimates are thus strictly first-order and may be of some question. However, because of their large magnitude, it appears hardly

- 
- \* The exactness of this normalization is not quite known, however, it does permit gross comparison of data.
  - \*\* The estimates of total air radiation used for these comparisons are only those of the one-atmosphere case, since at this pressure the approximate factor of two relationship,  $E_t \approx 2E_c$  was known to exist. Also, it should be pointed out that the extended continuum-radiation estimates,  $E_c$ , go as  $(\rho/\rho_0)^2$  at constant flight velocity rather than  $(\rho/\rho_0)^{1.7}$  as used in this comparison.
  - \*\*\* A radiator not included in the existing theories for the continuum-radiation for nitrogen is the negative ion of nitrogen. Some recent work by Boldt<sup>68</sup> who has measured the  $N^-$  radiative cross sections over a rather limited wavelength range, appears to provide the first experimental evidence of its existence. Boldt's<sup>68</sup> measurement indicates that as much as 50 percent of the continuum radiation at 10,500 °K and at 5300 Å is due to the  $N^-$  ions.



65-5560

Figure B-7 COMPARISON OF NITROGEN UV (0-0.11 μ) ESTIMATED CONTINUUM RADIATION WITH EXPERIMENTAL DATA COVERING THE 0.25-2.5 μ SPECTRAL RANGE

unlikely that the UV-region can be ignored in measuring total radiation. Therefore, questions arise as to the validity of the shock-tube data presented in figure 9, which presumably represented total radiation. The methods employed (see references 1, 6, 52 - 54) do not imply complete scan of the UV-region (below  $0.1\mu$ ).

## 5. PLASMA DIAGNOSTIC TECHNIQUES AND EXPERIMENTAL APPARATUS - A STANDARD ARC SOURCE

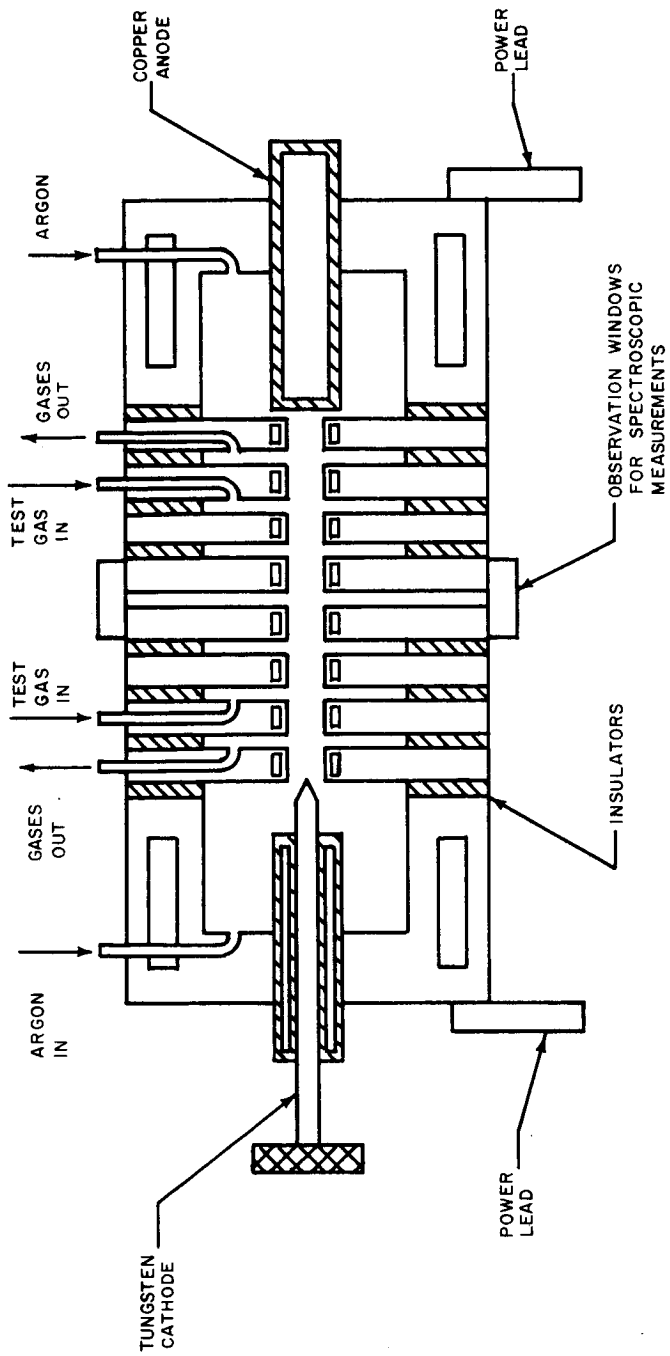
A diagram of the mechanically constricted arc which has been used extensively and successfully for measurements of radiation from a plasma is shown in figure B-8. The arc column is confined to a 5-mm diameter channel by a series of water-cooled washers. These constrictors are electrically insulated from one another and are spaced so that the arc column may be observed between any two constrictors or between the electrodes and a constrictor. The test gas or blanket gas for the electrodes is introduced into the arc channel between the constrictors. The present configuration utilizes a tungsten cathode and a copper anode both blanketed in argon and the gas or gases to be investigated and introduced on each side of the center observation chamber. The argon-test gas mixture exits from the arc head halfway between the observation chamber and the electrodes, providing a column of stagnant test gas plasma for study.

### a. Power Supply

The arc power is supplied from 84 truck batteries in 4 banks of 21 which may be used in parallel or series combinations to yield voltages of 252, 504, or 1008 volts. Control of the arc current, which is usually 50 amperes  $\pm$  0.001 amperes, is provided by a 24-ohm variable air-cooled ballast resistor capable of handling current up to 200 amperes and a water-cooled stainless steel tube with a sliding contact. The batteries are charged by a three-phase, full-wave silicon diode rectifier on the 220 volts AC service line.

### b. Spectroscopic Equipment

Spectroscopic measurements are made with a Bausch and Lomb (B & L) dual-grating stigmatic spectrograph, which has two gratings with first-order dispersions of 4 Å/mm, and 8 Å/mm, respectively. An image of the arc or a N.B.S. standard lamp is focussed on the spectrograph slit, and the spectrum is obtained photographically or photoelectrically. The latter provision is a modification of the B & L, in which a photomultiplier housing is substituted for the normal plate holder. There are two photomultipliers within the housing which may be driven across the spectrum for wavelength scanning purposes. Radiation measurements in the infrared have been made with a Perkin-Elmer Monochromator with a globar as a radiation standard.



NOTE: SHADED AREAS INDICATE WATER COOLING PASSAGES

Figure B-8 SKETCH OF CONSTRICTED ARC

65-5561



c. Conversion of Intensity Measurements to Radial Intensities

All measurements of the spacial distribution of radiation emitted by the cylindrical column of the arc give an intensity originating from a narrow slice of the column perpendicular to the axis of the arc. Since this radiating slice of gas has a temperature gradient causing some portions of the slice to emit more radiation per unit volume than other, it is necessary to convert the measured intensities to radial intensities. Due to the cylindrical symmetry of the arc column, this conversion may be obtained by solution of the following Abel integral equation:

$$S(x) = 2 \int \frac{I(r)r dr}{\sqrt{r^2 - x^2}} \quad (B-5)$$

where

$x$  = coordinate perpendicular to an arc axis and the optical axis

$r$  = radial coordinate of arc column

$R$  = boundary radius of arc

$S(x)$  = measured intensity as a function of  $x$  watts/cm<sup>2</sup>

$I(r)$  = radial intensity in watts/cm<sup>3</sup>

A number of numerical solutions of this integral equation have been used including those given by Pearce,<sup>71</sup> Bockasten,<sup>72</sup> and Barr.<sup>73</sup>

d. Typical Radiation Measurements

Temperatures for a nitrogen plasma were determined from the absolute intensity of the 4935 Å atomic nitrogen line whose transition probability according to Richter<sup>74</sup> is  $A = 2.24 \times 10^6 \text{ sec}^{-1}$ . They also have been made from electron number density measurements using the half-width of the hydrogen Beta line. Hydrogen is introduced into the arc in the amount of 1 percent. The temperature determined from this  $H_{\beta}$  measurement was found to agree within 2 percent of the temperature using the absolute intensity measurements of the 4935 Å nitrogen line.

Measurements of the continuum radiation were made with a pure nitrogen plasma at regions of the spectrum which suffer from a minimum of interference from atomic and molecular band lines. The contribution of the line radiation in the visible spectrum is easily minimized by using the high-dispersion grating spectrograph.

e. Generalized Spectral Distribution Equations

The radiation for a slab of gas in thermodynamic equilibrium at temperature T and x centimeters thick can be predicted from the following equation

$$\frac{dI}{dA d\Omega d\lambda} = (1 - e^{-a'_\lambda x}) \frac{dB(\lambda T)}{dA d\Omega d\lambda} \quad (B-6)$$

where  $B(\lambda T)$  is the Planck function for the blackbody intensity,  $(1 - e^{-a'_\lambda x})$  is the emissivity of the radiating gas,  $a'_\lambda$  is the apparent absorption coefficient corrected for the radiation added by induced emission. The ratio of the apparent absorption coefficient and the true absorption coefficient is

$$\frac{a'_\lambda}{a_\lambda} = \left( 1 - e^{-\frac{hc}{\lambda k T}} \right) \quad (B-7)$$

By combining equations (B-4) and (B-7) and using the first term of the series expansions of  $e^{-a'_\lambda x}$ , the approximate formula for the radiation emitted from an optically thin layer is obtained.

$$\frac{dI}{dA d\Omega d\lambda} = a_\lambda \times 2hc^2 \lambda^{-5} e^{-\frac{hc}{\lambda k T}} \quad (B-8)$$

Equation (B-8) may be used for experimentally determining the absorption coefficient by measuring I and T.

## APPENDIX C

### EVALUATION OF EXPERIMENTAL RESULTS OF A MATERIAL SUBJECT TO RADIATIVE HEATING

A diagram of the experimental apparatus used in a materials test under pure radiative fluxes is shown in figure C-1. A gas-stabilized arc column was maintained between a thoriated-tungsten cathode and a copper anode as shown. The viewing port (a quartz window) allowed a complete view of the arc column. A radiometer was used to measure the emitted radiation per unit arc-column length. Spectral radiance was also determined with a Littrow mount prism spectrograph. (One of the curves of spectral radiance of argon in this device is shown in the following section.) The distance  $R$  (see figure 14) from the geometrical center of the generator to the face of the radiometer is large in comparison to the dimensions of the observed arc column so that the exposed column could be treated, for a first approximation, as a point source. Neglecting the effect of the window, less than 10 percent, the radiant intensity  $I_r$ , at the receiver is related to the total radiant energy  $E$ , of the exposed column by

$$I_r = \frac{E}{4\pi R^2}$$

Division of the total radiant energy by the exposed length of arc column provided the emitted radiation per unit length of the observed column. This estimation was checked by varying both the distance  $R$  and the exposed length of arc column, and the results agreed within experimental error. It was interesting to note that this first-order approximation was only 20 percent higher than the results obtained from the spectral radiance measurements obtained spectrographically. For the materials testing, the model was located directly opposite the viewing port normal to the arc column. To compensate for material recession during the test and hence the change in incident flux, the following analysis was applied: Assuming  $l$  is the distance of the front surface of the model to the center of the arc column and  $l_0$  is this distance at time  $t_0$ , then:

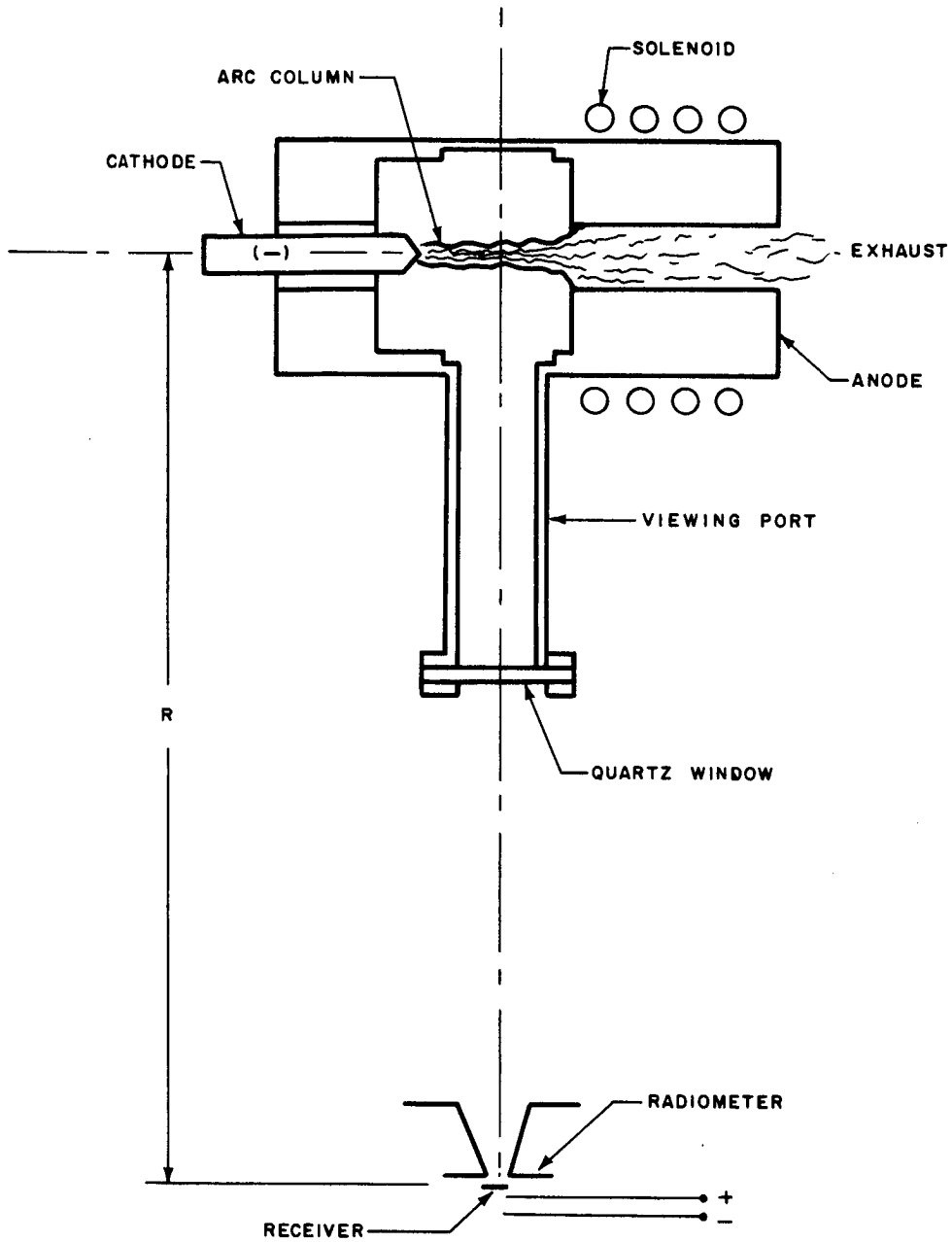
$$\frac{dl}{dt} = k_1 \dot{q}_r$$

and

$$\dot{q}_r = \dot{q}_r(l_0) \frac{l_0}{l}$$

$$\frac{dl}{dt} = k_1 \dot{q}_r(l_0) \frac{l_0}{l}$$

$$\frac{l^2}{2} + C = k_1 \dot{q}_r(l_0) l_0 t$$



65-5562

Figure C-1 RADIANT HEATING SOURCE

$$l^2 - l_0^2 = 2 k_1 \dot{q}_r (l_0) l_0 t$$

A plot of  $l^2 - l_0^2$  versus  $\dot{q}_r (l_0) t$  yields a straight line with a slope of  $5.25 \times 10^{-3} \frac{\text{in.}^2}{\text{kw/cm}^2\text{-sec}}$  (admittedly inconsistent units).

Therefore,  $2k_1 l_0 = 6.59 \times 10^{-3} \left( \frac{\text{in.}}{\text{sec}} / \frac{\text{kw}}{\text{cm}^2} \right) \text{ in.}$  For these tests  $2l_0 = 0.394 \text{ in.}$ ; therefore:

$$k_1 = 1.67 \times 10^{-2} \frac{\text{in.}}{\text{sec}} / \frac{\text{kw}}{\text{cm}^2}$$

The material being tested has a density of  $1.65 \text{ gm/cm}^3$  or  $4.2 \text{ gm/cm}^2\text{-inches}$ . Therefore, a recession rate of  $1 \text{ in./sec}$  is a mass loss rate of  $4.2 \text{ gm/cm}^2\text{sec}$ ; hence  $\dot{m} = 7.02 \times 10^{-2} \text{ gm/kilojoule}$ .

From this a material performance of  $Q_T^*$  can be calculated:

$$Q_T^* = 14.3 \text{ kilojoules/cm}$$

or

$$Q_T^* = 3,430 \text{ cal/gm}$$

To relate this performance to the performance of the material that might be observed in a straight convective heating test, reflection must be accounted for. A reasonable value of material emissivity with a surface temperature of  $3000^\circ\text{K}$  is 0.75. Reflection of incident flux would reduce  $Q_T^*$  by 25 percent, and reradiation would reduce it by 10 percent (Note: Under the present test conditions, blocking could not be considered as a significant factor.) With these reductions,  $Q_T^*$  is reduced by 37 percent to 2500 cal/gm. Recognizing that this evaluation is rough and preliminary, it is noted that this value is almost identical with the  $Q^*$  for this material obtained in straight convective-heating simulation facilities. The plot of the data points on the  $l^2 - l_0^2$  versus  $\dot{q}_r (l_0) t$  graph is shown as figure C-2.

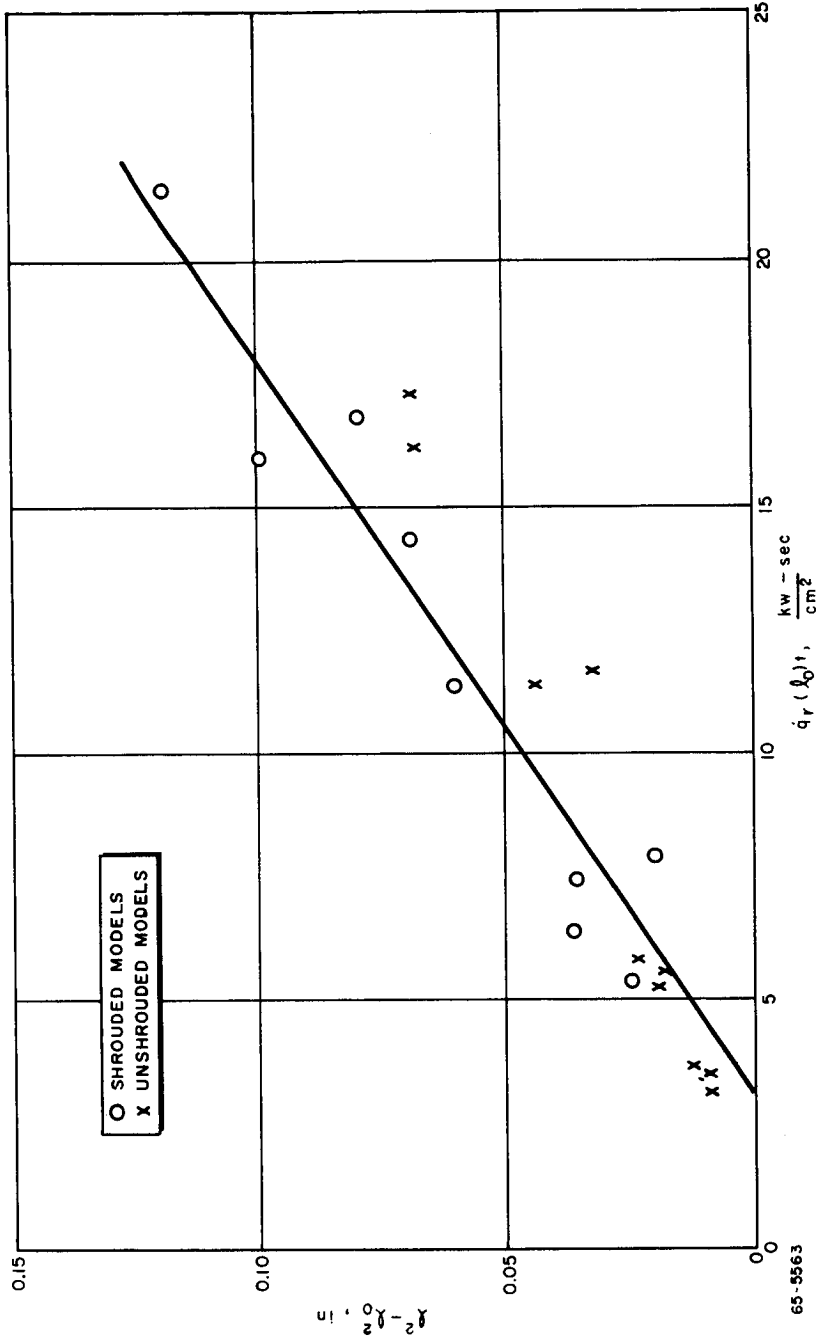


Figure C-2  $l^2 - l_0^2$  VERSUS  $q_r^2 (l_0)^2$

## APPENDIX D

### THE EFFECT OF ELECTROMAGNETIC RADIATION ON SOLIDS

Radiation carries with it an electromagnetic field which is perpendicular to the direction of the propagation of radiation. When such an electromagnetic wave impinges on the surface of a metal, an oscillating electric field is set up in the metal. Its free electrons begin to oscillate due to the electromagnetic field. The oscillating electrons collide with the atoms of the metal and transfer to them part of their energy. The atoms take up this energy in form of lattice vibrations and the metal heats up. The net effect of this process is that the metal absorbs the impinging radiation and becomes hot.

Not all of the energy of the free electrons is transmitted to the atoms of the metal. As the oscillating velocity of the electrons increases under the effect of the electromagnetic wave, the electrons begin to emit radiation and the entire material becomes a radiator. Since part of the incident radiation is reradiated, it does not increase the temperature of the substance.

The effect is different on dielectrics which do not have free electrons. Their electrons can oscillate only with the natural frequency of the atom to which they are bound. If the impinging radiation has a frequency identical with or close to the natural frequency of the atoms, the radiation is absorbed, producing the same effects as in metals. If radiation of a different frequency impinges on a dielectric, it will not be absorbed and the dielectric will not heat up.

From these, it follows that two important parameters determine the effect of radiation on a substance. The first is the spectral distribution of the impinging radiation; the second, the oscillating frequency of the elementary particles of the substance. These two will determine what fraction of the radiant energy is absorbed and what fraction is reradiated by a substance.

The spectral distribution of the radiation is defined by the nature of the source and the applied filters. The absorbed fraction is defined by the radiation parameters of the solid.

#### 1. THEORY OF THE THERMAL RADIATION PARAMETERS

##### a. Thermal Radiation Parameters of an Ideal Specimen

The interaction of thermal radiation with matter arises almost entirely from interactions between the electric and magnetic fields of the radiation and the motion of free and bound electrons in the material. Thus, when a beam of thermal radiation is incident on a material surface, the periodic electric field of the radiation excites oscillations of the free and bound electrons in

the material. The resulting current and space charge densities in the material then react back on the radiation field to produce the characteristic phenomena of reflection, absorption, refraction, etc., which are observed at a material surface. The basic equations governing this process are of course, Maxwell's equations for the electro-magnetic field, which for a periodic radiation field  $e^{-i\omega t}$ , become

$$\begin{aligned} \nabla \times \vec{E} &= \frac{i\omega}{c} \vec{B} & \nabla \cdot \vec{E} &= 4\pi\rho \\ \nabla \times \vec{E} &= \frac{1}{c} (4\pi\vec{j} - i\omega\vec{E}) & \nabla \cdot \vec{B} &= 0 \end{aligned} \quad (D-1)$$

where  $\omega$  is the angular frequency of the radiation,  $\vec{E}$  and  $\vec{B}$  are the total electric and magnetic fields, and  $\vec{j}$  and  $\rho$  are the current and charge densities induced in the material by the radiation. The effect of material properties enters into equation (D-1) through the relation between the induced current  $\vec{j}$  and the exciting field. In most cases it is a good approximation to take simply\*

$$\vec{j} = \sigma \vec{E} \quad (D-2)$$

where the conductivity  $\sigma$  is a complex constant which depends on the frequency of the radiation and the material temperature, and, of course, also on the particular material under consideration. For nonisotropic materials,  $\sigma$  may also depend on the crystal orientation.

The meaning of equation (D-2) is that the current density  $\vec{j}$  at any point in the material is simply proportional to the electric field strength  $\vec{E}$  at that point. The real part of  $\sigma$  gives the component which is 90 degrees out of phase with  $\vec{E}$ .

The entire effect of the material properties on the radiation is contained in equation (D-2), so that the optical properties of the bulk material are completely characterized by giving the value of the single complex number  $\sigma$  as a function of frequency and temperature.

The reflection of radiation from a completely homogeneous slab of material with a perfectly smooth surface can be readily calculated from the solution of equation (D-1) and (D-2) once the value of  $\sigma$  is known. From this solution, one finds the reflection coefficient  $r_0$  for an infinitely thick slab to be

\* An apparent exception to equation (D-2) is the anomalous skin effect, where the current density at one point in the material depends on the field strength at neighboring points. Although this effect is quite important for metals at cryogenic temperatures, it is probably not a significant effect at the elevated temperatures of interest in the present work and will be neglected in the subsequent discussion.



$$r_o = \frac{1}{2} \left| \frac{\cos \theta - \sqrt{(n-ik)^2 - \sin^2 \theta}}{\cos \theta + \sqrt{(n-ik)^2 - \sin^2 \theta}} \right|^2 + \frac{1}{2} \left| \frac{\sqrt{(n-ik)^2 - \sin^2 \theta} - (n-ik)^2 \cos \theta}{\sqrt{(n-ik)^2 - \sin^2 \theta} + (n-ik)^2 \cos \theta} \right|^2 \quad (D-3)$$

where  $\theta$  is the angle of incidence of the radiation, and the index of refraction  $n$  and absorption constant  $k$  are two real numbers which describe the optical properties of the material and which can be defined in terms of the complex conductivity  $\sigma$  by the relation

$$n - ik = 1 - \sqrt{\frac{4\pi i \sigma}{\omega}} \quad (D-4)$$

The subscript  $o$  on  $r_o$  indicates that equation (D-3) applies only to an ideal surface and will in general not be equal to the reflection coefficient actually observed for a real material specimen. The quantity  $r_o$  given by equation (D-3) is the quantity which was defined above as the reflectivity of the material and is an intrinsic property of the material, independent of the surface preparation.

Since equation (D-3) applies to an infinitely thick, and hence completely opaque slab, the emissivity can be found directly from equation (D-3) by means of Kirchoff's law,

$$\epsilon_o = 1 - r_o \quad (D-5)$$

$$\epsilon_o = 1 - \frac{1}{2} \left| \frac{\cos \theta - \sqrt{(n-ik)^2 - \sin^2 \theta}}{\cos \theta + \sqrt{(n-ik)^2 - \sin^2 \theta}} \right|^2 - \frac{1}{2} \left| \frac{\sqrt{(n-ik)^2 - \sin^2 \theta} - (n-ik)^2 \cos \theta}{\sqrt{(n-ik)^2 - \sin^2 \theta} + (n-ik)^2 \cos \theta} \right|^2 \quad (D-6)$$

Equation (D-6) thus describes the angular distribution of the spectral emissivity of an ideal surface in terms of the optical constants  $n$  and  $k$  of the material. As in the case of the reflectivity  $r_o$ , this equation is, of course, not generally applicable for the emittance of a real material specimen.

Any other thermal radiation parameter (e. g., polarization, phase shift due to reflection, etc.) of an ideal surface can be expressed in terms of the optical constants  $n$  and  $k$  by similar methods to those which were used in obtaining equations (D-3) and (D-2). The resulting formulas are not given here, but they can be obtained readily from the solution of equations (D-1) and (D-2), or from literature.

## b. Theory of the Optical Constants

As pointed out previously, in an ideal sample of any material all the thermal radiation parameters are determined if one knows the two optical constants  $n$  and  $k$ , or alternatively, the complex conductivity  $\sigma$  for the material as a function of wavelength and temperature. A number of theories have been proposed to determine these constants for various materials and conditions. For a metal, it is well known that at low frequencies the current  $\bar{j}$  is essentially in phase with the field  $\bar{E}$  and the conductivity  $\sigma$  in equation (D-2) is just equal to the direct current value  $\sigma_0$ . Substituting this value for  $\sigma$  in equation (D-4) and noting that for low frequencies  $1 \ll \frac{4\pi\sigma_0}{\omega}$ , one obtains

$$n \approx k \approx \sqrt{\frac{4\pi\sigma_0}{\omega}} \quad (D-7)$$

As shown originally by Hagen and Rubens,<sup>76</sup> and abundantly verified since,<sup>77, 78</sup> equation (D-7) is in essential agreement with experimental data for wavelengths longer than about  $10 \mu$ , but becomes rapidly poorer for shorter wavelengths, until, in the visible spectrum, it apparently bears no relation whatever to the observed data. The first attempt to explain this discrepancy was made by Drake<sup>79</sup>, who treated a metal as a sea of electrons which were free to move under the influence of the electric field but were subject to a damping force arising from collision with the lattice. This model thus predicted that for radiation frequencies comparable to or greater than the collision frequency of the electrons in the lattice, the electron current would no longer be able to follow the applied field and the conductivity  $\sigma$  would become complex. Thus, there would be a relaxation frequency related to the electron collision frequency, for which the character of the observed reflection would change more or less abruptly. Although this model was successful in predicting many of the qualitative features of the observations on metals at shorter wavelengths, notably the transparency of the alkali metals in the ultraviolet, it was not able to give quantitative agreement with the experimental data. Subsequent work on the problem has tended to confirm the general correctness of Drude's model for the conduction process in a metal, but has refined his treatment in two main ways: (1) By including several different kinds of free and bound electrons having a spectrum of resonant frequencies and relaxation times,<sup>80</sup> and (2) reformulating the arguments in terms of the modern band theory of solids. A good survey of the present state of the theory is given in the recent review article by Givens.<sup>81</sup> In general, one may say that the theoretical formulation of the problem has probably now been worked out adequately and that the main features of the spectral distribution (such as the internal photoelectric effect) are understood, but that a satisfactory theory has yet to be developed for determining many of the internal relaxation times and energy levels which would be required to carry out an actual calculation of the optical constants of a real material

at finite temperatures. At present, in fact, the only reliable source of data on the relaxation times required for such calculations appear to be experimental measurements of the optical constants themselves. Thus, although the theoretical treatment of the optical constants of metals is very valuable for the correlation of experimental data and for the determination of fundamental material properties from optical measurements, it cannot presently be used to obtain accurate theoretical values of the optical constants themselves from measurements of other material properties or from basic theory. Accordingly, the optical constants required would have to be obtained from experimental measurements.

c. Thermal Radiation Parameters of a Real Specimen

The emittance or reflectance of any actual specimen of a material may differ from the ideal values given by equations (D-3) and (D-6) if the specimen fails to fulfill any of the conditions set forth in the definition of the ideal specimen. These conditions are that (1) the specimen must be opaque, (2) the optical constants must be the same throughout the specimen, and (3) the surface must be optically smooth. The first condition is seldom a problem with metals and will not be discussed further here. The remaining two conditions are significant in determining the emissivities of metals in many practical situations.

The most common situation for which the second condition of a homogeneous specimen is not fulfilled is one in which the optical constants of the material near the surface of the specimen are different from those of the bulk material. This may occur, for example, for a specimen in which the surface is covered by a layer of oxide or adsorbed gas, or in which the density and crystal structure of the surface layer has been altered by some polishing process. Experimentally, it has been found that even a monomolecular surface layer of material can cause a detectable change in the reflection of radiation from a metal.<sup>82</sup> Since such surface layers are always present under ordinary atmospheric conditions, it is evidently important to take account of their effects in comparing the emittances of various specimens, unless they have been specially treated under high vacuum conditions to ensure the absence of surface layers.

The effects of a uniform surface layer on the thermal radiation parameters of a specimen can be calculated from equations (D-1) and (D-2) if the optical constants  $n$  and  $k$  and the thickness  $d$  of the surface layer are known. The calculation is essentially similar to that used in obtaining equation (D-3) for an ideal sample, but considerably more tedious.<sup>75, 83</sup> Since the optical constants of a thin film may differ from those of the bulk material, it is important to use measured values of  $n$  and  $k$  for the surface film in making these calculations. Such calculations have been carried out and compared with experimental observations in a few cases, and appear to account satisfactorily for the effects of surface layers on the thermal radiation parameters.<sup>82, 83</sup>

The third condition which must be satisfied by an ideal specimen, as defined above, is that the surface must be optically smooth. This condition is again unlikely to be satisfied by a given specimen unless very special care is exercised in its preparation and treatment, and can account for substantial deviations between the emittances of different specimens of the same material which are supposedly identical. The primary effect of surface roughness on the emittance is to increase the apparent emissivity of the surface by increasing the effective radiating area. Thus, a square specimen 1 cm on a side, for which the apparent microscopic surface area would be  $A = 1 \text{ cm}^2$ , might have a true microscopic surface area  $S$  equal to 5 or 10 times  $A$  due to the effects of surface roughness. If it is assumed that each little element of the surface radiates like an ideal specimen of the material, then the total radiation emitted from the surface would be

$\epsilon_0 \sigma T^4 S = \frac{S}{A} \epsilon_0 \sigma T^4 A$ . Because of the surface roughness, much of this emitted radiation would be reflected from the surface several times before it could escape and thus would be partially reabsorbed by the surface. For a material surface having an area ratio  $\frac{S}{A}$ , the average number of times which the radiation would be reflected from the surface before escaping would be approximately  $\frac{S}{A} - 1$ , so that to a first approximation the apparent emittance of the surface would be

$$\epsilon = \epsilon_0 \frac{S}{A} \epsilon_0 \left( \frac{S}{A} - 1 \right) = \epsilon_0 \frac{S}{A} (1 - \epsilon_0) \left( \frac{S}{A} - 1 \right) \quad (\text{D-8})$$

A better approximation for the emissivity would take account of the fact that all the radiation emitted from an actual surface will not be reflected the same number of times, but rather part of it will escape immediately with no reflection at all, part of it will be reflected once, part twice, and so forth. Thus if  $f(n)$  represents the fraction of radiation reflected  $n$  times, then the emittance  $\epsilon$  of the surface will be given by

$$\epsilon = \epsilon_0 \frac{S}{A} \sum_{n=0}^{\infty} f(n) (1 - \epsilon_0)^n \quad (\text{D-9})$$

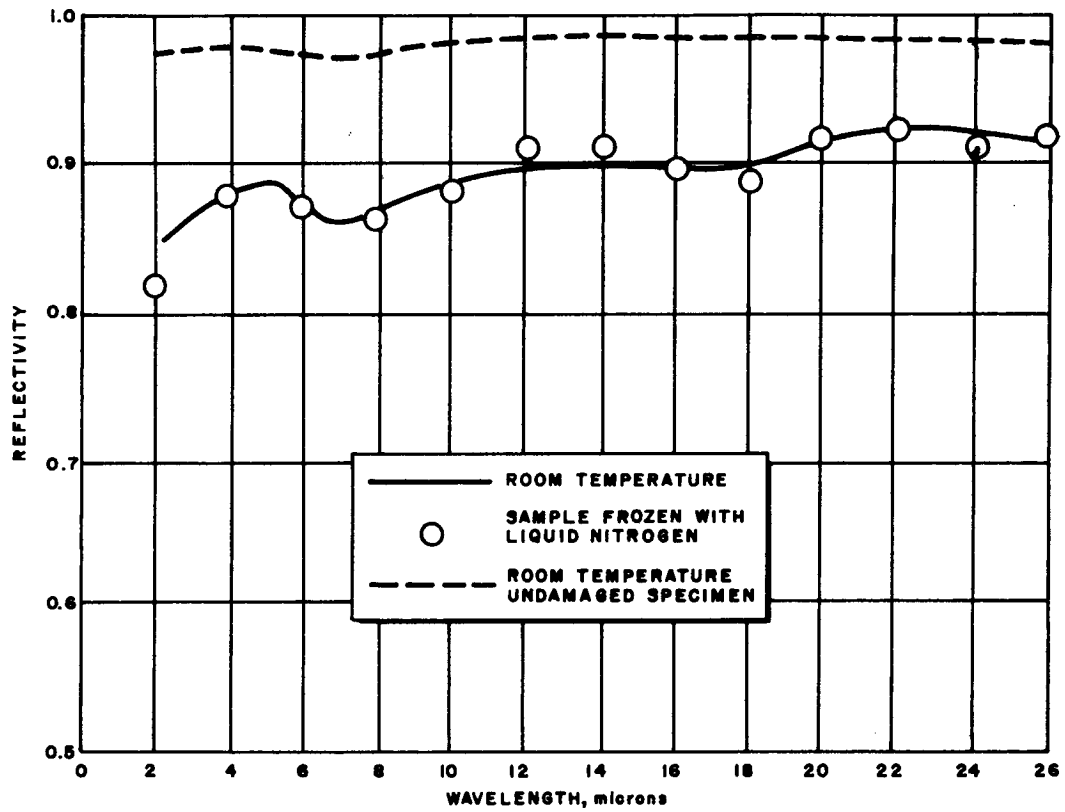
It is conjectured that for a large class of surfaces, the distribution function  $f(n)$  will depend primarily only on the surface area ratio  $\frac{S}{A}$ , so that equation (D-9) will give a formula for the emittance of a specimen with a rough surface in terms of the emissivity  $\epsilon_0$  of the bulk material and the surface area ratio  $\frac{S}{A}$  of the specimen.

In deriving equation (D-9), it was assumed that each element of the surface radiates like an ideally flat surface. According to the theory of radiating systems (antenna theory),<sup>75</sup> this will only be true for surface features which are large compared to the wavelength of the radiation, while the radiation will drop off very rapidly for surface features which are small compared to the wavelength. Very small irregularities in the surface (of the order of atomic dimensions) accordingly would not be expected to contribute significantly to the emitted radiation and should be neglected in determining the surface area  $S$  in equation (D-9). Thus, in applying equation (D-9), the surface area  $S$  should be measured with a resolution comparable to the wavelength of the radiation being studied, i. e., about 1 micron.<sup>4</sup>

## 2. CHARACTERIZATION OF SURFACES

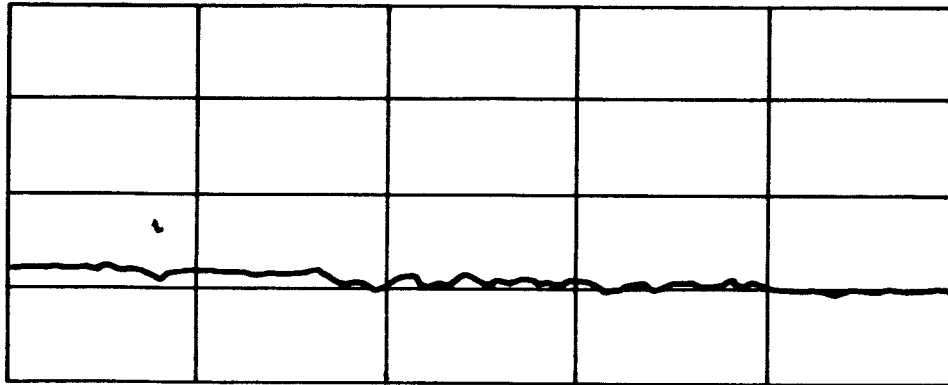
In a recent article, Richmond<sup>84</sup> of the National Bureau of Standards, points out that emittance should be considered a volume property rather than a surface property, and that the contributing volume depends upon the transparency, or opacity, of the material. The contributing volume of a relatively opaque metal, therefore, would only be a few atomic diameters thick, and in practice could be described by the "surface conditions," whereas the contributing volume of a glass or semitransparent ceramic could be up to several inches thick. Experiments at Avco RAD have indeed substantiated Richmond's statement. From observations of work in progress at RAD on a NASA contract,<sup>85</sup> it was noted that the reflectance of such metals as silver, gold, tungsten, aluminum, and stainless steel decreased after the surface was roughened by simulated micro-meteorite bombardment. Figure (D-1) illustrates the effect of such roughening in the case of silver. In the case of a semitransparent material such as aluminum oxide, however, changes in surface roughness from 25 microinches to greater than 200 microinches produced no discernible change in the emittance.<sup>86</sup> Figure (D-2) shows profiles, as determined by Talysurf, of two obviously different aluminum surfaces that exhibited the same emittance, illustrating the apparent lack of importance of the surface finish of a transparent or semitransparent material.

The work done on the NASA contract not only illustrates the effect of the surface conditions on the emittance of metals, but also indicates the shortcomings in the methods of describing or characterizing surface finishes. In this program, the method used to describe the surface consisted of measuring the depth of pits by focusing a microscope on the surface of the metal and then on the bottom of the pit and recording the travel between each setting and determining the diameter of each pit by direct measurement of enlarged photographs of the surface area. Although this method appears to give a satisfactory indication of the average depth to diameter ratio for pits in a particle impacted specimen, it would not be practical for typical machined surfaces or for application to large areas.



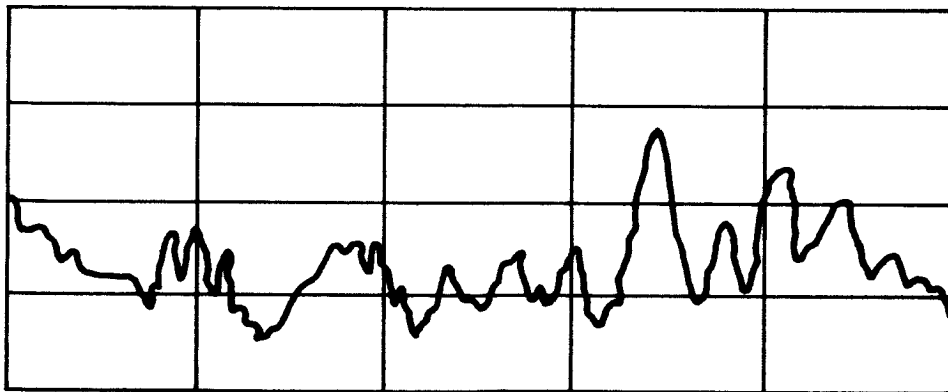
65-5564

Figure D-1 REFLECTIVITY OF SILVER AFTER DAMAGE BY PARTICLE IMPACT



POLISHED  
11-A-1

MAGNIFICATION:  
HORIZONTAL=100X  
VERTICAL=1000X



UNPOLISHED  
11-A-2

65-8866

Figure D-2 TALYSURF PROFILE OF ALUMINA SURFACE

For the most part, however, previous workers in the field of emittance measurements have made little or no attempt to characterize the surfaces on which the measurements were made. In some of the importance of the surface conditions were recognized, attempts to qualitatively describe the surface were made. Terms such as "polished," "oxidized," "sandblasted," etc., were used. Such descriptions are qualitative at best and leave much to be desired. This situation is illustrated in table D-1, where emittance data available in the literature for copper are collected. The great discrepancies can be explained by the vagueness and sometimes total lack of surface definition.

The main reason for this is the fact that no satisfactory methods exist which would characterize surface conditions numerically, so that two surfaces could be quantitatively related to one another. Also lacking is a system to express unequivocally the characteristics of a surface.

TABLE D-1

TOTAL NORMAL EMISSIVITIES OF COPPER

Surface Definition	Temperature	$\epsilon$	Reference
Polished	242° F	0.023	24
Polished	212° F	0.052	25
Polished	Room Temperature	0.15	26
Polished	Room Temperature	0.117	27
Polished	Room Temperature	0.03	28

Two methods are used presently to define surface texture. The first method consists of the descriptive definition of the surface preparation process, listing such data as quality of abrasives, length of polishing time, equipment used, etc. The major shortcoming of this method is that even the best defined and controlled surface preparation process does not necessarily result in identical surfaces on two specimens of the same material. Differences in crystal structure, in previous thermal history of the specimen, in the rate of wear of tools during the process, in the pressure applied in polishing cause such variances in the surface texture which cannot be avoided. The difficulty of surface definition increases if the method of preparation is not known, or if it is known to differ from the standardized process. No means are available to apply a correction factor to the emittance value measured on such a sample.

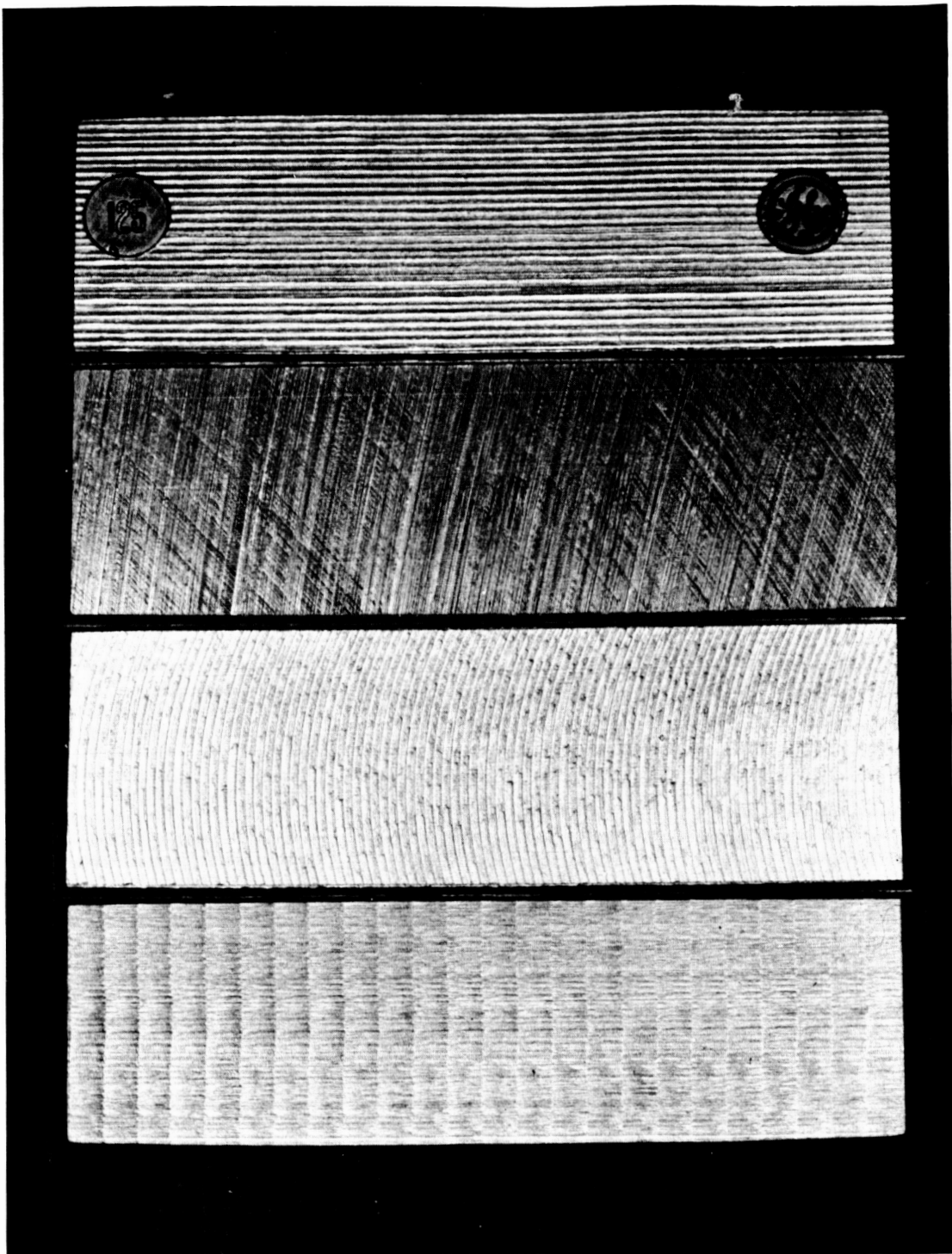
The second method is based on the optical or mechanical scanning of the surface profile. Observation with a microscope is very simple and the techniques are



well developed. Records are easily obtained, but the interpretation of the results is highly subjective, and no methods have been developed so far for numerical evaluation of a representative surface. At best this method can only yield a yes/no type of answer as the identity of two surfaces. There is no possibility to compare numerically two different surfaces or to establish a proportional, numerical order of merit.

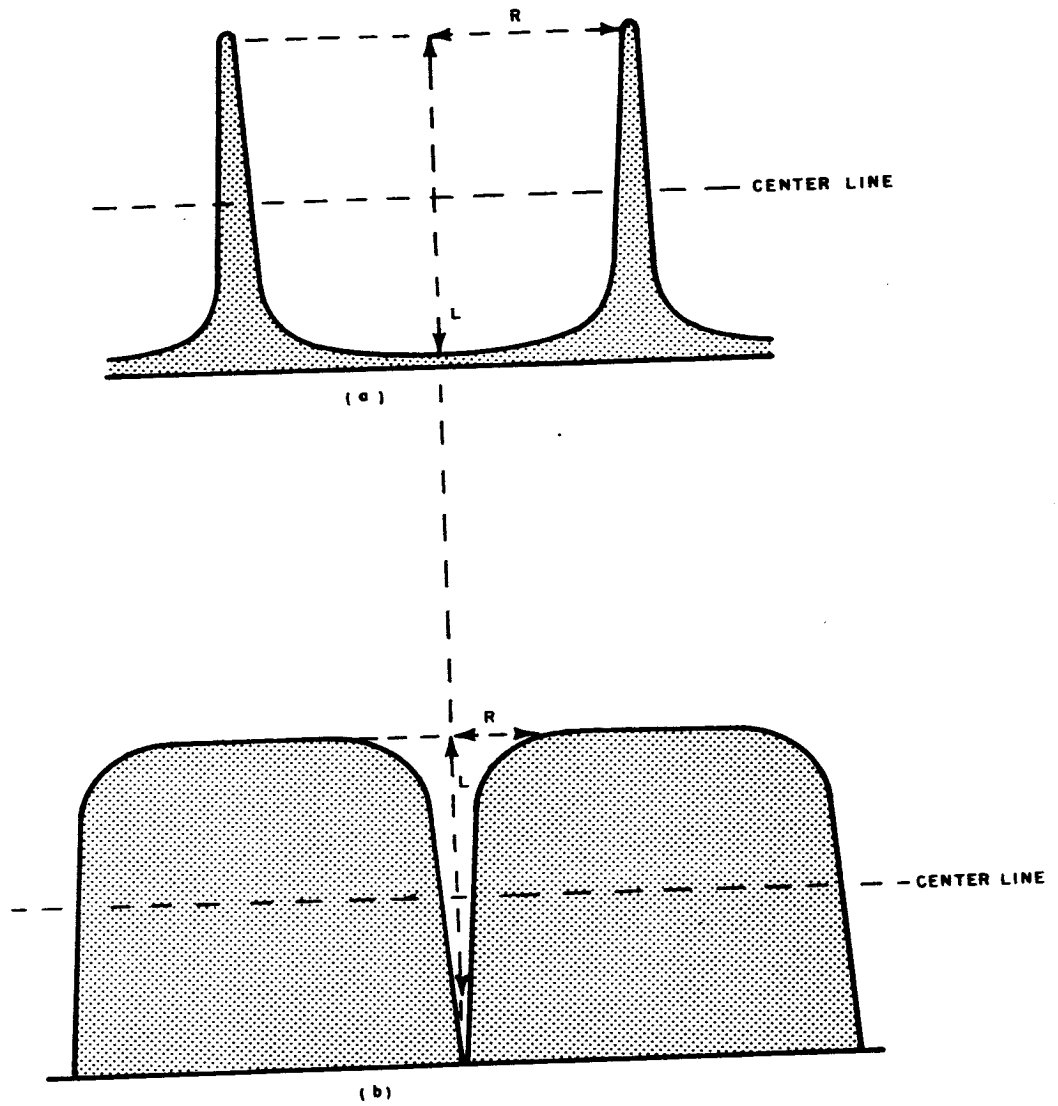
Techniques for mechanically measuring the surface roughness have long been established. This is ordinarily done by drawing a fine stylus across the surface to be measured. The stylus follows the contour of the surface and can either record a trace of the contours or indicate a numerical average to describe the surface roughness. This average is obtained by integrating the area under the trace of the contours of the surface and reporting it as a root mean square (RMS) value or as a center line average (CLA). Although both these values are numerical representations of the surface, they are not unequivocal representations. This is illustrated in figure D-3, which shows four obviously different surface finishes all of which were described as a 125-microinch RMS finish. The lack of equivalence of these four finishes indicates that it is not enough to integrate the ordinate height of the surface contour over a unit length, but that an additional factor must be included.

The need for an additional factor is further illustrated in figure D-4. Both the a and b curve would yield the same RMS-value in Talysurf measurement because the height of the peaks and the depth of the valleys, when measured from the centerline, is identical in both cases as is the number of peaks and valleys per unit length. Nevertheless, experience and observation suggests that the emittance of two surfaces, symbolized by "a" and "b", is different. The valleys on these surfaces can be considered as cavities with a depth of L and an orifice radius R. The effective emissivity of artificial blackbody cavities has been investigated by Buckley<sup>(87)</sup>, Gouffe<sup>(88)</sup>, and Laszlo.<sup>(89)</sup> It was found that, if all other parameters (shape, wall emissivity) are kept constant, the effective emissivity can be expressed as a function of L/R. Figure D-5 illustrates this correlation for two different shapes and for three different wall emissivities ( $\epsilon$ ). As the L/R value increases, so does the effective emissivity. In figure D-4, the L/R value is much smaller than in figure D-4b. Applying the above method of evaluation, the effective emittance of surface "a" is lower than that of "b," in spite of identical RMS-values.



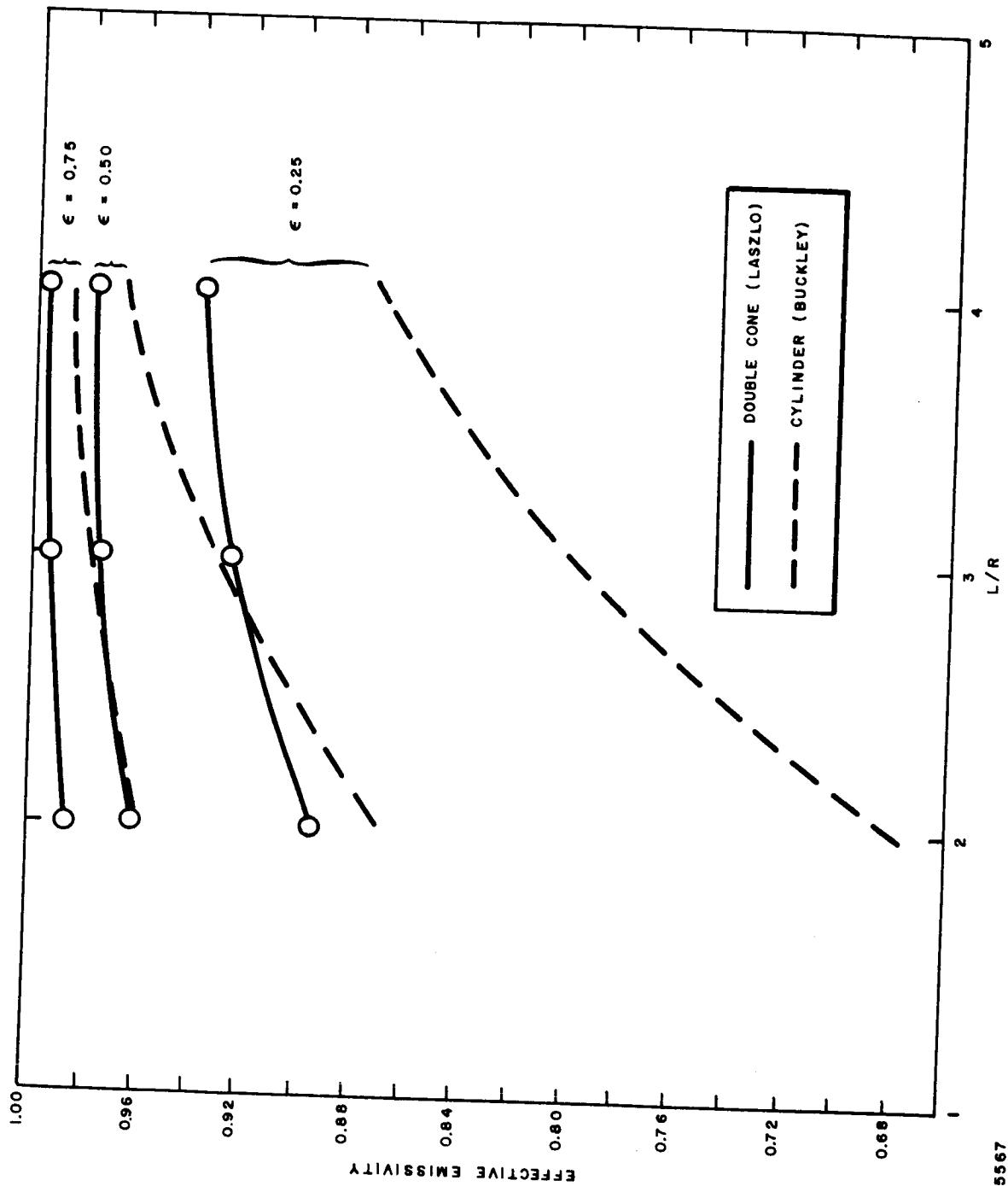
65-2646

Figure D-3 Four 125 Microinch RMS Finishes



65 - 5566

Figure D-4 ILLUSTRATION OF DEFICIENCIES OF RMS METHOD IN DEFINING SURFACE ROUGHNESS



65-5567

Figure D-5 COMPARISON OF THE EFFECTIVE EMISSIVITY OF THE CYLINDER WITH THAT OF NEW SHAPE BLACK BODY

## APPENDIX E

### REFERENCES

1. Nerem, R. M. and G. M. Strickford, Shock Layer Radiation During Hypervelocity Re-entry, AIAA Entry Technology Conference, Williamsburg and Hampton, Va. (October 1964).
2. Nardone, M. C., R. G. Breene, S. S. Zeldin, and T. R. Riethof, Radiance of Species in High Temperature Air, GE R63SD3, General Electric Space Sciences Lab. (June 1963).
3. Kivel, B. and K. Bailey, Tables of Radiation from High Temperature Air, Avco-Everett Research Report 21 (December 1957).
4. Allen, R. A. and A. Textoris, New Measurements and a New Interpretation for High Temperature Air Radiation, Presented at the AIAA Aerospace Sciences Meeting, New York, Preprint No. 64-72 (January 1964).
5. Page, W. A., Shock-Layer Radiation of Blunt Bodies Traveling at Lunar Return Entry Velocities, Presented at the IAS 31st Annual Meeting, New York, N. Y. (21-23 January 1963).
6. Hoshizaki, H., Equilibrium Total Radiation Measurements in Air at Super-orbital Entry Velocities, Lockheed Missiles and Space Co., Report No. 6-90-63-97 (October 1963).
7. Allen, R. A., P. H. Rose, and J. C. Camm, Nonequilibrium and Equilibrium Radiation at Super-Satellite Re-entry Velocities, IAS Preprint No. 63-77, Presented at IAS 31st Annual Meeting, New York, N. Y. (January 1963).
8. Howe, J. T. and J. R. Viegas, Solutions of the Ionized Radiating Shock Layer, Including Reabsorption and Foreign Species Effects, and Stagnation Region Heat Transfer, NASA TR R 159 (November 1962).
9. Midterm Progress Report, Integrated Wall Construction For Re-entry Vehicles, RAD-SR-64-115, Avco Research and Advanced Development Division (April 1964).
10. Carlton, James S., Experimental Study of Radiative Transport from Hot Gases Simulating in Composition the Atmospheres of Mars and Venus, AIAA Paper No. 63-455 (August 1963).

11. Gruszczynski, J. S. and W. R. Warren, Jr., Experimental Heat Transfer Studies of Hypervelocity Flight in Planetary Atmospheres, AIAA Entry Technology Conference, Cambridge, Mass., Paper No. 63-450 (August 1963).
12. Thomas, G. M. and W. A. Menard, Experimental Measurements of Non-equilibrium Radiation from Planetary Atmospheres, AIAA Entry Technology Conference, Williamsburg and Hampton, Va. (October 1964).
13. Breene, R. G., Jr. and M. C. Nardone, Radiant Emission in the Atmospheres of the Terrestrial Planets, Symp. on Dynamics of Manned Lifting Planetary Entry, John Wiley and Sons (1963).
14. Fairbairn, A., The Spectrum of Shock Heated Gases Simulating the Venus Atmosphere, AIAA Entry Technology Conference, Cambridge, Mass., Paper No. 63-454 (August 1963).
15. Allen, R. A., A. Textoris, and J. Wilson, Measurements of Free-Bound and Free-Free Continua of Nitrogen, Oxygen and Air, Avco Everett Research Report RR 195 (September, 1964).
16. Breen, R. G., M. Nardone, T. R. Riethof, and S. Zeldin, "Radiance of Species in High Temperature Air, G. E. R625052, General Electric Space Sciences Laboratory (July 1962).
17. Meyerott, R. E., J. Sokologg, and R. W. Nicholls, Absorption Coefficients of Air, Geophys. Res. Paper 68, (July 1960). (Also LMSD 288052, Lockheed Aircraft Corp., 1959.)
18. Diaconis, N. S., H. E. Weber, and W. R. Warren, Jr., Techniques for Severe Radiative and Convective Heating Environments for Materials Evaluation, Third Hypervelocity Techniques Symposium, Denver, Colorado (March, 1962).
19. Lundell, J. H., W. Winovich, and R. M. Wakefield, Simulation of Convective and Radiative Entry Heating, Second Hypervelocity Techniques Symposium, Denver, Colorado (March, 1962).
20. Howe, J. T., Shielding of Partially Reflecting Stagnation Surfaces Against Radiation by Transpiration of an Absorbing Gas, NASA TR R-95 (1961).
21. Lundell, J. H., R. M. Wakefield, and J. W. Jones, Experimental Investigation of a Charring Ablative Material Exposed to Combined Convective and Radiative Heating in Oxidizing and Nonoxidizing Environments, AIAA Entry Technology Conference, Williamsburg and Hampton, Va. (October, 1964).

22. Louis, J. F., R. Decher, R. A. Allen, and T. R. Brogan, Simulation of Re-entry Radiation Heat Transfer, Avco Everett Research Laboratory (August, 1963).
23. Hermann, M. and R. Liebermann, An Investigation of Radiation Emitted from a High Temperature Arc Column and Its Potential as a Source for High Radiant Heat Flux Simulators, R530-63-82, Avco Research and Advanced Development Division, Technical Release (November 1963).
24. Apollo Monthly Progress Report, RAD SR-64-287 Avco Research and Advanced Development Division (November 1964).
25. Stein, E., R. Shaw, and M. Hermann, Ablation Tests on Apollo Materials Subjected to Radiation Heating from the Arc Imaging Furnace, R720-63-903, Avco Research and Advanced Development Division, Technical Release (December 1963).
26. Foex, M., Concerning Several Devices for the Utilization of Imaging Furnaces, Proceedings Int. Conf. Image Furnace Techniques, Cambridge, Mass., Plenum Press, Inc., New York, N. Y. (1964).
27. Laszlo, T. S., Unpublished Data.
28. Glaser, P. E., Imaging Furnace Developments for High Temperature Research, J. Electrochem. Soc. 107, No. 3, (1960).
29. Cook, J. C., A 400 KW Pressurized Arc Imaging Furnace, Proceedings Int. Conf. Image Furnace Techniques, Cambridge, Mass., Plenum Press, Inc., New York, N. Y. (1964).
30. Horning, D. O. and E. R. Parket, Arc Image Furnace, AFOSR TR-59-88 (May 1959).
31. Denney, K. L., McDonnell Aircraft Corporation, St. Louis, Mo., Private Communication to T. S. Laszlo.
32. Null, M. R. and W. W. Lozier, Carbon Arc Image Furnaces, Rev. Sci. Inst., Vol. 29, No. 2, 163-70 (February 1958).
33. Hazlett, T., University of California, Livermore, California, Private Communication to T. S. Laszlo.
34. Farmer, R. W., An Arc-Imaging Furnace for Materials Research, ASD-TDR-63-312, (May 1962).

35. Latil, J. P., Automatic Recarboning of Carbon-Arc Lamps, Jour. of the SMPTE Vol. 66,(June 1957).
36. Ploetz, G. P., H. F. Cox, and L. C. Larson, The Carbon Vapor Lamp: A Thermal Radiation Source for Imaging Furnaces, Proceedings Int. Conf. Image Furnace Techniques, Cambridge, Mass. Plenum Press, Inc., New York, N. Y. (1964).
37. Cotton, E. S. Quartermaster Research and Engineering Center, Natick Mass., Private Communication to T. S. Laszlo.
38. Maust, E. E. and W. E. Warnke, The Performance and Operating Characteristics of an Image Furnace Having 60-inch Paraboloidal Mirrors, Bureau of Mines Report of Investigations 5946 (1962).
39. Recharadson, D. L., A Thermal Radiation Heat Source and Imaging System for Biomedical Research, Proceedings Int. Conf. Image Furnace Techniques, Cambridge, Mass., Plenum Press, Inc., New York, N. Y. (1964).
40. Thouret, W. E. and H. S. Strauss, High Wattage Xenon and Mercury Vapor Compact Arc Lamps as Radiation Sources for Imaging Furnaces, Conference on Imaging Techniques, Cambridge, Mass. (4-5 October 1962).
41. May, C. E., NASA Lewis Research Center, Cleveland, Ohio, Private Communication to T. S. Laszlo (1962).
42. Young, L. L. and F. H. Webb, Jr., Super-Radiance Source of Improved Spectral Composition with Integral Radiation Directing Means Especially Suitable for Use in Solar Simulators, Internat. Symp. on Solar Radiation Simulation. Los Angeles, Calif. (January 1965).
43. Hermann, M., and R. Liebermann, An Investigation of Radiation Emitted for a High Temperature Arc Column and its Potential as a Source for High Radiant Heat Flux Simulators, R530-63-82, Avco Research and Advanced Development Division, Technical Symposium, Denver, Colorado (March, 1964).
44. Diaconis, N. S., H. E. Weber, and W. R. Warren, Jr., Techniques for Severe Radiative and Convective Heating Environments for Materials Evaluation, Third Hypervelocity Techniques Symposium, Denver, Colorado (March 1964).
45. Jaatinen, W. A., E. A. Mayer, and F. R. Sileo, New Approach to Sources for Solar Simulation, Internat. Symp. on Solar Radiation Simulation, Los Angeles, Calif. (January 1965).



46. VanOrnum, D. G., Vortex Stabilized Radiation Sources for Improved Solar Simulation. Internat. Symp. on Solar Radiation Simulation, Los Angeles, Calif. (January 1965).
47. McGinn, J. H., A New Type Arc for Producing High Temperature, High Purity Plasma Jets; Proc. 5th Int. Conf. of Ionization Phen. in Gases, Munich, North-Holland Pub. Co., Amsterdam (1961).
48. Lundell, John H., NASA Ames Research Center, Moffett Field, Calif., Private Communication to T. K. Pugmire.
49. Bakish, R., (ed.). Introduction to Electron Beam Technology, John Wiley & Sons, Congress No. 62-17262 (1962).
50. Fromm, D., Absolute Spectral Distribution Measurements of Xenon High Pressure Discharges. U. S. Army Engineer Research and Development Laboratories (May 1963).
51. Genarco Inc., Jamaica, New York
52. Flagg, R. F. Stagnation-Point Radiative Heat-Transfer Measurements at Supersatellite Velocities, Avco Research and Advanced Development Division Wilmington, Mass. RAD-TM-63-77 (December 1963).
53. Nerem, R. M., Stagnation Point Heat Transfer in High Enthalpy Gas Flows, Part I and Part II, Ohio State University Aerodynamic Laboratory Final Report, prepared under contract AF33(657)-10110, Research and Technology Division, Air Force Systems Command, Wright-Patterson Air Force Base, Dayton, Ohio, FDL-TDR-64-41 (March 1964).
54. Page, W. A. and J.O. Arnold, Shock Layer Radiation of Blunt Bodies Traveling at Reentry Velocities, " NASA TR-R-193 (April 1964).
55. Wick, B. H., Radiative Heating of Vehicles Entering the Earth's Atmosphere, Presented to the AGARD Fluid Mechanics Panel, Brussels Belgium, (NASA Document No. N62-12453) (3-6 April 1962).
56. Laird, J. D., and K. Heron, Shock Tube Gas Dynamic Charts" Part I Equilibrium Argon-Free Air from 3,000 to 40,000°K, Avco Research and Advanced Development Division, TM 64-12 (10 April 1964).
57. Ziemer, R. W., Extended Hypervelocity Gas Dynamic Charts for Equilibrium Air, Space Technology Laboratories, Inc., Report STL-TR-60-0000-09093 (14 April 1960).
58. Personal Communication with K. Heron who had Previous Communication with Hoshizaki.

59. Feldman, S., Hypersonic Gas Dynamic Charts for Equilibrium Air, Avco Everett R. R. 40 (1957).
60. Morris, J. C., et al, Research on Radiation from Arc Heated Plasma, Prepared for Aeronautical Systems Division, Wright-Patterson Air Force Base, Dayton, Ohio, Avco Research and Advanced Development Division Contract No. AF33(616)-8390, Quarterly Progress Reports 1-12 (1960-1964).
61. Unsold, A. Physik der Sternatmosphären, 2nd ed., Springer, Berlin, 163-74 (1955).
62. Burhorn, F. and R. Wienecke, A. Phys. Chemie 213 37 (1960); 215, 269 and 285 (1960).
63. Flinn, D. Q. and T. R. Munson, Equilibrium Composition and Thermodynamic Properties of N, C, O. A Mixtures to 40,000°K, Avco RAD-TM-64-11 (March 1964).
64. Burgess A. and M. F. Seaton, A General Formula for the Calculation of Atomic Photo-Ionization Cross Section. Monthly Notices Roy. Astron. Soc., 120, P121-151 (1960).
65. Bethe, H. A. and E. E. Salpeter, Quantum Mechanics of One-and-Two Electron Atoms, Academic Press (1957).
66. Lindenmeis, C. Avco-Everett Research Note 157 (September 1959).
67. Griem Hans R., Plasma Spectroscopy, McGraw-Hill Book Co., (1964).
68. Boldt, G., 2. Physik 154 330-338 (1959).
69. Morris, J. C. et al, Research on Radiation from Arc Heated Plasma, Avco RAD, RAD-TR-64-10 (9 July 1964).
70. Allen, R. A. and A. Textoris, Evidence for the Existence of N<sup>-</sup> from the Continuum Radiation from Shock Waves Journal of Chem. Phy. Vol. 40, No. 11, 3445-3446 (June 1964).
71. Pearce, W. J., Calculation of the Radial Distribution of Photon Emitters in Symmetric Sources, Conference on Extremely High Temperatures pp. 123-134, Boston, Massachusetts (1958)
72. Bockasten, K., JOSA 51, 953 (1961).
73. Barr. W. L., JOSA 52, 885 (1962).

74. Richter, F., *Astrophys.* 51 177 (1961).
75. Stratton, J. A., Electromagnetic Theory, McGraw-Hill N. Y. (1941).
76. Hagen, E. and H. Rubens, *Ann. Physik II*, 873 (1903).
77. Hurst, C., *Proc. Royal Soc. (London)* A142 466 (1933).
78. Leigh, C. H. and S. J. Walnik, *Emissivity of Metals after Damage by Particle Impact*, Avco RAD-SR-61-58 (21 July 1961).
79. Drude, P., *Theory of Optics*, Longmans Green and Co., N. Y. (1902).
80. Roberts, S., *Phys. Rev.* 100, 1667 (1955).
81. Givens, M. P., *Optical Properties of Metals*, in: Solid State Physics 6, F. Seitz and D. Turnbull, Academic Press, N. Y. (1958).
82. Roberts, S., *Phys. Rev.* 118, 1509 (1960).
83. Partori, T., *J. Opt. Soc. Am.* 52, 918 (1962).
84. Richmond, J. R., NB.S. Wash., D. C., *Coatings for Space Vehicles First Symposium - Surface Effects on Spacecraft Materials*, May 1959, Edited by Francis J. Clauss, Copyright 1960 by John Wiley & Sons, Inc.
85. Leigh, C. H., *Spectral Emissivity of Metals after Damage by Particle Impact*, Final Report Contract NAS8-1642 Avco RAD Technical Report RAD-TR-62-38 (13 August 1962).
86. Gannon, R. E. and B. Linder, *The Effect of Surface Conditions and Porosity on the Emittance of Alumina*, Presented at the 14th Pacific Coast Regional Meeting, American Ceramic Society, San Francisco (October 1961).
87. Buckley, H., *On the Radiation from the Inside of a Circular Cylinder*, *Philosophical Magazine*, 4, 753 (1927); 6, 447 (1928), 17, 377 (1934).
88. Gouffee, A., *Corrections D'ouverture des coups-noir artificiels, compte tenu des diffusions multiples internes*, *Revue D'Optique*, 24 (1-3), (January - March 1945).
89. Laszlo, T. S., *On Radiant Energy in High Temperature Research*, *Solar Energy*, Vol. V., No. 4 (October-December 1961).

DISTRIBUTION

<u>Addressee</u>	<u>No. of Copies</u>
NASA Manned Spacecraft Center (+1 reproducible) Structures and Mechanics Division Thermo-Structures Branch/ES3 2101 Webster-Seabrook Road Houston, Texas 77058 Attention: Mr. D. H. Greenshields	25
NASA Manned Spacecraft Center General Research Procurement Branch/BG751 2101 Webster-Seabrook Road Houston, Texas 77058 Attention: Mr. Paul Liebhardt	3
NASA Manned Spacecraft Center Technical Information Division Documentation Section/BF332 2101 Webster-Seabrook Road Houston, Texas 77058 Attention: Miss Retha Shirkey	4
Central Files Research Library(+1 reproducible)	1 67